NTNU – Trondheim
Norwegian University of
Science and Technology

Structural Framework of the Statfjord Formation (Rhaetian-Sinemurian) in the Oseberg South Field, Norwegian North Sea

Jeffrey John Catterall

Petroleum Geosciences
Submission date: May 2012
Supervisor: Stephen John Lippard, IGB

Norwegian University of Science and Technology
Department of Geology and Mineral Resources Engineering

Acknowledgements

First and foremost, I would like to thank Statoil ASA for the opportunity to work on this project, and for providing me with a place to sit in the Bergen office while writing the thesis. In addition, I would like to thank both of my supervisors Hugo Sese at Statoil and Stephen Lippard at NTNU for their support and feedback throughout the project, and also to Jim Daniels who helped turn this project into one suitable for a Master's thesis.

I have received support from many individuals from the Oseberg South Petroleum Technology Group. Their constant feedback, mentorship, and support during the many aspects of this project have been greatly appreciated.

Lastly, thank you to all of my friends and fellow classmates that have made my two years at NTNU such a wonderful experience.

Jeffrey John Catterall
June 2012

Abstract

The Statfjord Formation (Rhaetian-Sinemurian) produces from six fields across the North Sea, but no discoveries have yet been made in the 12 exploration wells across the Oseberg South Field. The field has undergone two major periods of rifting in the Permian-Triassic and from the mid-Jurassic to Early Cretaceous. The Statfjord Formation was deposited during the Permian-Triassic post-rift period, but its tectonic influence on the paleogeography of the formation is not well understood.

An isopach map produced from seismic interpretation and RMS modelling of the Statfjord Formation showed a westward thickening trend towards the present-day Viking Graben. This study presents results obtained using new, high-quality OBC seismic data that has allowed for faults throughout the field to be mapped in great detail. Supported by stratigraphic correlations and biostratigraphy, the mapping has showed that most faults can be assigned to either of the main rifting phases or their associated post-rift subsidence histories. Large, east-dipping faults are believed to have originated during the Permo-Triassic rifting, with evidence of movement into the Cretaceous. Large thickness increases of the formation over the westward dipping Oseberg and Brage Faults, as well as syn-rift sediments within some grabens in the J structure indicate movements of these faults during deposition.

Biostratigraphic data show that the lowermost part of the Statfjord Formation was approximately the same thickness across the field until the Late Triassic, constraining the initiation of the Oseberg and Brage Faults to the Early Jurassic. Interpretations from timelines correlated within the Statfjord Formation suggest that the rate of subsidence along different faults was not consistent through time. Thickness changes along strike of the fault indicate that the movement along the fault was diachronous. This study aims to show that major fault activity influenced the deposition, and possibly preservation potential of sediment in the Statfjord Formation.

The second phase of rifting is believed to have initiated many of the faults within the field, as well as reactivated the Oseberg and Brage Faults. Additional NW-SE faults in the Omega structure show no evidence of syn-rift sediments at the Statfjord Formation level, suggesting a mid-Jurassic post-rift origin. Similarly oriented faults were seen in the C structure, however, the presence of syn-rift sediments was difficult to ascertain, and no conclusions about the timing of initiation were made.

Table of Contents

Table of Figures

Table of Tables

1. Introduction

The Oseberg South (Oseberg Sør) field was discovered by well 30/9-3 in 1984, and comprises production licenses PL079 and PL104. It is currently licensed by: Statoil Petroleum AS (49,3 %, operator); Petoro AS (33,6 %); Total E&P Norge AS (10,0 %); ExxonMobil E&P Norway AS (4,7 %); and ConocoPhillips Skandinavia AS (2,4 %). It was brought on production in February 2000, and as of January 2012, the field has produced 48,17 million Sm3 (net oil equivalents) from the Jurassic Tarbert, Ness, (Brent Group) and Heather Formations (Figure 2). A total of 18 exploration wells have been drilled in the period from 1983 to 2009, while 73 development wells (including injection, observation, and production) have been drilled from 1998 to 2011. While production from the Brent Group and Heather Formation has been the focus of exploration activity, eleven of the exploration wells have penetrated the Statfjord Formation (Table 1). These exploration wells were placed optimizing targets in the Brent Group, and thus not ideally placed for a Statfjord Formation target, however, the information obtained has been valuable in understanding the geology of the Statfjord Formation.

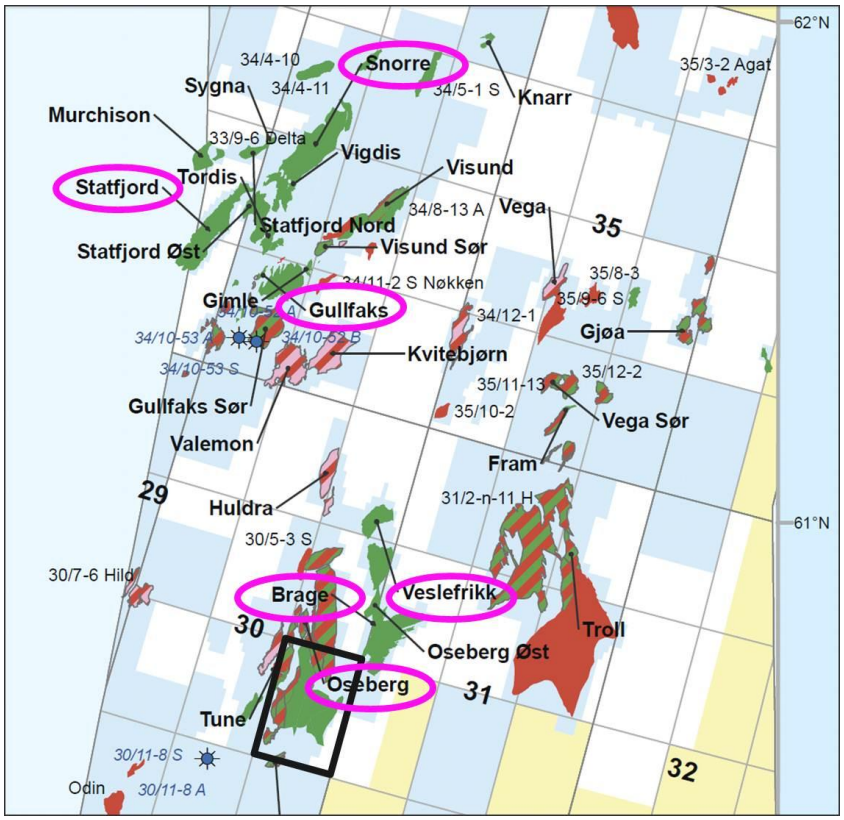

Figure 1: Regional overview of the Norwegian North Sea license areas off the Norwegian coastline; the black outline highlights block 30/9 and the approximate location of the Oseberg South field, and the magenta circles show fields that currently produce from the Statfjord Formation (NPD 2011).

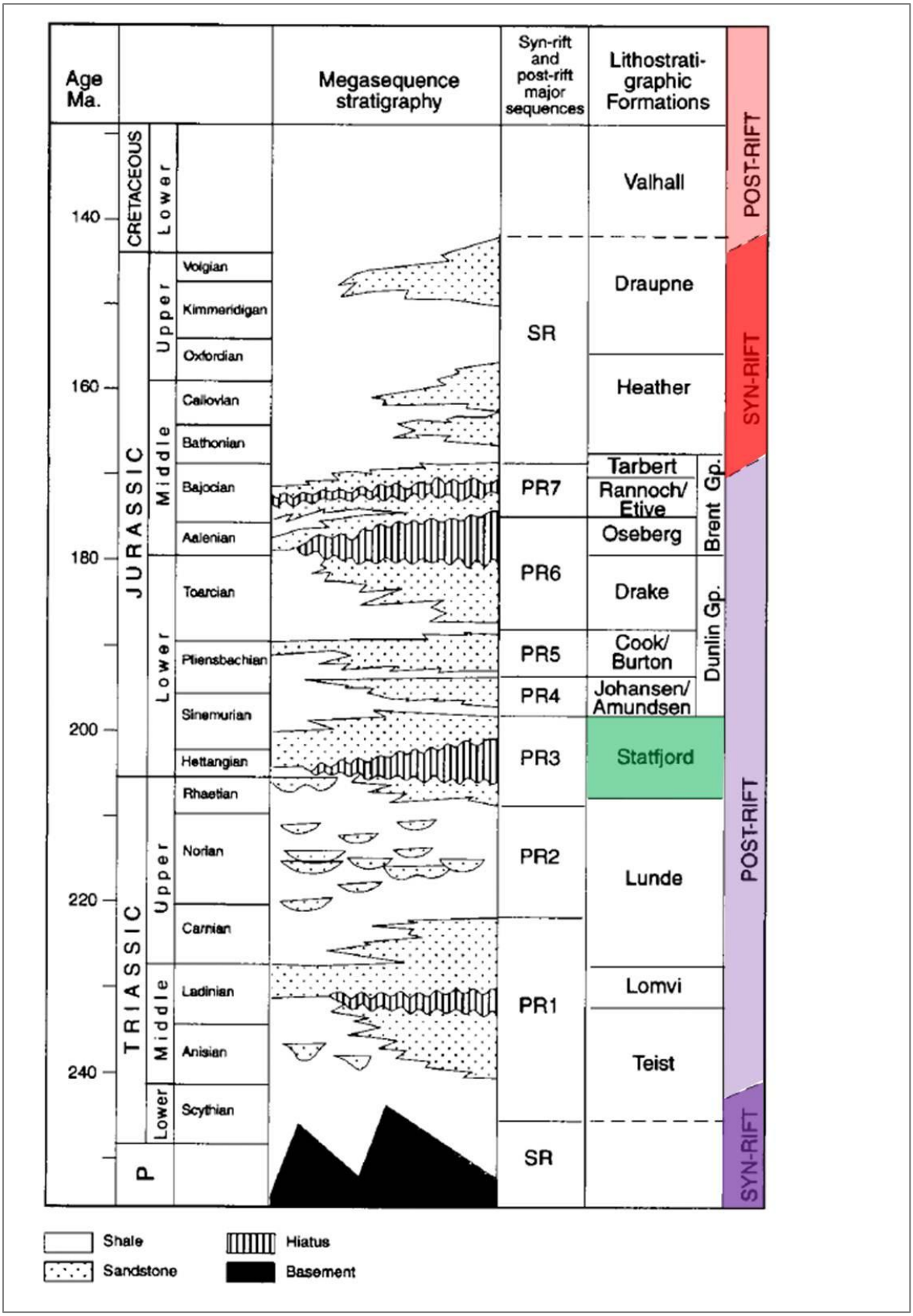

Figure 2: Stratigraphic section of the northern North Sea, showing formations and associated timing with respect to two major rifting events (modified from Færseth 1996).

Interest in the Statfjord Formation has increased in the Oseberg South field owing to several factors. Across the Viking Graben in the North Sea, six fields produce from the Statfjord Formation (Brage, Oseberg Main, Veslefrikk, Gullfaks, Statfjord, & Snorre) in the Norwegian sector, and from two fields (Alwyn and Brent) in the British sector (Ramm & Ryseth 1996, Ryseth & Ramm 1996; Figure 1). The nearby production from the Oseberg Main field from the Statfjord Formation has spurred more interest in the outlying areas, including Oseberg South. Until recently, the understanding of deeper horizons such as the Statfjord Formation has been inhibited mainly by the high uncertainties created due to poor seismic data quality and few well penetrations. However, three separate Ocean Bottom Cable (OBC) seismic surveys were shot over the J structure (2008), the C structure (2010), and remaining parts of the field (2010), all of which were merged in 2010 to create one large survey that was used for interpretations in this thesis (Figure 3). The resulting processed data provided significantly better imaging than the previous streamer data (Figure 4). As precursor to this project, the author of this thesis interpreted the Statfjord Formation horizon on the 'fast-track' OBC dataset in the summer of 2011, creating the first structural map of the Statfjord Formation across the Oseberg South field. Further understanding of the structural architecture of the formation will aid in determining if and when charging of the formation may have occurred, and possibly regarding potential areas of higher reservoir quality.

1.1 Objective

As of January 2012, 11 of the 18 exploration wells (Table 1) have penetrated the Statfjord Formation within the Oseberg South Field, in addition to one Statfjord Formation target drilled at 30/9-24T2. All of the drilled wells tested water, with the exception of 30/9-13S, which showed signs of gas in the petrophysical logs. Despite the lack of hydrocarbons found in the Statfjord Formation exploration wells so far, one cannot discount the possibility of hydrocarbons existing in other structural blocks, many of which contain untested structural highs. The depth of the reservoir and hydrocarbon charging history increases the complexity in exploring the Statfjord Formation, but it is hoped that mapping from the new OBC data can help increase the understanding of the formation, and reduce associated risks. As such, the main purpose of this thesis is to create a structural framework model of the Statfjord Formation, where better understanding of the structural configuration and the structural history will help in mitigating further exploration risk. Creating a structural model is one of the first steps in the eventual development of a full scale reservoir model, which will be outside the scope of this thesis. However, the structural model will require many input parameters, including the seismic interpretation of the horizons of interest; the creation of synthetic seismic traces to tie the petrophysical well data to the seismic; major fault

interpretation; formation tops and thicknesses from logs; and conceptual stratigraphic interpretation from logs and core.

The deliverables of this thesis include:

- Logged Statfjord Formation core, where available, with interpretations of depositional environment.
- Biostratigraphic correlation, confirming age equivalents, where possible.
- Consistent formation top picks.
- Appropriate tie of geological well data to seismic by creating seismic synthetic data, where possible.
- Mapping of interpretation of the top, middle, and base Statfjord Formation markers, and interpretation of major faults.
- Built structural model of the Statfjord Formation at Oseberg South in RMS.
- Suggested naming scheme and litho-zonation of the formation.

In addition to the aforementioned deliverables, the thesis intends to address several questions:

- Consistency of the structural development of the field from published data and interpretations from the Oseberg South field, and implications on the understanding of the field.
- The reliability of biostratigraphic data in determining the relative subsidence rates from one block to another, and its value in developing consistent zonation criteria that can be used not only for the existing wells, but for future wells in the field, and correlation to other fields.
- Evidence of syn-depositional sediments, indicating fault movement during deposition of the Statfjord Formation.

Table 1: List of wells that penetrate the Statfjord Formation in Oseberg South.

Well	Fluid	Triassic Penetration	Core
30/9-3A	Water	Yes	No
30/9-4S	Water	No	Yes
30/9-5S	Water	Yes	Yes
30/9-6	Water	No	No
30/9-7	Water	No	No
30/9-9	Water	No	No
30/9-10	Water	No	No
30/9-11A	Water	No	No
30/9-13S	Gas?	No	No
30/9-15	Water	No	No
30/9-16	Water	No	Yes
30/9-24T2	Water	Yes	No

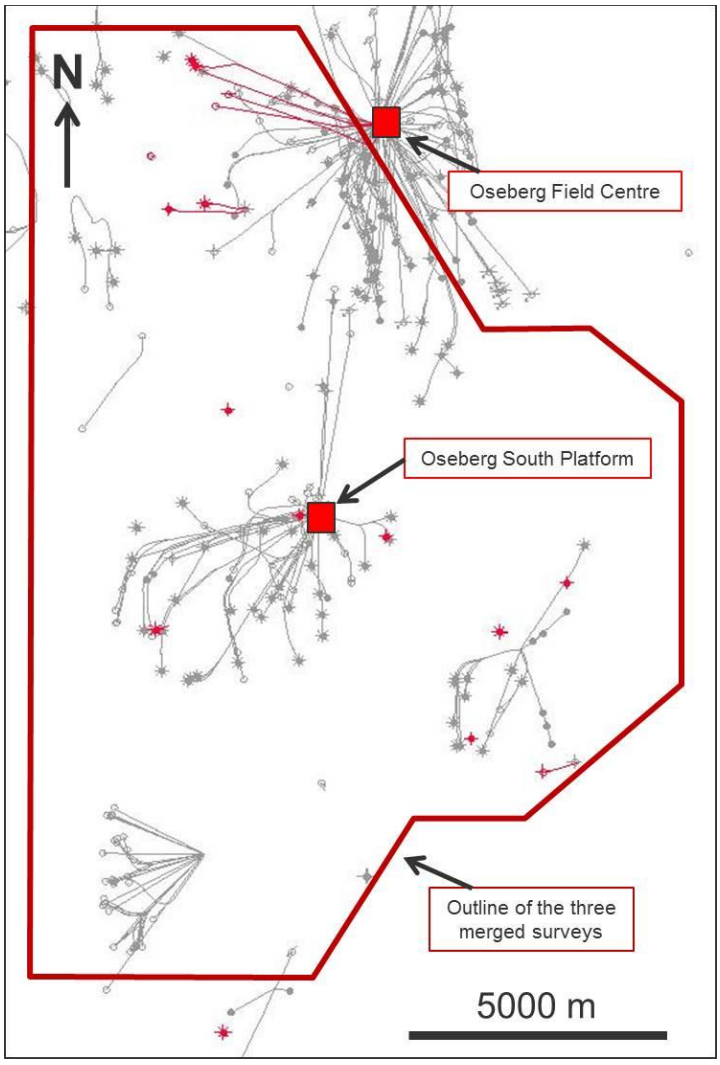

Figure 3: The outline of the OBC dataset shot in 2010 is highlighted with a red outline. Exploration wells that penetrated the Statfjord Formation are also highlighted in red.

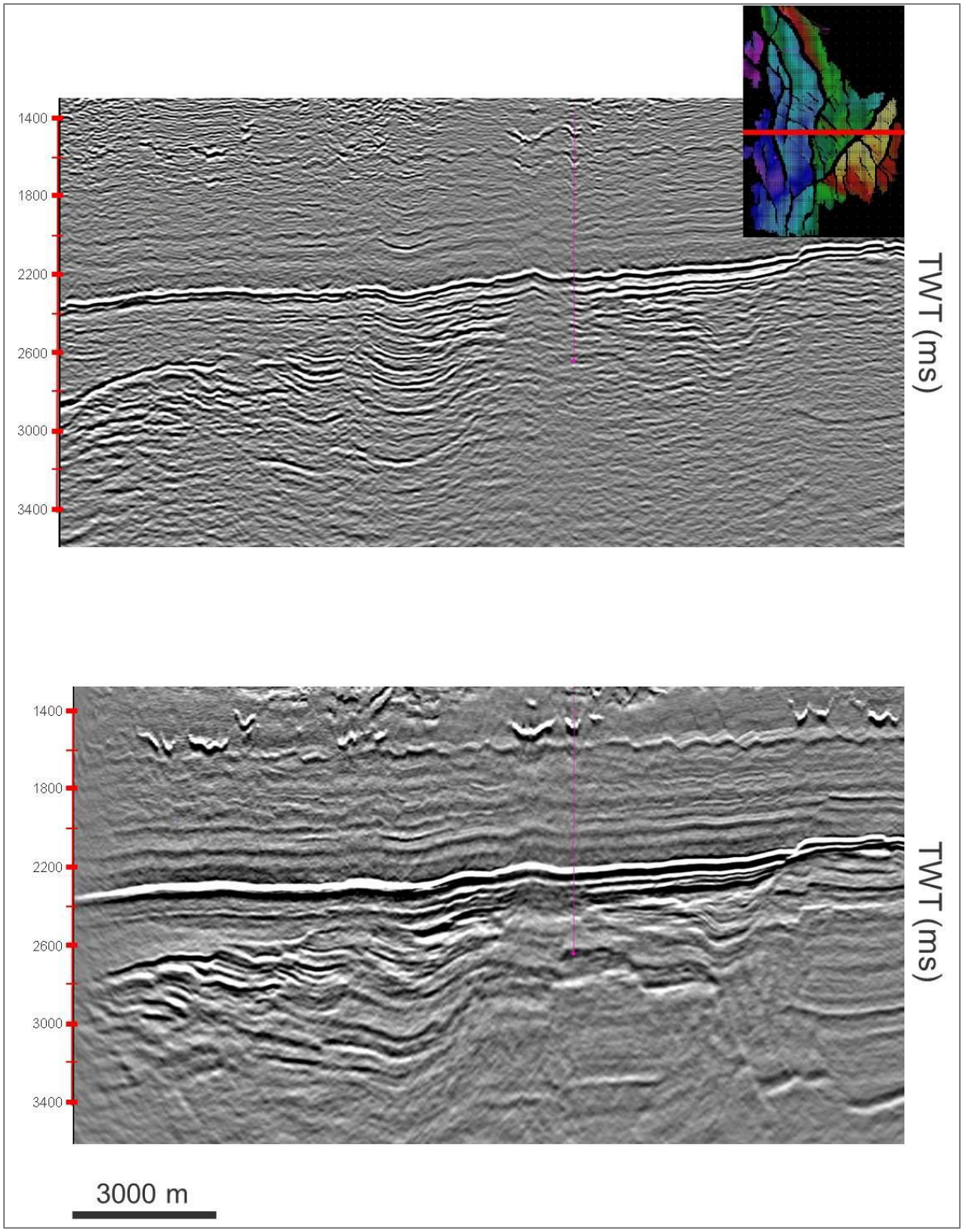

Figure 4: Visual quality comparison between the old streamer data (top) and the new OBC data obtained in 2010 (bottom). Both sections are in TWT (ms).

2. Background Geology

2.1 Stratigraphy

The Statfjord Formation is regionally extensive across much of the Norwegian and British sectors of the North Sea. The current stratigraphic nomenclature used for the Statfjord Formation and its associated members was defined by Deegan & Scull in 1977, and further supported in 1984 by Vollset & Doré. Deegan & Scull (1977) defined the Statfjord Formation based on well 33/12-2 (Mobil, Figure 6) in the Norwegian waters of the North Sea, with interpretations partially based on the work from Yonge *et al.* (1975) and Bowen (1975). The formation is divided into three members, from oldest to youngest: the Raude Member, the Eiriksson Member, and the Nansen Member. The aerial extent of each member is seen in Figure 5.

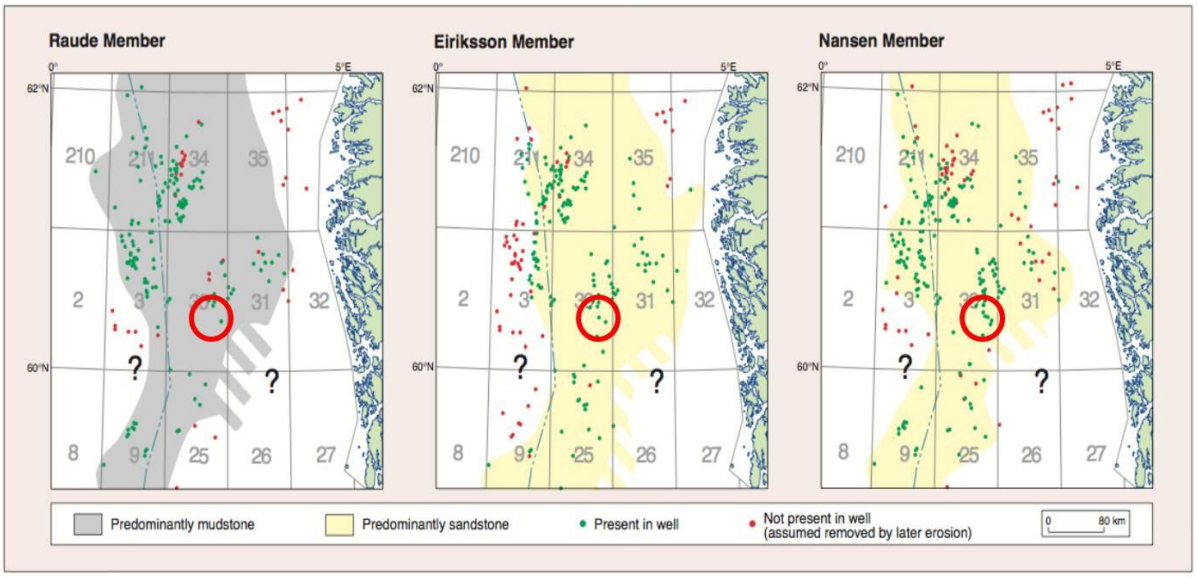

Figure 5: Maps showing the approximate aerial distribution of the three members that comprise the Statfjord Formation in the North Sea (from Millennium Atlas). The Oseberg South Field is highlighted with a red circle.

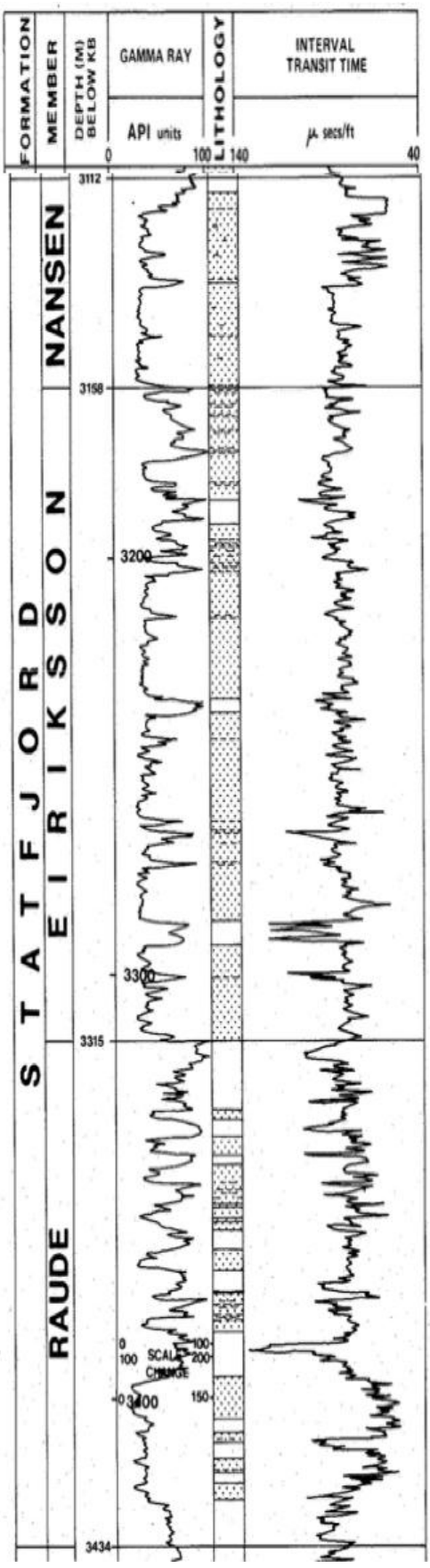

Figure 6: Type well (33/12-2) used by Deegan and Scull (1977) for definition of the Raude, Eiriksson, and Nansen Members of the Statfjord Formation.

The Raude Member was basally defined as the point where a transition occurs between the underlying shalier formation (Lunde Formation), and the massive sandstones of the Statfjord Formation (Deegan & Scull 1977). The boundary is also marked by the end of pervasive red beds that belong to the Lunde Formation, however, this boundary is only well defined in areas where the Statfjord Formation has fully developed (Deegan & Scull 1977). Outside of the areas in the Brent and Statfjord Fields, the lithological base of the Statfjord Formation becomes increasingly difficult to define. Petrophysically, where the Raude Member is well defined, its lower boundary can be defined on the gamma ray and sonic logs as a coarsening upward unit. Lithologically, the unit comprises alternating layers of sand and shale, with sand percentages ranging from 15 to 75 (Deegan & Scull 1977). The sandstones are generally fine to medium grained, poorly to moderately sorted, micaceous with a kaolinitic matrix, with occasional carbonaceous debris. The coarsening upward profile that is sometimes used to define the base of the Raude Member contains a mix of silty claystones, grey arkosic sandstones, and dolomitic limestones (Deegan & Scull 1977). Structures within the member include cross-bedding and scour and fill features, which the authors interpreted as deposited within a braided stream dominated, fluvial environment.

The Eiriksson Member is distinguished from the underlying Raude Member due to the pervasiveness of the sand bodies and ability to correlate from well to well, as opposed to the patchy sands that are associated with the Raude Member (Deegan & Scull 1977). In type well 33/12-2, the sandstones are on average five metres thick, while the interbedded shales are 2.5 m thick. The sandstones appear more mature, containing less kaolinite and mica than the Raude Member (Deegan & Scull 1977). Sands are medium to coarse grained, with granules, pebbles, and lignite fragments sometimes concentrated along the bedding foresets and within channel features (Deegan & Scull 1977). The top of the member contains marine fossils and glauconite, and the authors suggest deposition within a marginal marine environment.

The Nansen Member caps the Statfjord Formation, and is distinguished from the underlying Eiriksson Member by its prominent white sandstones with calcite cement, with the upper boundary marked by the presence of marine shales from the Dunlin Group (Deegan & Scull 1977). The carbonaceous material seen in the underlying formations is nearly absent, and marine fossils are contained within the shale beds. The member is best developed in the British sector, and towards the east, the sandstones beds grade into calcareous siltstones and shales (Deegan & Scull 1977).

Both Deegan & Scull (1977) and Vollset & Doré (1984) note that these divisions are only well defined in the area surrounding the type well, and further towards the east, or in areas where

the Statfjord Formation is significantly thinner than the type well, these differentiations become more difficult, or are nearly impossible to define. The stratigraphic chart from Ryseth (2001), Figure 7, illustrates this.

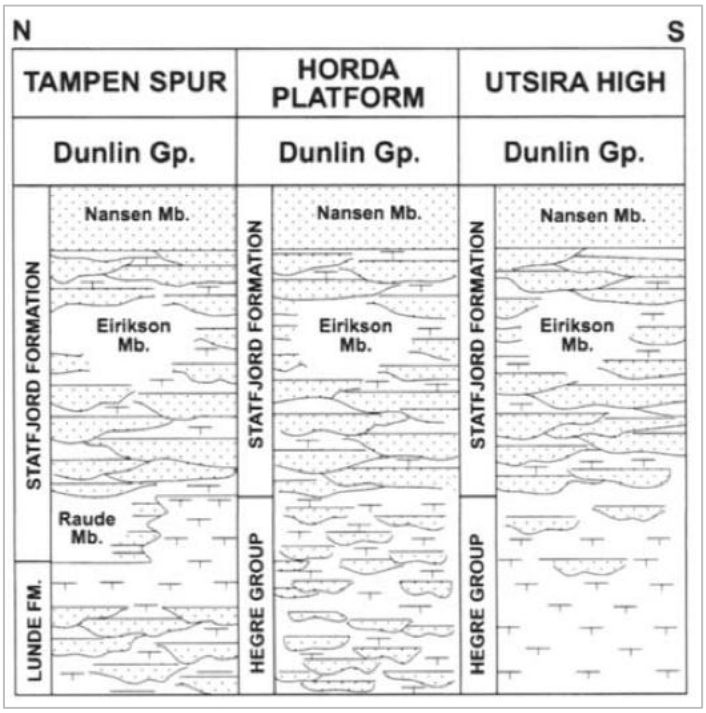

Figure 7: Stratigraphy of the Statfjord Formation in the Tampen Spur, Horda Platform, and Utsira High areas of the North Sea (Ryseth 2001).

Defining the lower part of the formation can sometimes be difficult, with the biostratigraphic dating aiding in defining the lower boundary. Underlying the Statfjord Formation, the Lunde Formation contains several fossils, including *Riccisporites tuberculatus*, which is of Rhaetian age, and is absent in the Statfjord Formation (Eide 1989, Ryseth 2001). Sinemurian age in the upper parts of the Statfjord is defined by the presence of C*orollina* and *Cerebropoolenites* (Raunsgaard and Lund 1980). The presence of *Liasidium variabile* in some parts of the Statfjord Formation reiterates a Sinemurian age, and also proves the presence of marine depositional conditions. From these observations, the Statfjord Formation is Rhaetian-Sinemurian age.

2.2 Regional Statfjord Sedimentology

The sedimentology of the Statfjord Formation was based mainly on the facies scheme by Ryseth (2001) that had been further refined from facies schemes and interpretations done by Ryseth & Ramm (1996) and Røe & Steel (1985). The project done by Ryseth & Ramm (1996) investigated the alluvial architecture and differential subsidence within the Statfjord

Formation. In the study, they developed a group of facies assemblages from the 61 cores available from the Tampen Spur and Horda Platform areas. Of the three assemblages that were created, Assemblages 1 and 2 belonged to the Eiriksson Member, while Assemblage 3 belonged to the Nansen Member.

The sharp basal surface of Assemblage 1 is typically overlain by conglomerates or coarse grained sandstones, and fine upwards. Structures within the unit may comprise planar laminated, cross-stratified, massive sandstones, ripple- and parallel-laminated sandstones (Ryseth & Ramm 1996).

The constituents of Assemblage 2 are significantly different from that of Assemblage 1. Assemblage 2 is a generally heterogeneous unit, with alternating layers of mottled red/grey mudrocks with fine to very fine beds of sandstone. Laminated mudrocks, rootlets, thin coal beds, and nodular carbonate cementations may also be encountered throughout the formation. The mottled mudstones and carbonate nodules are typical of the lower part of the formation, while the upper part contains the coal deposits. The trace fossil *Planolites* is found occasionally throughout both Assemblage 1 and 2 (Ryseth & Ramm 1996).

Assemblage 3 is seen in the Nansen Member, and reflects marine influenced structures that include lenticular laminae and symmetrical ripple laminations (Ryseth & Ramm 1996). Along with marine influenced structures, a wider variety of trace fossils exists, including: *Asterosoma, Palaeophycus, Teichichnus, Skolithos,* and *Planolites*. All but *Asterosoma* are generally found in brackish water environments (Pemberton *et al*. 1992), with *Asterosoma* more conducive to shallow marine settings (Seilacher 2007). In addition, a flooding surface can typically be seen at the base of this assemblage.

Ryseth & Ramm (1996) further assigned environmental interpretations to each of the assemblages. Figure 8 shows three interpreted log sections of each of the assemblages. The fining upward nature of the packages within Assemblage 1 is apparent, with thicknesses of the packages on the scale of three to six metres. The grouping of sedimentological features, namely cross-stratification, planar lamination, and ripple lamination, are characteristic of settings where tractional currents prevail (Ryseth & Ramm 1996, Miall 1992) and are typical of depositional within a fluvial setting (Collinson 1986).

Observations from Assemblage 2 indicated two different main depositional environments, reflecting a change in climatic conditions during the Late Jurassic and Early Jurassic (Ryseth & Ramm 1996). The lowermost section was dominated by red colouring and nodular carbonates, the latter of which representing an immature soil carbonate build-up. Overall, this represented an oxidizing environment that allowed for the development of soils (Ryseth

& Ramm 1996). The upper part of the formation showed the opposite type of environment, i.e., reducing. Mottled red and grey mud sediments were abundant, with some rootlets showing signs of the reducing conditions. These rootlets, along with sporadic coal seams help reiterate the reducing conditions, and show that the environment was conducive to soil production.

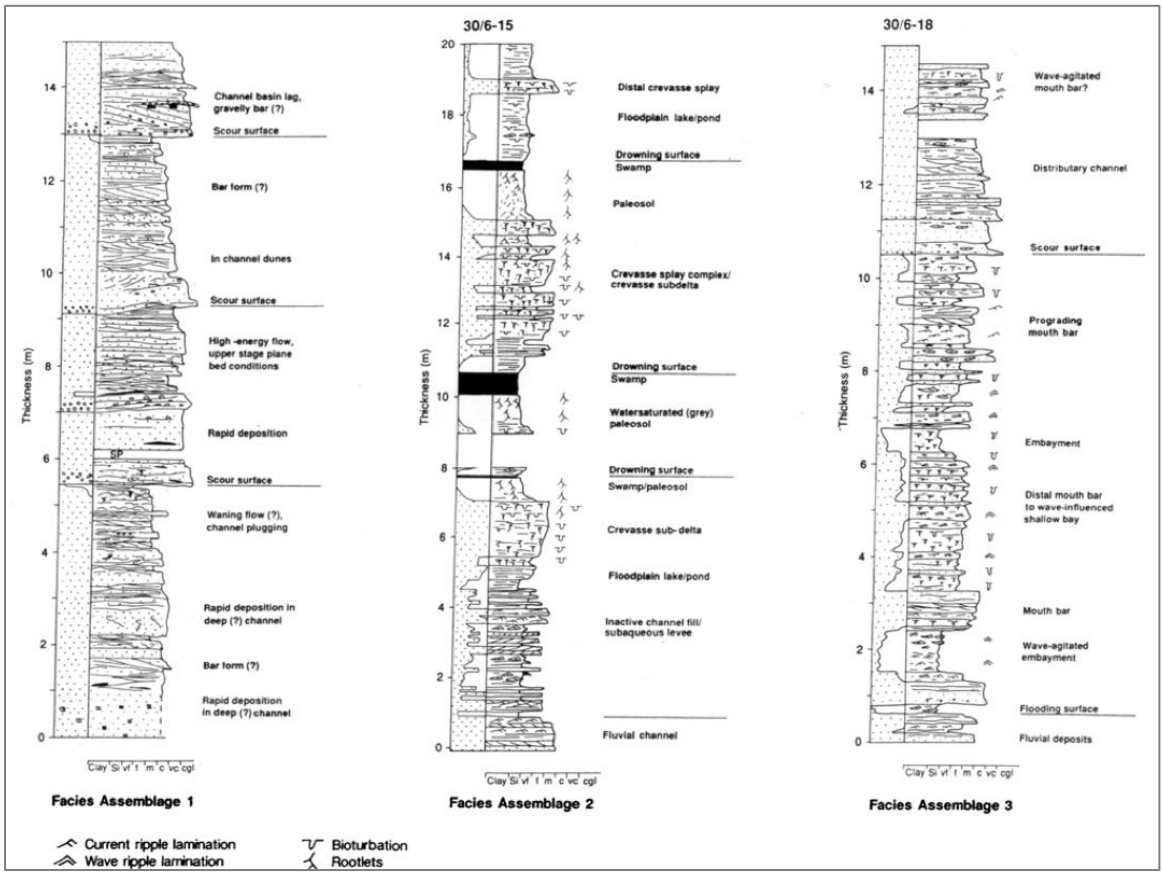

Figure 8: Core descriptions showing the different facies assemblages in wells on the eastern edge of the Viking Graben (from Ryseth & Ramm 1996).

Another typical relation that was seen in Assemblage 2 was the alternation of laminated mudrocks and rippled sandstone layers (Ryseth & Ramm 1996). This assemblage was typical in the upper parts of the Statfjord Formation, and is thought to represent the shifting of environments from standing water within lakes or ponds, and subsequent crevasse splay deposits (Ryseth & Ramm 1996).

Assemblage 3 contained evidence of deposition within marginal marine conditions. The presence of a flooding surface at the base, along with burrow diversity, and overall vertical coarsening led Ryseth & Ramm (1996) to define this interval as transitional marine between the underlying fluvial deposits of the Eiriksson Member, and the overlying marine rocks of the Dunlin Group. Sandier intervals within Assemblage 3 were thought to represent coastal

embayments or distributary channels and wave-influenced mouth bar systems depending on the grain size and sedimentary structures present (Ryseth & Ramm 1996).

In Ryseth (2001), more detailed interpretations of the assemblages were performed on cores from 23 wells in the Tampen Spur, Horda Platform, and Utsira High regions. A total of 10 lithofacies descriptions were made (Table 2), with their respective relationships aiding in the palaeogeographic reconstruction of the Statfjord Formation during deposition. Notes regarding some of the descriptions help in pointing out the most relevant details for interpreting the sediment relationships.

Table 2: Table showing a summary of lithofacies and associated interpretations (from Ryseth 2001).

Summary of lithofacies types identified in the alluvial part of the Statfjord Formation

Lithofacies	Description	Association [a]	Interpretation
Gm	Massive to crudely stratified, extraclast conglomerate. Sharply based, fining upwards into sandy lithofacies.	Shc, Sm	Channel bedload, lags, gravel bars.
Se	Massive to crudely stratified intraclast conglomerate. Sharply based, with siderite nodules, mudclasts and coal pieces.	Sm, Shc, Sx	Channel bedload, lags, scour fills.
Shc	Medium- to coarse-grained, pebbly sandstone. Crude to well-defined horizontal lamination, sets up to 250 cm.	Sm, Sx	Channel bedload/saltation load, upper stage plane beds.
Sm	Fine- to coarse-grained, massive/disorganized sandstone. Units up to several m thick, with water-escape structures, convolute lamination.	Shc, Sx, Shf	Channel saltation/suspension load. Rapid deposition associated with water escape.
Sx	Fine- to coarse-grained and pebbly sandstone. Sets/cosets of trough and planar cross-stratification. Sets commonly 10–40 cm, maximum 200 cm.	Shc, Sm, Shf	Lower flow regime dune/bar accretion by tractional currents.
Shf	Very fine- to fine-grained sandstone. Planar lamination.	Sr, Sm, Fl	Upper flow regime plane beds, channel suspension load, waning flow.
Sr	Unidirectional ripple lamination. Very fine- to fine-grained sandstone.	Shf, Fl	Lower flow regime current ripples. Interbedding with Shf indicates rapid shifts between upper and lower stage, waning flow.
Fl	Laminated, dark grey mudrocks, occasionally bioturbated, with sandy streaks and lenses. Pyrite and siderite nodules.	P	Low-energy suspension fall-out in standing water (lakes, ponds), weak agitation during floods.
P	Destratified mudrocks and sandstones. Red/brown, mottled to grey with carbonaceous rootlets. Calcrete (red-beds) and siderite/pyrite (grey-beds).	C	Palaeosols, reflecting oxidized (red) and reducive (grey) soil conditions.
C	Coal and carbonaceous mudrocks, units up to 75 cm, rootlets below.	Fl	In-situ peat and swamps, protected from clastic input.

[a] This column summarizes common vertical lithofacies transitions.

Ryseth (2001) noted that the quartzitic and lithic fragments of lithofacies Gm and Shc were thought to represent proximal deposition within the system. However, the widespread occurrence of this facies in all three study areas excluded them from contributing greatly in the palaeogeographic interpretation. Cross-stratified sandstones were represented as lithofacies Sx, and were subsequently divided into either planar-tabular cross beds, or sets and co-sets of troughs. This distinguishing feature helped determine whether deposition took the form of bars, sand waves, and sand flats, or migration of dunes in deep channels, respectively (Ryseth 2001, Miall 1992).

Ryseth (2001) interpreted the massive sandstones (Sm) as the expression of the quick dumping of sediments within a channel system. These sandstones are typically

interstratified with structured deposits and can be overlain with horizontally stratified sandstones. Together, these associations reflect rapid sediment deposition followed by high flow conditions (Ryseth 2001).

As mentioned in Ryseth and Ramm (1996), evidence of oxidizing conditions that led to the development of soil horizons was typical of the lower half of the Eiriksson Member. These horizons were expressed as red to grey paleosols, and associated calcrete nodules. Deposits of the upper half of the Eiriksson Member showed evidence of reducing conditions, and included grey mudstones with carbonaceous rootlets, and coal beds (represented by lithofacies C). Among the interstratified paleosols and coal beds of the upper Eiriksson Member were subaqueously deposited sandstones. Ryseth (2001) noted the importance of this observation as the bodies of standing water required for these deposits would have been more likely in the distal, and thus lower gradient areas of the fluvial system, which has implications in the palaeogeographic reconstruction.

The results from the authors are all reasonably similar in that it is agreed that the Statfjord Formation was deposited mostly within a terrestrial system, with eventual transgression that resulted in the massive sandstone deposits of the Nansen Member. The high variability of deposition within an alluvial system plays a critical role in successfully developing hydrocarbon fields, and the understanding of this variation will help to reduce, or better understand the risks involved with exploration in these areas.

2.3 Structural History

The North Sea is a structurally complex area that has undergone several phases of rifting throughout its history. The rift system in the North Sea, dominantly located in British and Norwegian territorial waters, is the location of many prolific oil fields, and comprises three main arms: the Moray Firth Basin, the Central Graben, and the Viking Graben. The Oseberg South field lies on the eastern edge of the Viking Graben, and the structural history focuses on this area. The Viking Graben itself is a roughly 40 km wide, mid-Jurassic-Cretaceous age feature, and is contained with a much wider sedimentary basin that is between 170 and 200 km in width (Færseth 1998).

The sedimentary basin of the northern North Sea is separated into three domains: north, central, and south (Figure 9). All three domains are defined in the east by the Øygarden Fault Complex, while the western edge is defined by the Alwyn-Ninian-Hutton (ANH) alignment in the northern domain, and by the Hild-Brent alignment in the central and southern domains (Steel & Ryseth 1990, Færseth 1996, Færseth & Ravnås 1998). Beyond

the western boundary of the sedimentary basin lies the Shetland Platform, while to the east of the basin lies the Norwegian mainland. As the Viking Graben is the most prominent structural feature within this sedimentary basin, it was thought that it was the only rifting event that had affected the basin. However, some authors in the 80s discussed the possibility of an earlier rifting event (e.g., Eynon 1981, Ziegler 1982, Wood & Barton 1983), which was confirmed by Badley *et al.* (1984), and subsequently assigned an age range of Permian-early Triassic (Steel & Ryseth 1990). In addition to the two rifting events, each had been followed by a phase of thermal cooling and subsidence of the crust, as described by Badley *et al*. (1984). It is believed that following the Permo-Triassic rifting, thermal cooling and subsidence of the crust continued to affect the basin for the next 70 Ma, nearly coinciding with the onset of the Jurassic extensional phase (ter Voorde *et al.* 1997a).

In addition to the major north-south oriented bounding features of the northern North Sea basin (the Øygarden Fault complex and the Hild-Brent alignment), similarly aligned major faults define parts of the basin. Several of these major features (e.g., the Oseberg, Brage, and Brage East Faults) are bounding faults of the Oseberg fault block, and have been discussed in detail in several publications (e.g., Badley *et al.* 1984, ter Voorde *et al*. 1997b, and Færseth & Ravnås 1998). These faults provide an important reference point for both the understanding of the interaction between the Permo-Triassic and Jurassic rifting events, and as a comparison between older published data, and the new interpretations from the OBC data at Oseberg South. These faults are seen in plan view in Figure 10, and in cross-section view in Figure 11.

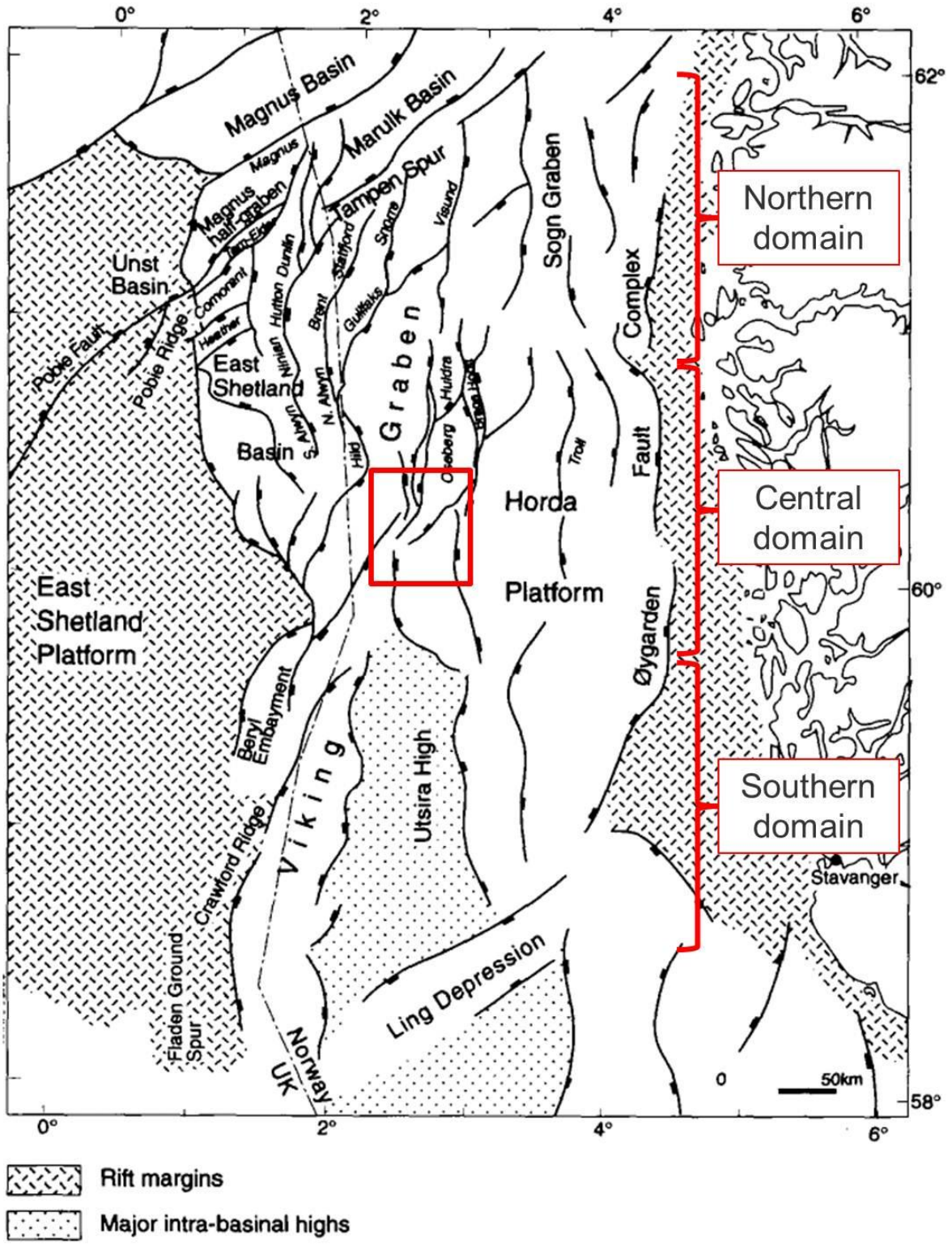

Figure 9: Structural elements of the northern North Sea, with the Northern, Central, and Southern domains of the Viking Graben highlighted. The approximate location of the Oseberg South field is highlighted with a red box (modified from Færseth 1996).

Evidence for the Permo-Triassic rift was discovered in regional seismic lines across the Horda Platform, which included the Oseberg field. The seismic lines showed a deep unconformity, below which a series of rotated fault blocks were visible (Badley *et al*. 1984). The deepest well at that time had not yet penetrated the unconformity, but dating from that well indicated that the unconformity must have an age older than the Early Triassic. Subsequent seismic interpretation by Steel & Ryseth (1990) confirmed a pre-Triassic age for the initiation for this early stage of rifting. More recent work by Færseth (1996) has better imaged the rotated fault blocks and subsequent syn-rift sediments (Figure 11). The figure, which shows a West-East cross-section over the Oseberg field, clearly shows the Hild-Brent alignment and Øygarden Fault Complex acting as the bounding features for this sedimentary basin. It is evident that the Permo-Triassic rifting event engaged the entire ~200 km width of the sedimentary basin, and that the axis of the graben was located east of the Oseberg Field under the present day Horda Platform. This stands in stark contrast to the Jurassic rifting event that created the Viking Graben, whose axis lies to the west of the Oseberg Field, and affected a mere 40 km width of the sedimentary basin. The size of the fault blocks also varies, with Permo-Triassic related fault blocks roughly 30-35km in width, and Jurassic fault blocks roughly 15-20km in width (Færseth & Ravnås 1998). Figure 10 shows that the Oseberg South Field lies in an area that was greatly affected by both of the rifting phases, making it a highly complex structure. However, the complexity also provides information that can help determine the timing of the faults within the field, and thus deduce the palaeogeography of the field during certain time periods.

Both Badley *et al*. (1984) and Steel & Ryseth (1990) recognized regional thickness trends within the Triassic and early Jurassic sediments. In particular, the thickness of these sediments increased towards the present-day Viking Graben, with the largest differences occurring across major faults. The thickness changes were thought to represent continued subsidence within the basin caused by thermal cooling after the Permo-Triassic rifting event had ceased (Badley *et al*. 1984, Steel & Ryseth 1990). In particular, Steel & Ryseth (1990) noted the most significant thickness change across a lineament that separates the Horda Platform from the Viking Graben. This lineament was not named, but is believed to represent the Oseberg Fault. Færseth & Ravnås (1998) agreed with this statement, although the timing of the Brage fault was still uncertain. The thickness differences in the Statfjord Formation across the Oseberg Fault change along the strike, with decreasing thickness variations moving southwards. The variations in thickness allowed Steel & Ryseth (1990) to postulate the relative post-rift subsidence rates during the 70 Ma after the cessation of Permo-Triassic extension, which likely influenced sedimentation patterns during that time. The overlying Dunlin Group also saw similar thickness trends across major faults,

further indicating the continuation of this post-rift thermal subsidence towards the beginning of the deposition of the Brent Group.

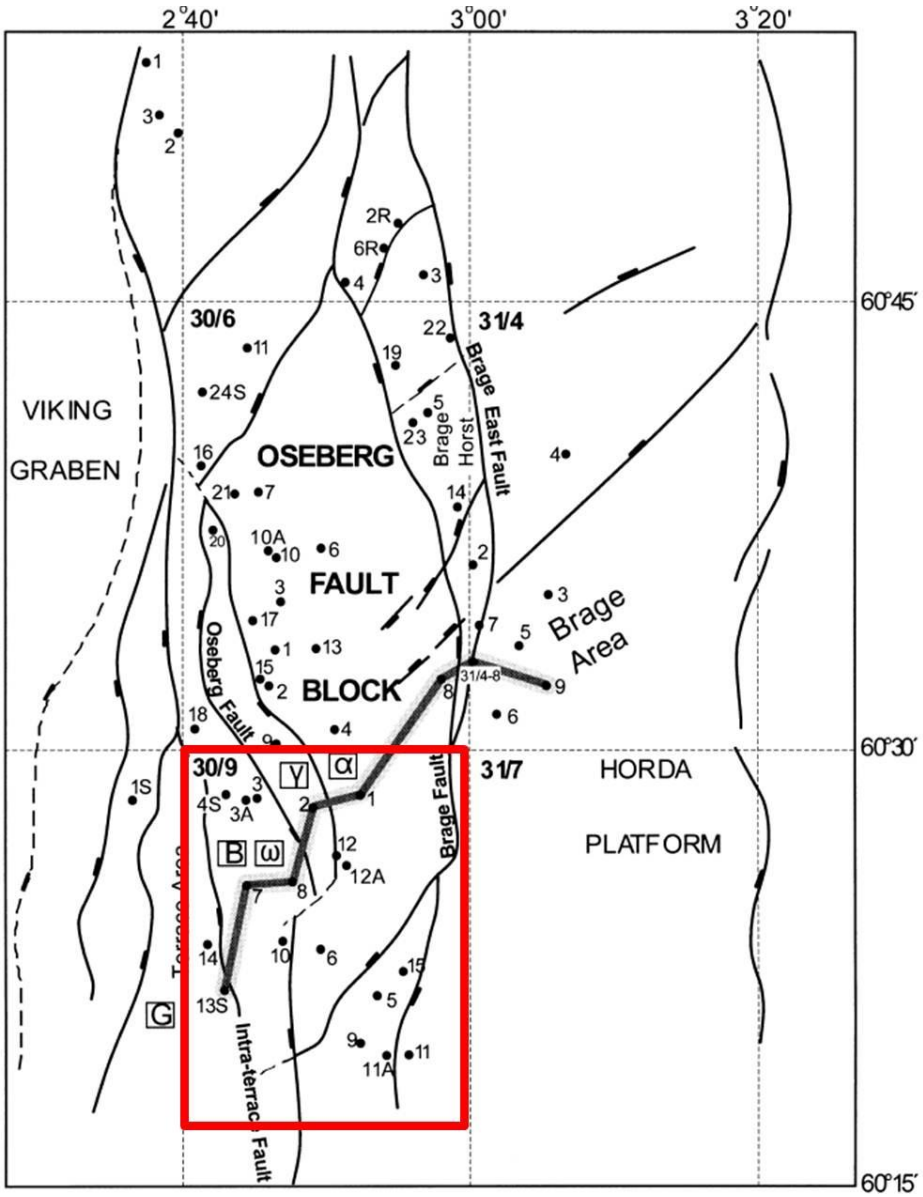

Figure 10: The Oseberg fault block, with the Oseberg South field highlighted in red. Well numbers refer to exploration wells, some of which are relevant to this thesis (from ter Voorde *et al*. 1997b).

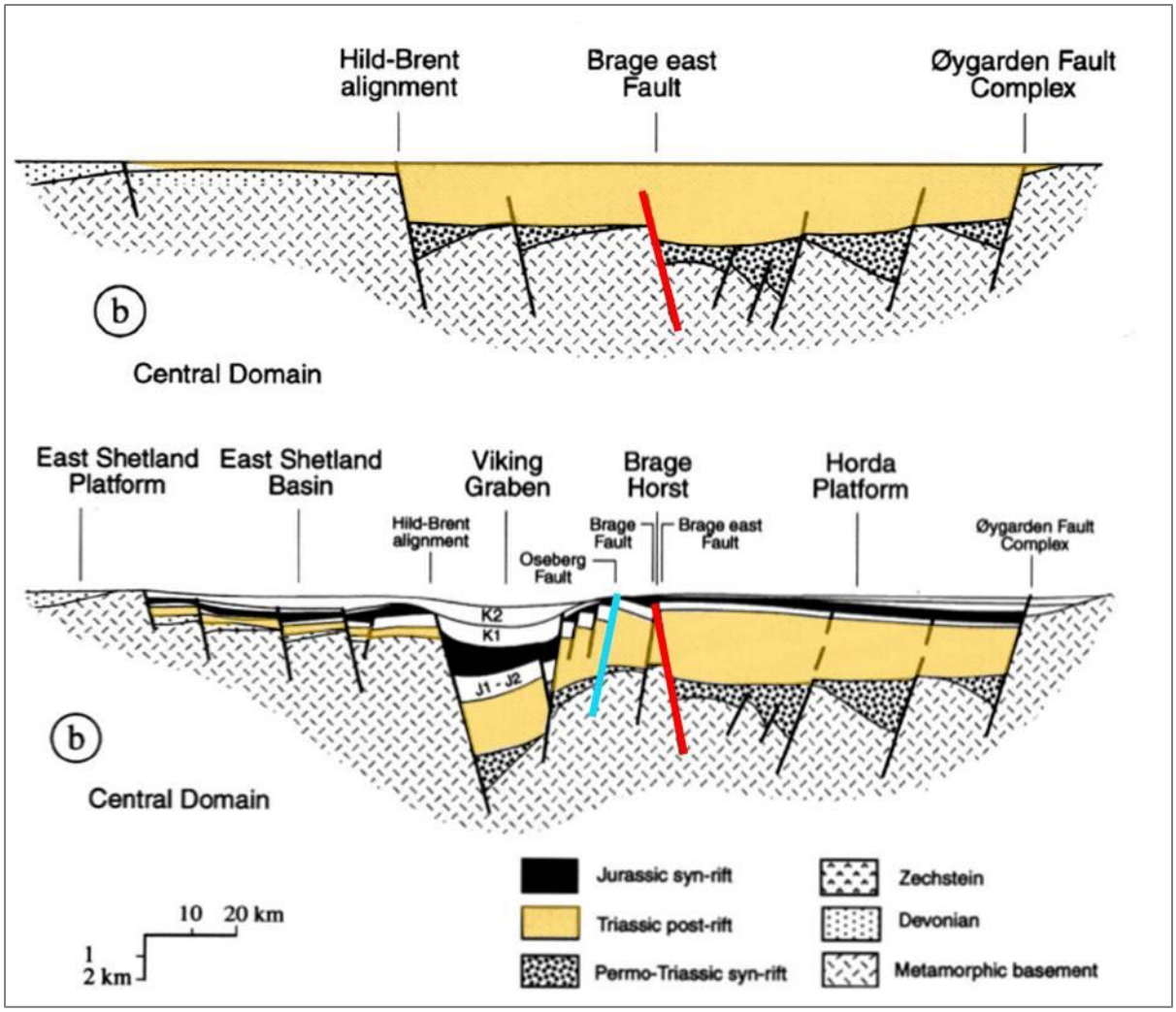

Figure 11: Schematic cross-sections show a summary of the main structural features of the northern North Sea sedimentary basin related to the Permo-Triassic rifting (top) and the Jurassic rifting (bottom). Triassic post-rift sediments that include the Statfjord Formation are highlighted in orange, and the major faults Brage East and Oseberg are highlighted in red and blue, respectively. Figure modified from Færseth (1996).

Adding complexity to the fault interpretations at Oseberg South, the dip directions of the major faults swing from the west towards the east at the southern end of the field, and are visible on the OBC seismic in the K structures. An important part of this project will be the comparison between the published literature and the interpreted data at Oseberg South. It is hoped that higher quality data will provide additional insight into the understanding of the structural evolution of the Oseberg South field area, which could perhaps have implications into the structural evolution on a more regional scale.

The rifting event associated with the formation of the Viking Graben began in the mid-Jurassic, and lasted approximately until the Early Cretaceous (e.g., Graue *et al.* 1987, Badley *et al.* 1988, Helland-Hansen *et al.* 1992, Johannesen *et al.* 1995, Ravnås *et al.*

1997, Færseth *et al.* 1997), with associated post-rift subsidence. This event is referred to as the mid-Jurassic rifting event throughout the remainder of this report, with the name referring to the onset of rifting, and not necessarily when it may have been most active. A cross-section across the Oseberg Field in Figure 11 shows the resulting fault configuration from this rifting event, with the Oseberg and Brage East Faults highlighted in blue and red, respectively. Numerous west-dipping faults puntuate the Oseberg Field, with many of the faults penetrating beyond the Statfjord Formation level. Færseth (1996) suggested that many of the major faults associated with the mid-Jurassic rifting were not initiated during this events, but were a consequence of the basin configuration that has resulted from previous rifting events. This implies that many of these major, west-dipping faults were initiated during the post-rift period following Permo-Triassic rifting. However, although initiated prior to the mid-Jurassic rifting, the field did not arrive in its present configuration until Kimmeridgian time in the Upper Jurassic (Færseth & Ravnås 1998, Ravnås *et al.* 2000). Additional evidence of reactivation was also seen on some of the major faults during this time (Færseth 1996).

3. Reservoir Modelling

The purpose of a reservoir model is to visualize and understand the behaviour of the reservoir throughout the development and production of the field. These models contain a large amount of data, including: fault and horizon interpretations from seismic, porosity and permeability values, net to gross sand ratios, fluid contacts, and facies interpretations, among others.

A logical process is used when building the model, which consists of structural and property modelling, with further modelling in each category.

- Structural modelling
    - Horizon modelling
- Property modelling
    - Facies modelling
    - Petrophysical modelling

Furthermore, the results from these processes are used to help determine the in-place volumes in the reservoir, and can be further used and refined during production of the field for better understanding of reservoir behaviour. In this thesis, structural and horizon modelling is performed, forming the basis of a complete reservoir model should this be desired in the future. For this project, IRAP RMS (or simply RMS) was used to complete the structural and horizon modelling.

The data used in the input into the modelling formed the bulk of the work for this project, and from it came improved understanding about the Statfjord Formation from a structural perspective, and also about the limitations of the data currently in use. The inputs for the model are split into two main categories, namely geological, which helps with defining the horizons, and geophysical, which helps with both the structural understanding and distribution of the horizons, as discussed below. The names and locations of the main structural blocks/areas that are referenced in this thesis are presented in a map in the Appendix.

4. Geological Input

Several sources of data were available to help refine and understand the geology of the Statfjord Formation at Oseberg South. As mentioned earlier, there are only three wells that fully penetrated the Statfjord Formation through to the Triassic Lunde Formation, so the interpretations have limited scope. Despite this, the results from the interpretations were consistent with regional findings from the literature regarding depositional environment of the Nansen Member of the Statfjord Formation across the Viking Graben. Petrophysical logs, core data, and biostratigraphic data were used to help define the geological understanding and horizon properties across the Oseberg South field.

4.1 Stratigraphic Zonation & Biostratigraphy

Evaluating the stratigraphy of the Statfjord Formation within the Oseberg South Field can be difficult due to the poor petrophysical log coverage that is available, however, biostratigraphic analysis was performed for most of the exploration wells. As most of these wells at Oseberg South fail to penetrate deeply into the Statfjord Formation, the biostratigraphic data was only used as a stratigraphic tool in three of the wells: 30/9-5S, 30/9-3A, and 30/9-24T2, all of which penetrated to the Triassic Lunde Formation (Figure 12). Discussions regarding biostratigraphic zonation in the Statfjord Formation revealed that previous interpretations have been especially difficult in the formation as the lithologies and palaeoenvironments of deposition give poor recovery of long ranging fossils (Valerie Charnock, per. comm. 2012). Regardless, the data was examined in an attempt to extract as much useful information as possible to aid in correlations and stratigraphic zonation.

The data was obtained from biostratigraphic reports prepared for Norsk Hydro AS (30/9-5S, 30/9-3A) and StatoilHydro (30/9-24T2) by Fugro Robertson Ltd. (formerly Robertson Research International Ltd). The reports are all now Statoil ASA internal documents.

The Statfjord Formation is divided into three members (the Raude, the Eiriksson, and the Nansen), however, the Raude Member is either absent, or is too difficult to distinguish from the other members due to its conformable nature at Oseberg South. Although these stratigraphy definitions have been published by the Norwegian Petroleum Directorate (see Deegan & Scull 1977 and Vollset & Doré 1984), Statoil also uses additional internal definitions that are helpful in both a seismic context, as well as in determining the overall deposition of the formation. The biostratigraphic information available has also further refined some of these interpretations, and ensures consistency of the picks where the information is available. It may also be helpful in better understanding how the formation

was deposited and perhaps the length of time it took for different parts of the formation to be deposited. Understanding this timing may also provide further insight into the timing of fault movement throughout the deposition of the formation.

The proximity of wells 30/9-24T2 and 30/9-3A in relation to one another makes correlation between the two based on petrophysical log properties relatively simple, however, correlating these markers with 30/9-5S in the J structure proved to be more difficult. In addition to the approximate 14 km distance between the wells, the Statfjord Formation at 30/9-5S is nearly 200 m thinner than the other two wells, and has markedly different petrophysical log characteristics (Figure 15).

From a biostratigraphic perspective, the quality and confidence of a time interval based on palynology or micropalaeontology changes depending on the sampling method. In reports, the biostratigraphic information is given based on first occurrence, and last occurrence, as read from the bottom of the well upwards (i.e., older to younger). The three main methods of obtaining these samples (drill cuttings, sidewall cores, and full core) affect the degree of confidence with which a first or last occurrence is noted, with full core providing the highest degree of certainty. When obtaining samples from drill cuttings, the circulating mud increases the uncertainty as to which interval the sample belongs to. Generally, the last occurrence of a fossil has a higher degree of certainty than the first occurrence as the sample for the first occurrence may have come from any of the zones located above its correct interval.

4.1.1 Formation Tops

Roughly half of the wells at Oseberg South had consistent formation tops picked, all of which used the naming convention from the Oseberg Main Field. Literature studies and reports from the Norwegian Petroleum Directorate report that the Statfjord Formation formally contains three members, namely, the Nansen, Eiriksson, and the Raude, with the latter indistinguishable in the Oseberg South Field. As Figure 13 shows, Statoil chooses to divide the formation into Lower, Middle, and Upper portions, with the Middle Statfjord providing a good seismic reflector across much of the field, as well as indicating what is thought to be a regional geological and correllable event. Overall, the tops picked in the Statfjord Formation across the Oseberg South field are: the top Statfjord, Eiriksson, Middle Statfjord, Lower Statfjord, and Base Statfjord (top Lunde Formation), as illustrated with well 30/9-3A in Figure 13.

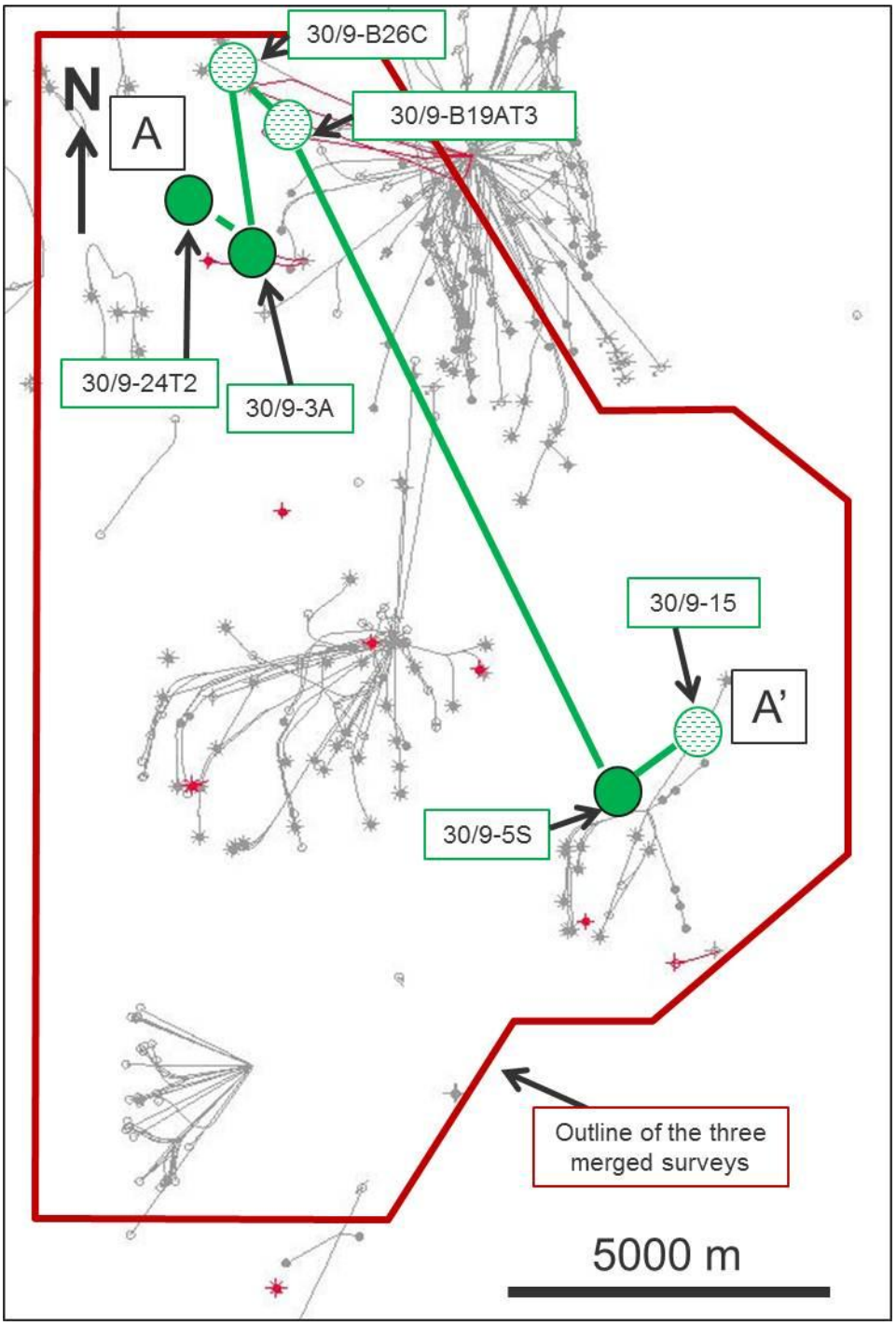

Figure 12: Six wells were used in the cross section, and three (solid green circles) were used in more detailed biostratigraphic analysis.

4.1.1.1 Top Statfjord

The top Statfjord Formation is a relatively simple and consistent pick across the field, and was made in all of the exploration wells that were available. It is defined as the sharp transition between the underlying marine sands of the Nansen Member, and the overlying marine shales of the Dunlin Group.

4.1.1.2 Eiriksson

The Top Eiriksson Member marks the transition between the underlying fluvial deposits that characterize much of the Statfjord Formation, and the overlying marine-influenced deposits of the Nansen Member. The Top Eiriksson Member has been picked in 12 of the wells, however, the degree of uncertainty is quite high in four of the wells as the logs end at or near where the Top Eiriksson Member is expected. In these wells, a spike in the Gamma Ray logs may be misinterpreted as the Top Eiriksson Member when it could in fact be a thin shale layer that is sometimes seen within the Nansen Member. In wells with deeper penetration into the Eiriksson Member, the shale marking the top of the member is consistently at least 10 m thick, and up to 20 m in some locales.

4.1.1.3 Middle Statfjord

The Middle Statfjord Formation marker is one of the more difficult tops to pick on petrophysical logs, and is best supported by lithological data from drill cuttings. On the Omega structure, the horizon is a roughly 20 m thick shale zone that can be rich in coal, and in most areas is underlain and overlain by sand sequences. This is not consistent in all structures though, as can be seen in well 30/9-3A (Figure 13). This pick becomes increasingly difficult over the J structure.

4.1.1.4 Lower Statfjord

This zone marks the base of the Middle Statfjord Formation, and represents the fluvial deposits that characterize much of the Statfjord Formation. This zone is highly variable throughout the Oseberg South Field, but is often picked as the first sand rich layer below the coaly Middle Statfjord Formation. However, in some areas, the top of this zone is shale rich, and needs to be distinguished from the overlying Middle Statfjord Formation based on lower coal content. This zone has been picked in six wells across the field.

4.1.1.5 Base Statfjord (top Lunde Formation)

The boundary between the Lunde Formation and overlying Statfjord Formation is believed to be transitional, representing a change from the shalier Lunde Formation to the sandier/fluvial Statfjord Formation. In the Oseberg South field, the Base Statfjord Formation has been picked as the boundary between the heterogeneous Statfjord Formation (alternating sand and shale packages), and the blocky shale layer at the top Lunde Formation. This pick has been made in three wells in the field, and on both the Omega and J structures, the boundary is quite consistent in the petrophysical logs.

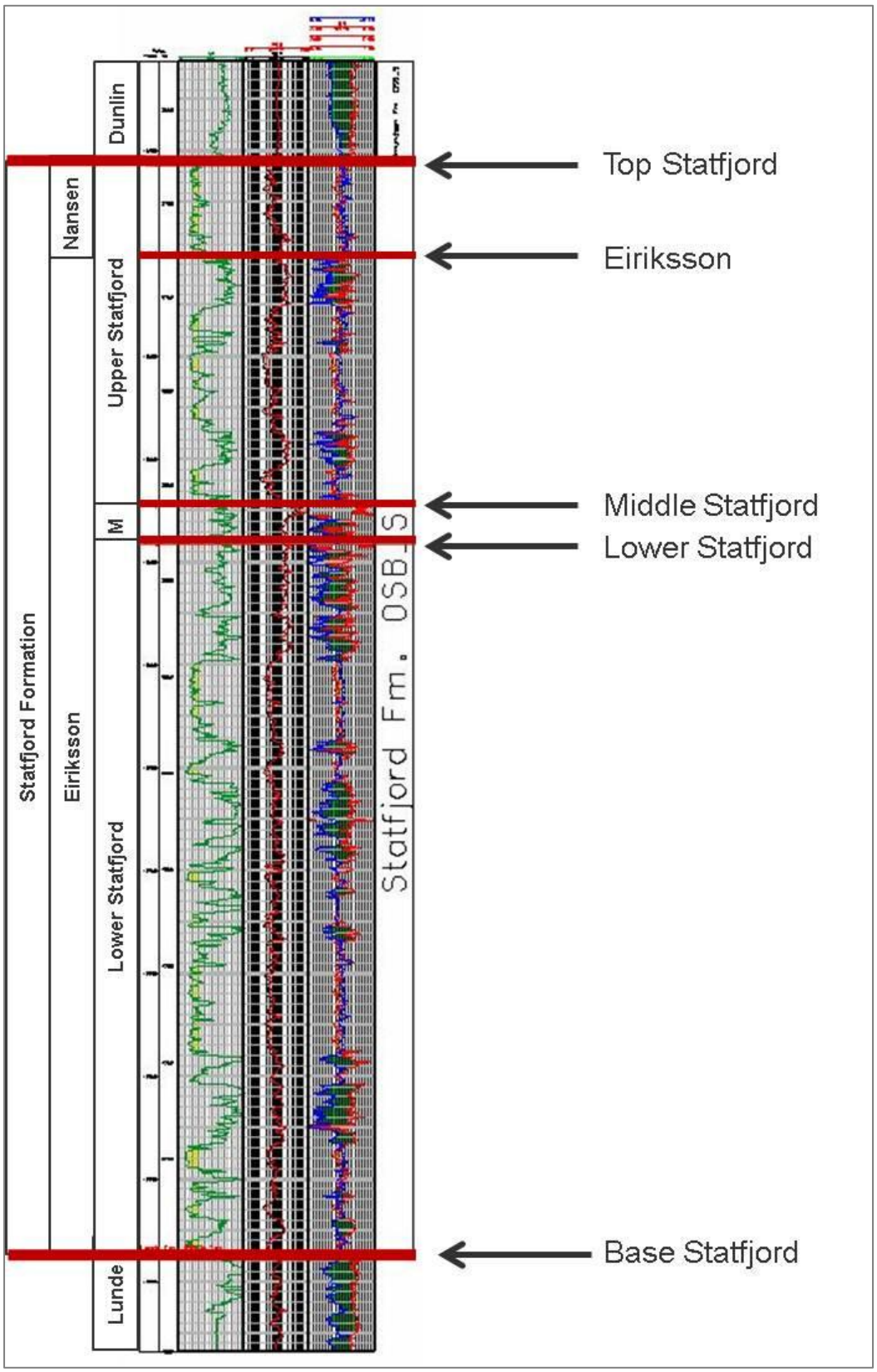

Figure 13: Petrophysical logs from well 30/9-3A showing the main formation tops picked in red. From left to right, the logs present are Gamma Ray (green; scale 0-150), Resistivity (red; scale 0.2 - 200), Neutron porosity (blue; scale 0.45 - -0.15), and Density (red; scale 1.95-2.95).

4.1.2 Biostratigraphy of individual wells

4.1.2.1 Well: 30/9-24T2

The biostratigraphic information from this well is the most recent dataset that exists for the Statfjord Formation in the Oseberg South field, having been completed in 2010. The Triassic Hegre Group (Lunde Formation) and has been cautiously defined biostratigraphically with the first abundant occurrence of *Ricciisporites tuberculatus*, which corresponds well to the transition from shale to mixed sand and shale that petrophysically defines the Top Lunde Formation (see Appendix for a biostratigraphic summary of each well). Within the Statfjord Formation, the top of Triassic interval is defined by the last common occurrence of *Ricciisporites tuberculatus* at a depth of 3636 mMD, which also coincides with an abrupt decrease in Gamma Ray readings from a mix of sand and shale towards a much cleaner section of sand.

The next biostratigraphically significant event occurs with the first appearance of *Microreticulatisporites fuscus* at around 3460 mMD, which is typical of the early Sinemurian. Discussions with Valerie Charnock revealed that determining the top Hettangian (i.e., early Sinemurian) has always been difficult to determine in the Statfjord Formation, but using some of the main fossils can help narrow the interval where this stage may end (Figure 14). In the absence of major fossil groups, the last occurrence of rare *Ricciisporites tuberculatus* provides confirmation that one is within the Hettangian. In this well, this was not encountered, and so the top Hettangian was placed just below the first occurrence of *Microreticulatisporites fuscus*, which is typical of the early Sinemurian. There is little of biostratigraphic significance near the Middle and Lower Statfjord well picks. The first occurrence of *Liasidium variable* occurs at 3228 mMD, which is indicative of marine conditions that characterize the Nansen Member. This coincides with the top of the Eiriksson Member in this well (3232 mMD), defining the end of the alluvial depositional conditions within the Statfjord Formation. The last occurrence of *Liasidium variable* occurs at 3186 mMD, roughly in the middle of the Nansen Member, and is indicative of late Sinemurian time (Statoil Internal Data 2012).

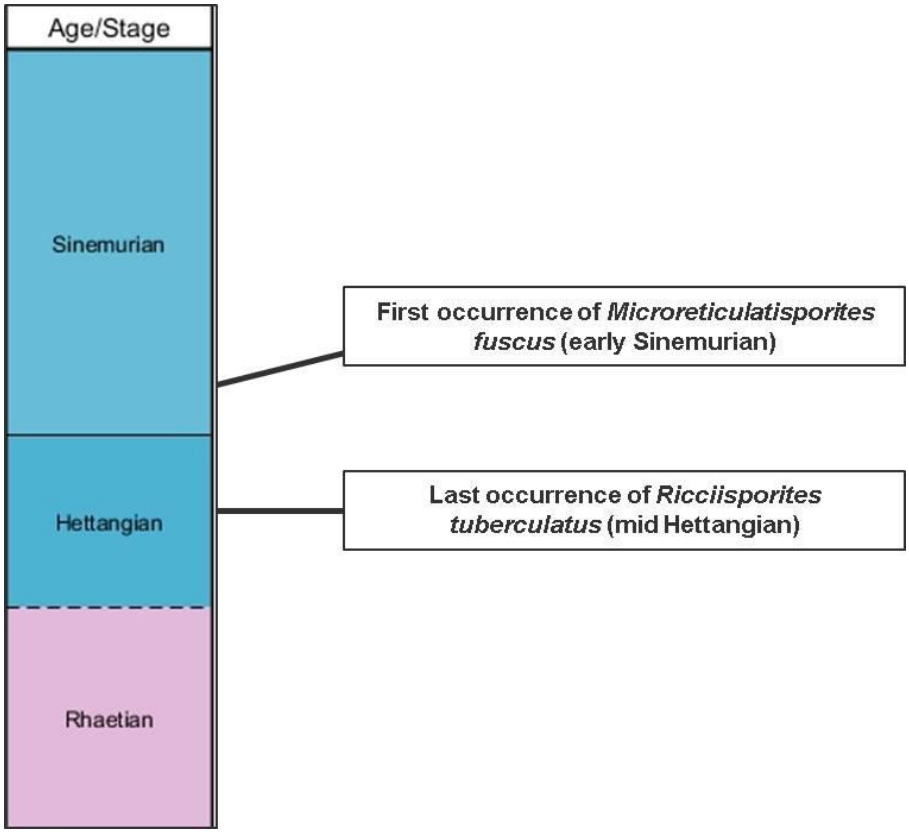

Figure 14: Schematic demonstrating the uncertainty regarding placement of the top Hettangian. As a result of few good palynological markers at top Hettangian, only a range can be given. Time scale created in Time Scale Generator software (Statoil).

4.1.2.2 Well: 30/9-3A

This well is located roughly 2,1 km SE of 30/9-24T2, and biostratigraphic analysis was completed in 1984. The petrophysical correlations between this well and 30/9-24T2 are generally quite consistent and easy to make, and has shown similar results in biostratigraphy.

The report (Miles *et al.* 1984) did not state the abundance of *Ricciisporites tuberculatus* within the well, which aided in determining both the Top Triassic and Top Lunde Formation in 30/9-24T2. Instead, the Top Lunde Formation was picked based on petrophysical log correlation, and the last occurrence of *Ovalipollis ovalis* at 4172 mMD was used to define the Top Triassic at 4248 mMD. This fossil is not commonly used to define this age group (Valerie Charnock, per. comm. 2012); however, the location of this fossil occurrence correlates well with the corresponding petrophysical logs from 30/9-24T2. *Microreticulatisporites fuscus* was not encountered to define the lowermost Sinemurian age, however, the last rare occurrence of *Ricciisporites tuberculatus* was encountered at 3960

mMD, indicating the highest known palynological evidence for Hettangian time in this well. This interval correlates reasonably well with the placement of the Top Hettangian in well 30/9-24T2, and shows that the isopach thickness from the Lower Statfjord Formation marker to the Top Triassic is roughly the same in both wells.

Miles *et al*. 1984 stated that *Liasidium variable* occurred at 3536 mMD, but did not note the first or last occurrence. This depth is located well into the overlying Dunlin Group, however, the well's proximity to 30/9-24T2 and good correlation quality make it likely that *Liasidium variable* was also present in the Nansen Member interval in well 30/9-3A. No other significant palynological information was recorded in this well.

4.1.2.3 Well: 30/9-5S

This well is located on the J structure, approximately 14km SE from well 30/9-3A, and shows significant differences in log character, as well as Statfjord isopach thickness from the previous two wells located on the Omega structure (Figure 15).

The Top Lunde Formation was picked on petrophysical logs in this well based in the first abundant occurrence of *Ricciisporites tuberculatus* at roughly 2942 mMD, with the Top Triassic placed at 2873 mMD as indicated by the last abundant occurrence of *Ricciisporites tuberculatus* that characteristically caps the Triassic.

The Top Hettangian has been difficult to place with any certainty in this well. *Microreticulatisporites fuscus* was not encountered, but the last rare occurrence of *Ricciisporites tuberculatus* was seen at 2849 mMD, indicating presence within the Hettangian. The last occurrence of *Trachysporites fuscus* was also mentioned in the report, which is not thought to be present far above the Top Hettangian. The actual depth was not reported, but interpretations from the report (Bysveen & van Veen 1986) have placed the Top Hettangian at 2730 mMD. There was a high degree of uncertainty in where to place the top of the Hettangian in this well, and the most that can be said that it likely lies somewhere between 2730 and 2849 mMD. As seen in Appendix, the Top Hettangian was placed at 2782 mMD based on possibility a possible correllable surface in the petrophysical logs, and assumes that this correllable surface represents a timeline. The high degree of uncertainty in the placement of the Top Hettangian creates difficulties when making interpretations, however, even with this uncertainty, the possible Hettangian interval is still thinner than those seen in the wells on the Omega structure. These thickness variations may help in understanding the relative rates of subsidence and movement of faults during this time. As with the previous two wells, *Liasidium variable* was encountered throughout core from the

Nansen Member with its first appearance at 2630 mMD, roughly corresponding to the Top Eiriksson Member.

4.1.2.4 Biostratigraphic Zone Limitations

There are several limitations and points to take note of regarding interpretations from biostratigraphic analysis. The small database of information within the field means that the interpretations are very preliminary, and could change significantly with the addition of more data. It is important to note that a common timeline may not correspond to a common log signature within the petrophysical well data, however, at Oseberg South, the timeline for the Top Triassic appears to correlate well with the petrophysical log data. In comparison, the timeline for the Top Hettangian is very uncertain, and could not be used confidently for correlation.

4.2 Biostratigraphic & Zonation discussion

A stratigraphic cross-section was made (Figure 15; Datum = Top Statfjord Formation) that included the three wells with biostratigraphic analysis, as well as three other wells that penetrated into the Middle and Lower Statfjord Formation levels. The three additional wells are 30/9-B26C and 30/9-B19AT3, located on the Gamma structure, and 30/9-15 located on the J structure. The wells located on the Gamma structure did not have any biostratigraphic analysis performed, and while the 30/9-15 well did, no Hettangian sediments were encountered.

The logs in the cross-section are all in true vertical depth, which may present problems when making interpretations regarding thickness trends across the field. However, the three wells with biostratigraphic data penetrated the Statfjord Formation at a vertical or nearly vertical orientation, and the dip of the fault blocks is low enough that with these large thicknesses, the differences between the true vertical depth and the true stratigraphic thickness were not enough to greatly influence the interpretations.

An obvious feature from the cross section is roughly 200 m decrease in the Statfjord Formation thickness between the Omega structure, and the well on the J structure. In combination with the approximate time correlations from the biostratigraphy, a zonation was created across the cross-section in order to make possible inferences about relative subsidence rates during certain time intervals.

The preliminary zonation is listed below:

- Zone D: Interval from Top Eiriksson Member to Top Statfjord Formation
- Zone C: Interval from Top Middle Statfjord Formation to Top Eiriksson Member
- Zone B: Interval from Top Triassic to Top Middle Statfjord Formation
- Zone A: Interval from Top Lunde Formation to Top Triassic

Zone A was the lowermost interval, which represents deposition of the Statfjord Formation during the Late Triassic time. The biostratigraphic and petrophysical correlations in this zone were common across the field, indicating that this zone was deposited within the same timeframe. The zone shows a relatively consistent thickness across these three wells, which are separated by two major faults (the Oseberg and Brage Faults) within the field. This indicates that during deposition of the early Statfjord Formation, the area was tectonically quiet, and not yet influenced by these two large faults. Steel & Ryseth (1990) stated that the early Statfjord appears to have been deposited in a broad alluvial plain, and the correlation data presented appears to support this, despite the small sample size.

Making timing inferences from the remaining data within the wells are difficult due to the challenges encountered in determining the Top Hettangian (interpretations shown in black in Figure 15). In the absence of a Hettangian timeline, the Middle Statfjord Formation was used as it is believed to have represented a regional event. Both the Nansen Member and Dunlin Group represented the transition between alluvial and mixed-marine, and to fully marine conditions, respectively, and so their correlative surfaces likely represent different time frames across the entire basin as transgression progressed. On a smaller scale though, these surfaces can be assumed to represent the same timeline. Thus, throughout the Oseberg South Field, the Top Triassic, the Middle Statfjord Formation, and the Top Eiriksson Member have been used as timelines.

The top of Zone B was placed using the Middle Statfjord Formation as a regional marker due to its aerial extent and good correlation properties. Based on this assumption, the thickness difference in Zone B from the wells on the Omega structure and the J structure is quite evident, with the latter showing a roughly 120m decrease in thickness. This difference suggests that the Oseberg Fault, Brage Fault, or both, were active during the deposition of the formation. Full penetration of the Statfjord Formation within the Gamma structure might provide more information regarding fault movement. Another feature of the zone is the stark contrast in the heterogeneities in the petrophysical logs. The base of Zone B in wells 30/9-24T2 and 30/9-3A show roughly 50 m of clean sand, while the remainder of the overlying section shows frequent alternations between sand and shale. In contrast, nearly the entire

section of Zone B in 30/9-5S consists of nearly homogenous sand with very little shale. Overall, the thickness of Zone B in the Omega structure is nearly twice that seen in the J structure.

Zone C is characterized by heterogeneous sand and shale packages and overall shows slight thickening from the J structure towards the Omega structure. The thickness difference in Zone C from the Gamma structure and the J structure was quite minor, with both around 85 m thick, while Zone C in the Omega structure averaged around 120 m thickness. Compared to Zone B, the smaller thickness differences from the Omega to J structure seem to indicate that the relative subsidence rates, and thus relative movement on the fault(s) was lower during this time period. The addition of two wells on the Gamma structure into the correlation provides inside into the movement on the Brage Fault. The similarity in thickness of Zone B in the J and Gamma structures suggests that the Brage Fault may not have been active during this time, and movement solely in the Oseberg Fault was responsible for the thickness differences.

Zone D is generally a thin zone that represents the Nansen Member, and it shows a consistent increase in the thickness from the J structure to both the Gamma and Omega structures. The difference in thickness is even quite large within the Omega structure, with wells 30/9-24T2 and 30/9-3A showing thickness of 80 and 44m respectively, a considerable change considering the mere 2.5 km distance between the wells. The change is conspicuous, however, the data has been double checked and this large thickness difference appears to be true. The source of such a dramatic change is unknown, but the 30/9-24T2 well is located close to the large Omega Fault, and it is possible that minor faulting near the western edge of the Omega structure has caused some overthickening in this area. Overall, the data suggests that both the Brage and Oseberg Faults were active during deposition of Zone D.

The timelines and correlations used in the wells seem to indicate that differential subsidence occurred on the faults throughout deposition of the Statfjord Formation, and that these subsidence rates changed with time.

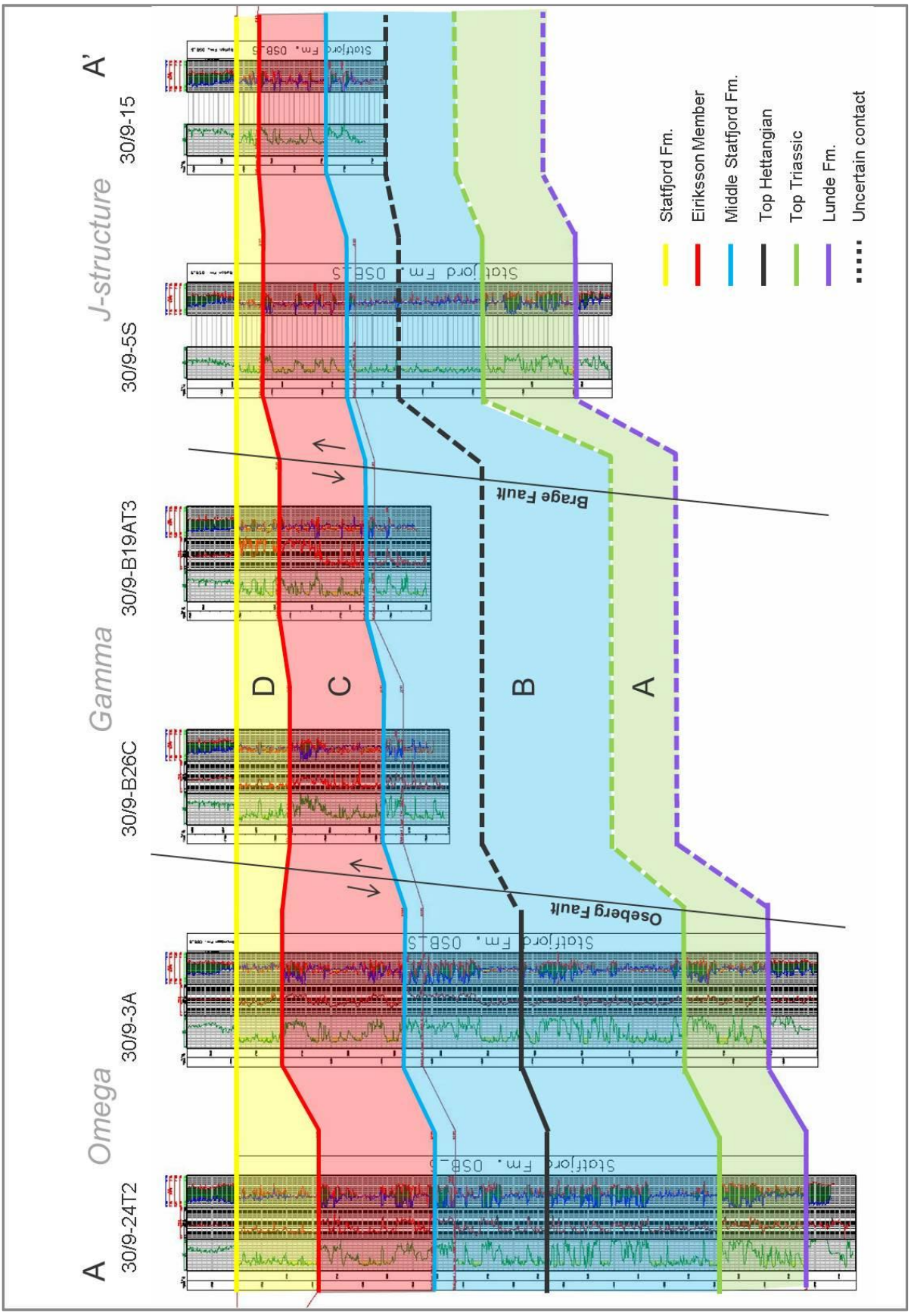

Figure 15: West to East stratigraphic cross-section (datum = Top Statfjord). See Figure11 for location of line of section.

4.3 Core Descriptions

Only three cores are available at the Statfjord Formation level at Oseberg South, from wells 30/9-5S, 30/9-4S, and 30/9-16 (Figure 16, Table 3), with the latter located south of the full fold data of the OBC seismic. The eight metres of core available from well 30/9-4S was mostly rubble, and was not logged for sedimentological purposes. Full core descriptions of the remaining two wells were digitized using the program WellCAD and can be seen in Figures 18-21.

Table 3: Cored wells within the Statfjord Formation, their stratigraphic location, and depth intervals.

Well	Interval	Depth Range (mMD)
30/9-5S	Nansen	2608 - 2626,2
30/9-16	Nansen	3459 - 3486,2
30/9-4S	Eiriksson	4268 - 4276,3

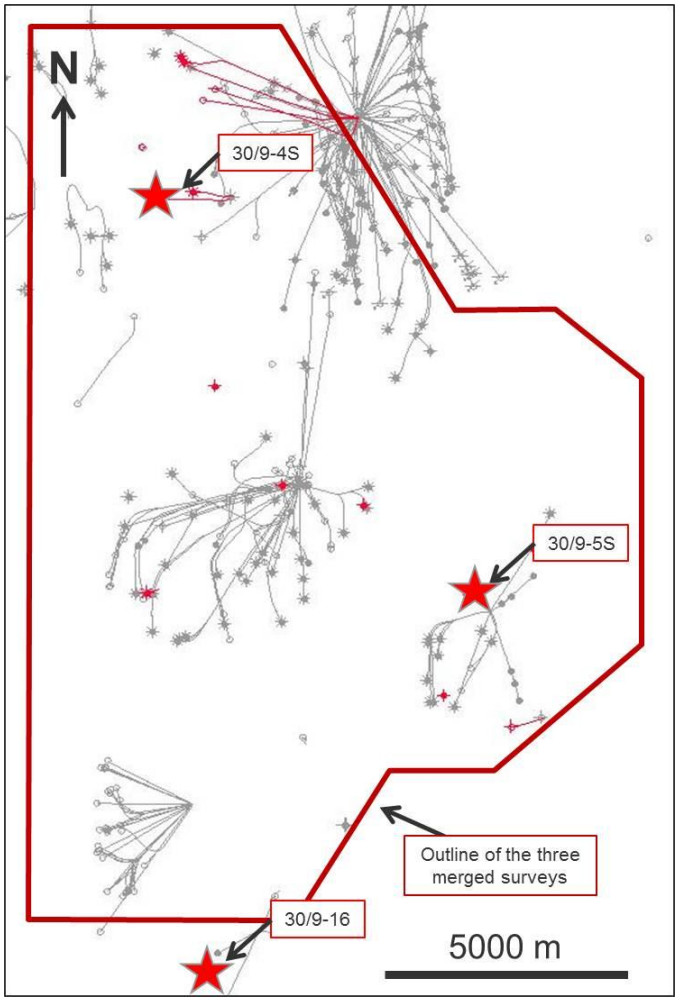

Figure 16: Map highlighting the cored wells in the Oseberg South field. Statfjord well penetrations are highlighted in red.

4.3.1 Facies

The facies scheme used in this thesis is based partially on Ryseth (2001), Miall (1992), and Aase (2011). It was based on comprehensive geological evaluations of the Statfjord Formation on a regional basis across the Viking Graben region (Table 4).

Table 4: Facies codes used in the core analysis. Modified from Miall (1992), Ryseth (2001), & Aase (2011).

Facies Code	Facies Description
Gm	Massive or crudely bedded gravel
Gx	Cross-bedded gravel
Sm	Massive or disorganized sand; very fine to very coarse
Sx	Cross-bedded sand; fine to very coarse
St	Trough cross-bedded sand; fine to very coarse
Sp	Planar cross-bedded sand; fine to very coarse
Sr	Ripple cross-laminated sand; very fine to medium
Sl	Low-angle cross-bedded sand; very fine to medium
Sh	Horizontally laminated sand; very fine to medium
Sfl	Flaser-bedded sand; very fine to medium
Sw	HCS/SCS and wave-ripped sand; very fine to very coarse
Sb	Thoroughly bioturbated sand; very fine to very coarse
Swa	Wavy bedding
Hl	Lenticular bedded heterolith
Fl	Finely laminated mud or mud dominated heterolith, occasionally bioturbated with sandy streaks. Pyrite and siderite nodules.
Fb	Strongly bioturbated mud or mud dominated heterolith
Fm	Massive mudstone
C	Coal or carbonaceous mud

The above facies codes were used to group similar geological settings together, and use some of these relationships to determine a possible depositional environment. For future modelling of the formation, a different facies scheme will be applied where the facies are grouped together based on their petrophysical properties and/or similar geometric configurations. Better understanding of the geological facies will help determine how to best divide the rock into the modelling facies, and understanding the orientation and expected flow properties for the rocks involved. The creation of modelling facies was not performed in this thesis.

The two core logged wells are located within the Nansen Member (Figure 17), with the lowermost metres of the core from 30/9-16 resting within what is believed to represent the uppermost Eiriksson Member. As both of the cores were taken within what the marine

influenced portion of the formation, the potential of applying results from the interpretations for the remainder of the fluvial dominated Eiriksson Member is limited. Better understanding of the facies of the Eiriksson Member will need to be obtained from future core, if and when the Statfjord Formation is penetrated again in the Oseberg South field. In the meantime, cores obtained from the Eiriksson Member in nearby fields can be used as an analogue in the absence of this information. Other information that can help characterize the formation include a regional understanding and palaeogeographic reconstruction of the Eiriksson Member; chip sample and sidewall cores that can show some of the prevailing diagenetic conditions; and the petrophysical log suites.

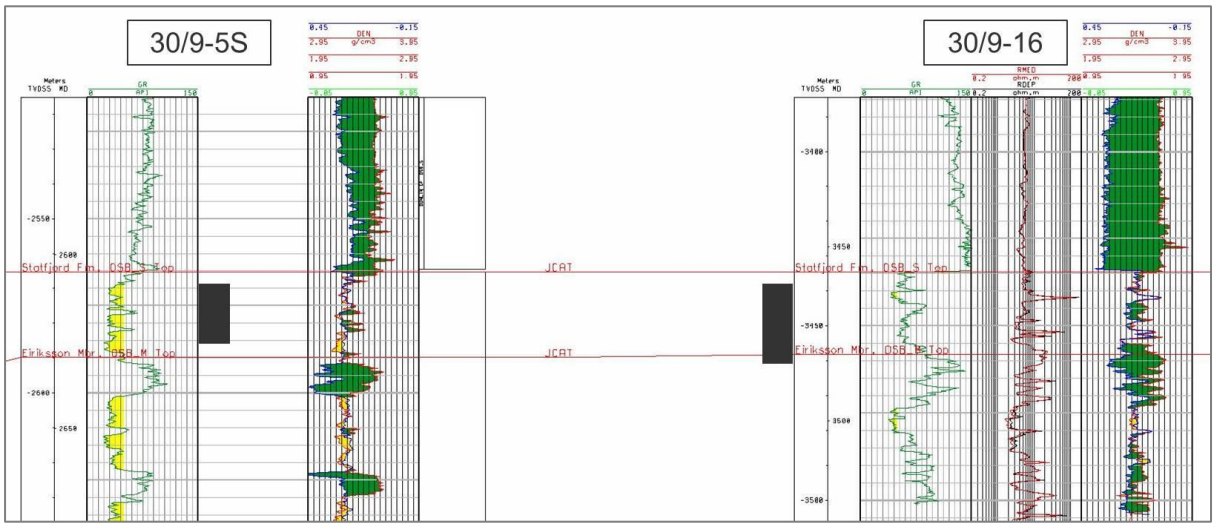

Figure 17: Petrophysical logs from wells 30/9-5S and 30/9-16, with the black bars representing the approximate interval that was cored.

4.3.2 Environmental Interpretations

Despite the similarities in the stratigraphic position of both of the logged wells, the core showed distinct differences in terms of both depositional environment, and reservoir properties. Figures 24 and 25 show plots of the porosity and permeability measurements, respectively, taken from core and core plugs throughout both of the wells. A considerable decrease in porosity and permeability values was seen in well 30/9-16, an expected trend with greater depth, which may also be confounded by the original depositional fabric and its diagenetic history.

Well 30/9-5S

The core from this well was roughly 18 metres in length, and contained several sections of rubble and unrecovered core. The core displayed visual porosity throughout, and the number of sections of rubble may demonstrate the lack of cementation in the section. Additionally, bioturbation was nearly absent within the entire core, except a two metre thick section at 2613 m.

The lower metre of the core displayed ripple-laminated medium-grained sand, with all of the ripples showing unidirectional orientation (Figure 22, Panel F). The ripples had a maximum height of 0,5 cm and combined with their unidirectional orientation, indicate deposition within a low energy, shallow water settings, and in the context of other interpretations from this core, possibly a crevasse splay.

The overlying few metres were dominantly rubble, but some competent sections showed a minimum 70 cm thick cross-bed set (Figure 22, Panel D), with the visibility of the bedding planes enhanced by the presence of interlaminated fine sediment. Visible porosity was present throughout this section, and the scale of the cross-beds and coarseness of the sediment indicates that this may have been deposited within a channel system, with the possible base seen in Figure 22, Panel E.

A roughly five metre thick section of low angle cross-bedded sand, mixed with sections of rubble overlies the interpreted channel sands. The section showed a slight coarsening upward profile, from medium to coarse sand, with a few thin streaks of very coarse material and minor coal layers near the top of the section. A minor (5 cm scale) bed of finely laminated muds/very fine sand was seen within the coarser low-angle cross-beds at 2620,8 m, which may indicate a brief shift in depositional regime. The overlying two metres contained the same fine sediments as the thin 5 cm bed, shifting between what can be classified as wavy and flaser bedding (Figure 22, Panel C). Some current ripples, including rare bi-directional ripples, were visible. This seven metre thick section exhibits a rapid shift in energy conditions and depositional environment, from higher energy conditions, perhaps along the side of a bar or channel, shifting towards lower energy conditions of the tidal flat containing flaser and wavy bedded sediments (Dalrymple 1992).

The overlying 3 metres from 2614,5 to 2617,5 m shows a series of rapidly shifting environmental conditions. The lower 1,5 m shows a coarsening upward sequence with few current ripples, with remaining 1,5 m showing several 0,5 m scale fining upward sections

that are marked at the base by well-rounded organic material (Figure 22, Panel B). Current ripples and sigmoidal cross bedding are also visible within these fining upward profiles.

The overlying metre of sediment shows a rapid shift between a 30 cm thick section of finely laminated muds, to a 30 cm fining upward section of sand with minor organic debris, and another 40 cm section of finely laminated muds. These muds are the only sections in this core that contained bioturbation, with both *Skolithos* and *Planolites* visible. The relative lack of diversity and number of trace fossils can be indicative of a stressed salinity environment (Pemberton *et al.* 1992) and in combination with the low energy muds present, may indicate deposition within a lagoonal environment, with the sandy beds representing possible storm or wash over deposits.

The remaining five metres of core at the top of the section is medium to coarse grained, with cross-bedding evident throughout. A nearly one metre scale cross-bed is located near the top of the section and displays a typical sigmoidal shape, with low angle beds at the bottom, higher angle in the middle, and low angle beds again at the top of the bed. Organic debris and small, centimetre scale layers of coal are common throughout the section, as is visible porosity. Some current ripples are also visible. Overall, this section appears to represent a channel system with organic debris from nearby sources.

The porosity and permeability data from this core shows excellent reservoir properties with most samples showing greater than 20% porosity, and a very high number with greater than 1 Darcy permeability. The interpreted channel sands showed the best reservoir properties, while the muddy section showed the lowest.

Overall, observations from this core seem to indicate deposition within a more active part of the depositional system, perhaps within tidal or distributary channels of the transitional marine system. The coarseness of sediment, common cross-bedded features, and general lack of bioturbation seem to support a high energy environment. The well's location on a possible paleo-high on the J structure may also have influenced the depositional environment during this time, although the full implications of this are not yet understood.

Well 30/9-16

The core from well 30/9-16 is 27,2 m in length and has full recovery with minor sections with rubble. The lowermost three metres of the core was characterized by moderate to intense bioturbation, and although most of the primary sedimentary structures were obliterated by bioturbation, some sigmoidal cross-stratification was noted. The trace fossil suite was quite diverse, with possible *Skolithos, Asterosoma, Rosselia*, and *Planolites* present, among

others. The diversity and abundance of the trace fossils suggest that this depositional environment was located in more fully marine waters, as opposed to brackish waters which generally show a less diverse selection of traces (Pemberton *et al*. 1992). The coarseness of the sediment and abundance and diversity of the traces suggest a depositional environment that was not very restricted, and may have been subject to high energy conditions. This is also reflected in the apparent storm beds and erosional surfaces seen in Figure 23, Panel J.

This heavily bioturbated section is overlain by a roughly five metre thick section of silt-size to fine sand-size material. The intensity of the bioturbation as well as the diversity of the trace fossils was reduced compared to the underlying layer. This may reflect rapid deposition of sediment within this section or perhaps a change in salinity conditions that hindered the development of trace-fossil creating organisms. Sedimentary structures present included low angle cross-beds, current ripples, possible hummocky cross-stratification, and thicker beds of coarser, cross-stratified sands possibly representing storm events (Figure 23, Panel I). The finely laminated silts may represent deposition within a low energy environment, which due to the lack of trace fossil diversity may be a restricted lagoon setting.

The overlying three metres from 3474 – 3477 m is characterised by moderate bioturbation, and common alteration of medium-grained sand with fine mud drapes. Double mud drapes were common throughout this section (Figure 23, Panel H) with ripples in between these mud drapes showing opposing flow directions. The ebb and flow of tides and the intermittent slack water period commonly creates these features, and is indicative of deposition within the sub-tidal zone of a tidal environment. This layer is capped by centimetre scale coal layers that display some internal faulting. A 7-8 m layer of dominantly massive sand overlies the previous section, and displays no identifiable trace fossils, and few sedimentary structures. Among the few structures present were possible cross-bedding with reduced dip angle higher in the section, many of which were highlighted by scattered organic debris. There was also a colour change within some layers, which appeared to be calcite cementation, as tested with hydrochloric acid. The scale of the bedding, lack of trace fossils, and relatively few sedimentary structures indicates that this section might have been quickly deposited in a high energy system, possibly within a channel system.

The overlying few metres appear to be part of the same sedimentary package, but display more visible internal structures that include tabular cross-bedding, some possible sigmoidal cross-beds, organic debris, and some deformation structures. An increase in organic debris is also evident, and the dip of the bedding is lower than encountered deeper within the section. It seems likely that this section is part of the same sedimentary package as below,

but represents deposition closer to the land/water interface (i.e., near the edge of the channel).

A distinct change in sedimentology is seen at roughly 3465,5 m depth, with the overlying three metres displaying a fining upwards profile with a thin layer of coarse material seen at the base. Wavy bedding and finely laminated muds are common, with the degree of bioturbation increasing upwards towards the finer sediment. There appears to be little diversity in the trace fossils, and it is possible that only *Planolites* is present. The fining upwards profile and wavy bedding indicates possible deposition within a quiet depositional environment, possible within the intertidal area of an estuary or bay, where brackish water conditions would support a low abundance and low diversity of trace fossils (Pemberton *et al.* 1992).

A more-or-less gradational contact caps this section, with the uppermost 3,5 metres of core exhibiting a high degree of bioturbation, with only faint relics of the primary depositional fabric remaining, seen as low angle cross-beds (Figure 23, Panel G). Shell fragments are common throughout, indicating deposition within a fully marine, or very close to fully marine conditions. As seen in Figure 17, this section of the core is located in the uppermost Nansen Member, and represents the last sandy sediments before inundation of the fully marine Dunlin Group shale.

The structures and sediments in core are consistent with literature descriptions of the Nansen Member from across the Viking Graben (e.g., Vollset & Doré 1984, Ryseth 2001). The sediments show significant and rapid changes in the depositional environment, which is expected in an alluvial to marine transitional environment. The sediments show deposition within lagoons or estuaries with occasional storm influence, possible bays, channel systems, and nearly fully marine environments near the top of the section. Porosity and permeability measurements from core plugs showed that there was a significant decrease in reservoir quality compared to samples from well 30/9-5S, but despite this, still contains a few sections with porosity greater than 15%, and permeability greater than 10 mD. As one might expect, the highest porosity and permeability values were seen within the interpreted channel sands. As they were one of the thickest facies encountered, they may represent a significant exploration target within the Nansen Member in the future.

Core Discussion

Overall, the interpretations from the core within the two wells are consistent with interpretations regarding the depositional environment in the Nansen Member. Although

well 30/9-5S did not show much marine influence, the depositional environment is believed to have been in the close vicinity of the transitional zone. The differences in the environments between the two wells demonstrate the variability of the formation, and the challenges that will be faced should the Nansen Member become a focus for future exploration alongside the Eiriksson Member. The lack of core within the Eiriksson Member that could be logged creates a problem for better understanding of the depositional conditions through the Eiriksson Member time, but in the absence of this data, regional data will have to suffice until more information is obtained. Once this data is obtained, a more detailed depositional history can be put together for the Statfjord Formation at Oseberg South. Core porosity and permeability measurements confirmed the decline in reservoir quality expected with depth (Figures 24 & 25) but results also showed that even with greater depths, reservoir quality sands exist, and can represent future exploration targets.

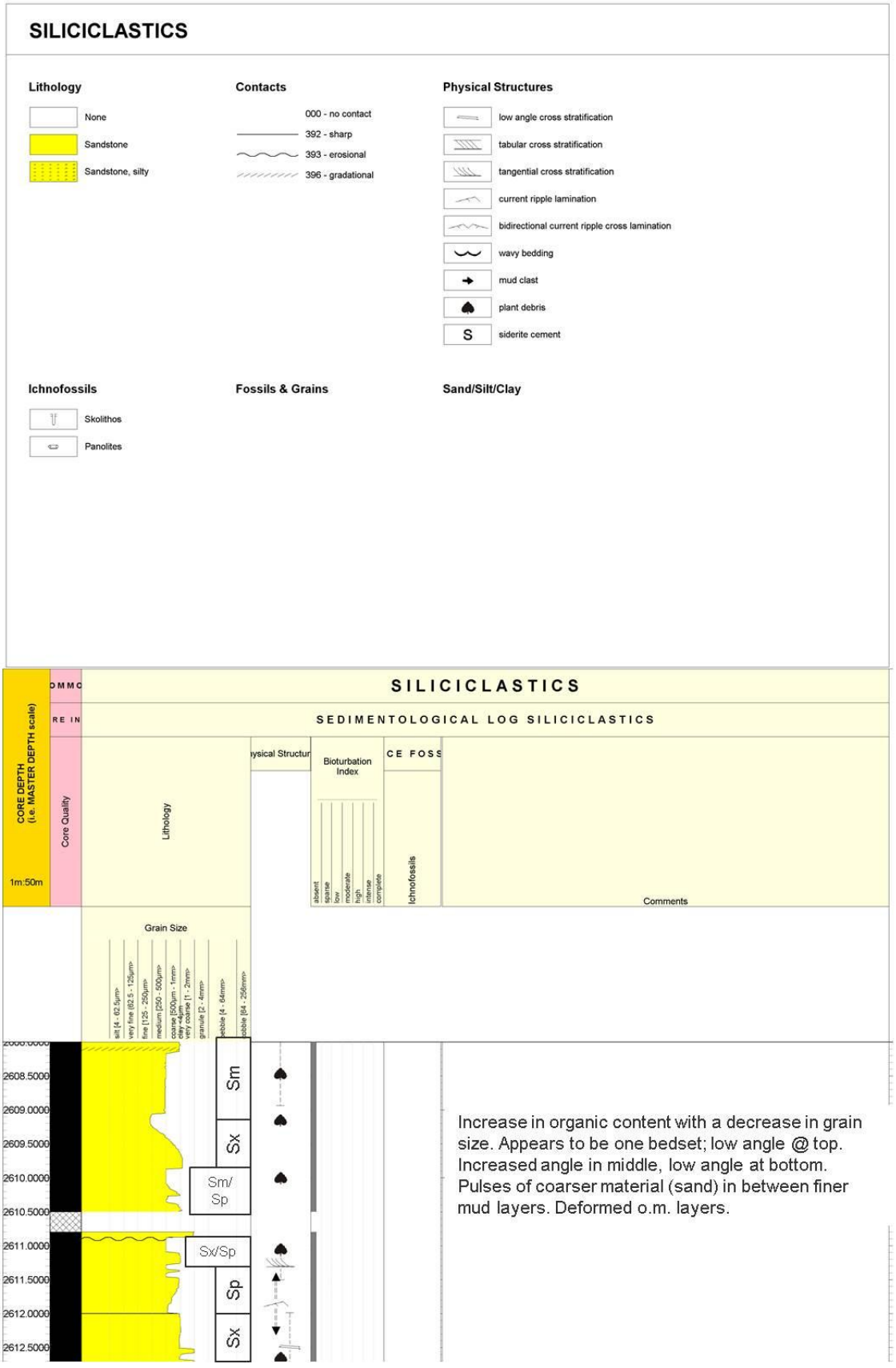

Figure 18: Core log from well 30/9-5S, depth 2608 m - 2612,5 m.

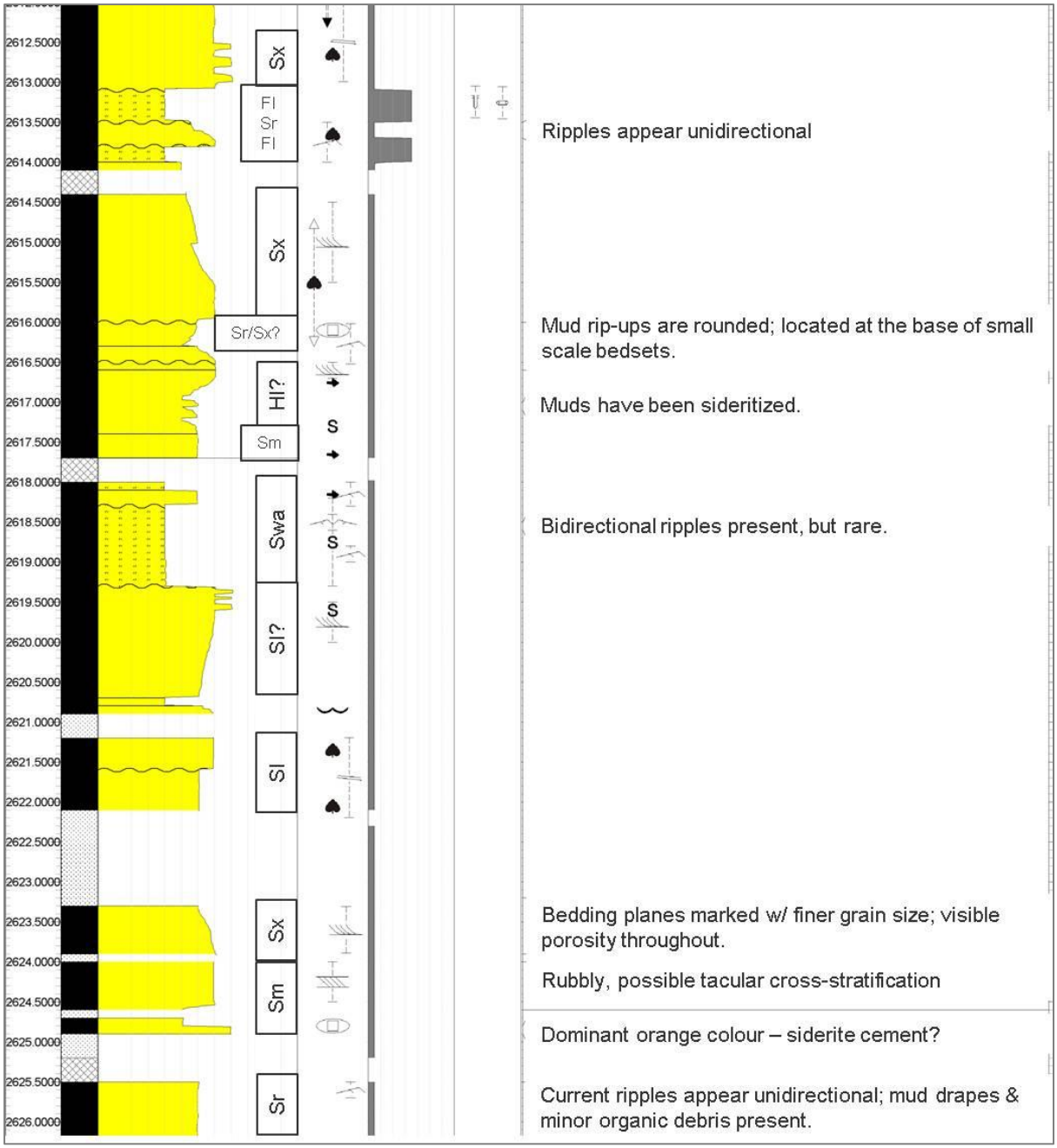

Figure 19: Core log from well 30/9-5S, depth 2612,5 m - 2626,2 m.

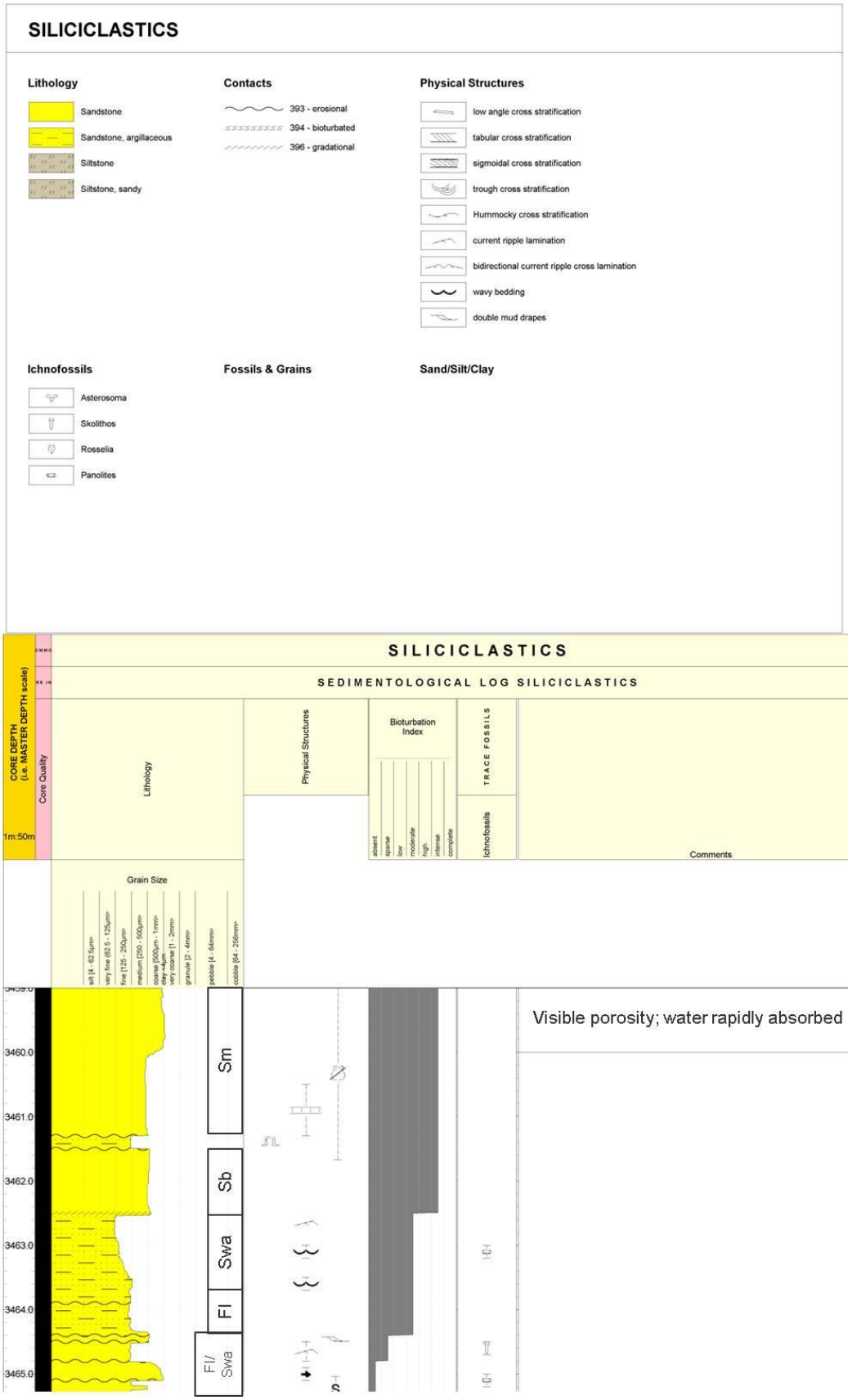

Figure 20: Core log of well 30/9-16, depth range 3459 m - 3465,1 m.

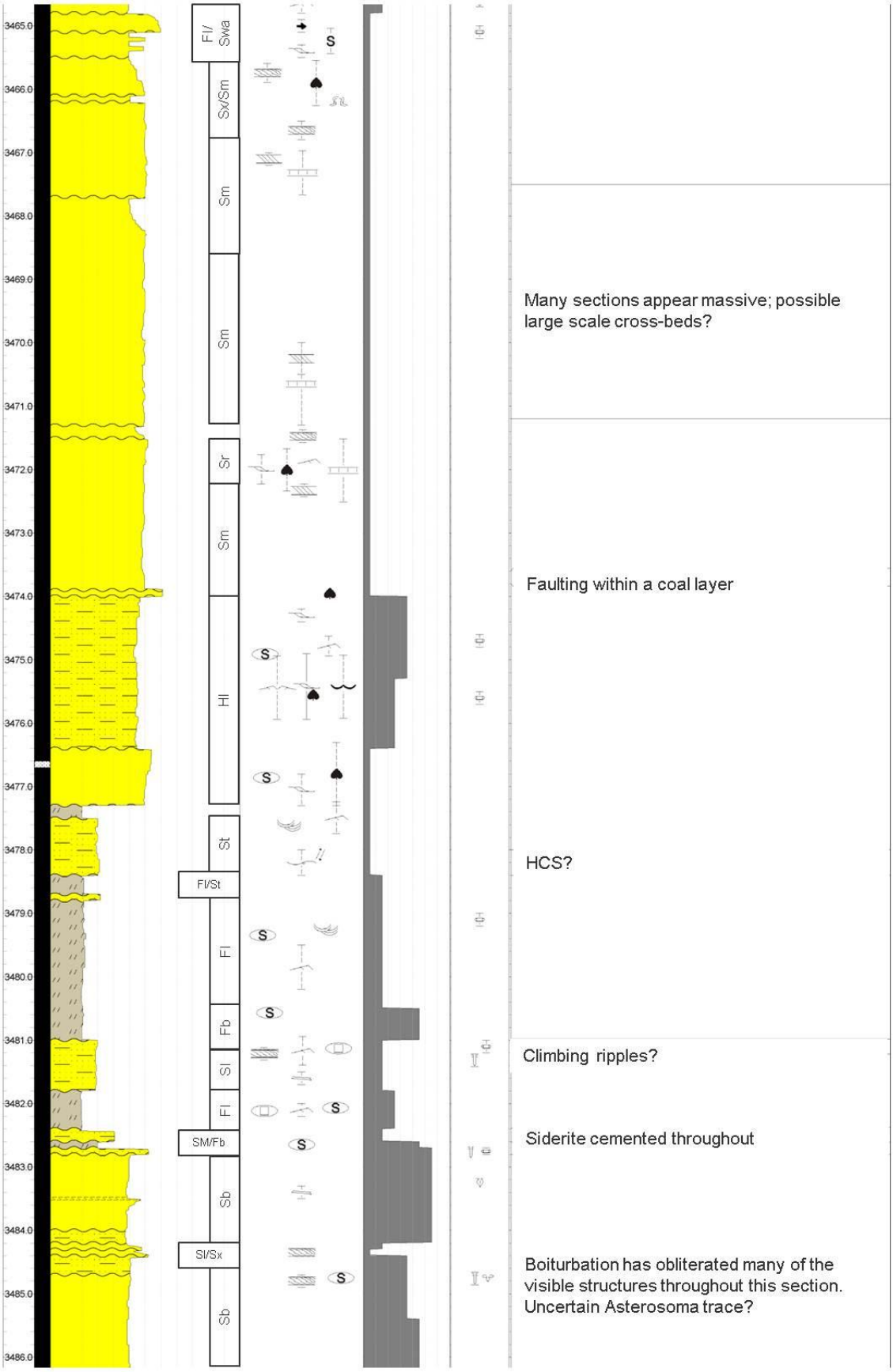

Figure 21: Core log of well 30/9-16, depth 3465 m - 3486,2 m.

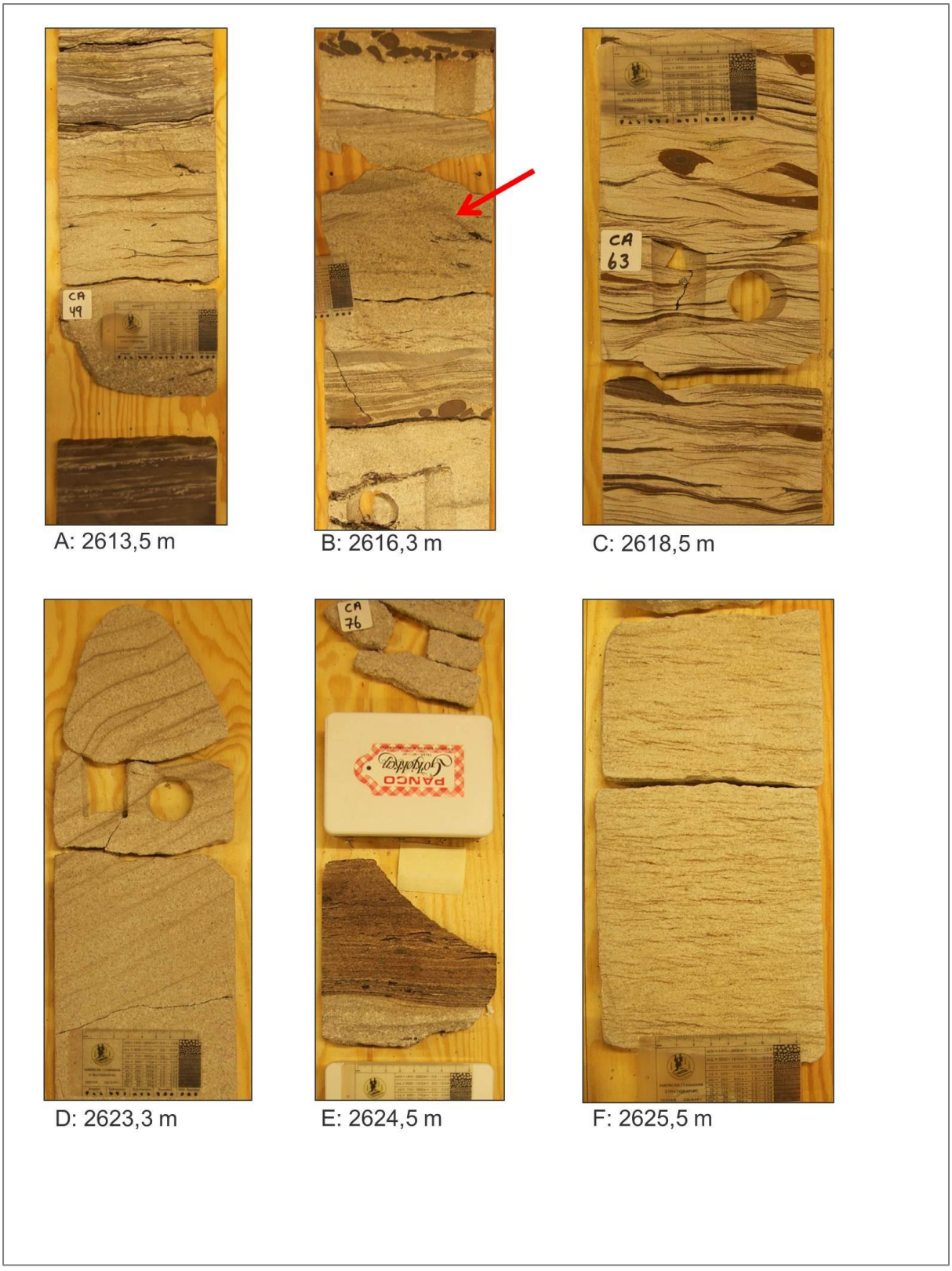

Figure 22: Core photos from well 30/9-5S. A: Ripple laminated sands located between fine grained and bioturbated mud beds. B: Rounded mud clasts are seen at the base of some beds, note current ripples denoted with the red arrow. C: Wavy bedding. D: Large scale cross-beds, the bedding planes are outline by fine material. E: The red bed represents a possible channel base. F: Current ripples that appear unidirectional; possible crevasse splay deposit.

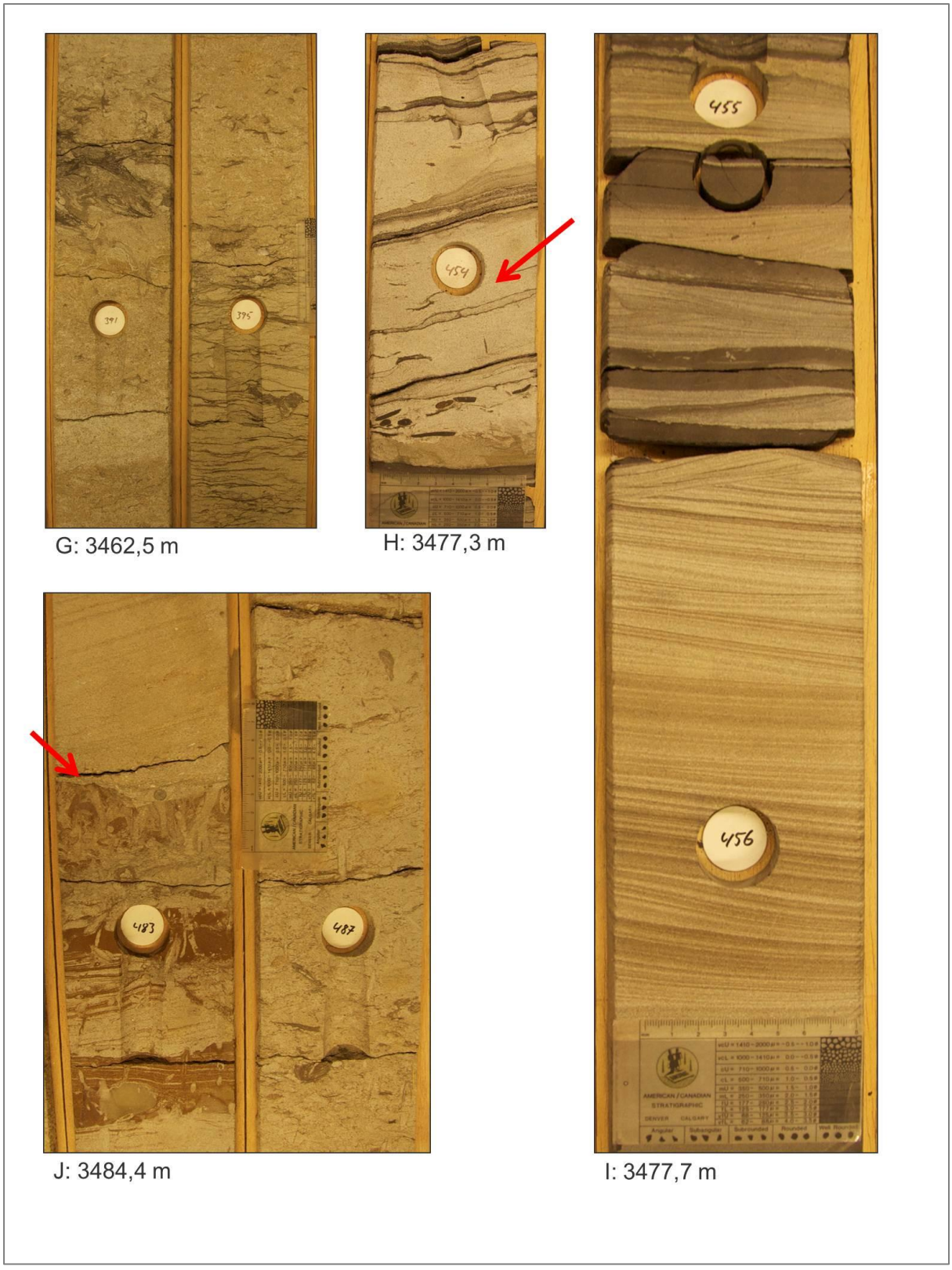

Figure 23: Core photos from well 30/9-16. G: Transition between underlying wavy bedding and overlying bioturbated sands. H: Double mud drapes denoted by the red arrow. I: Possible storm beds; HCS? J: Scoured boundary overlying a heavily bioturbated section of sand (red arrow).

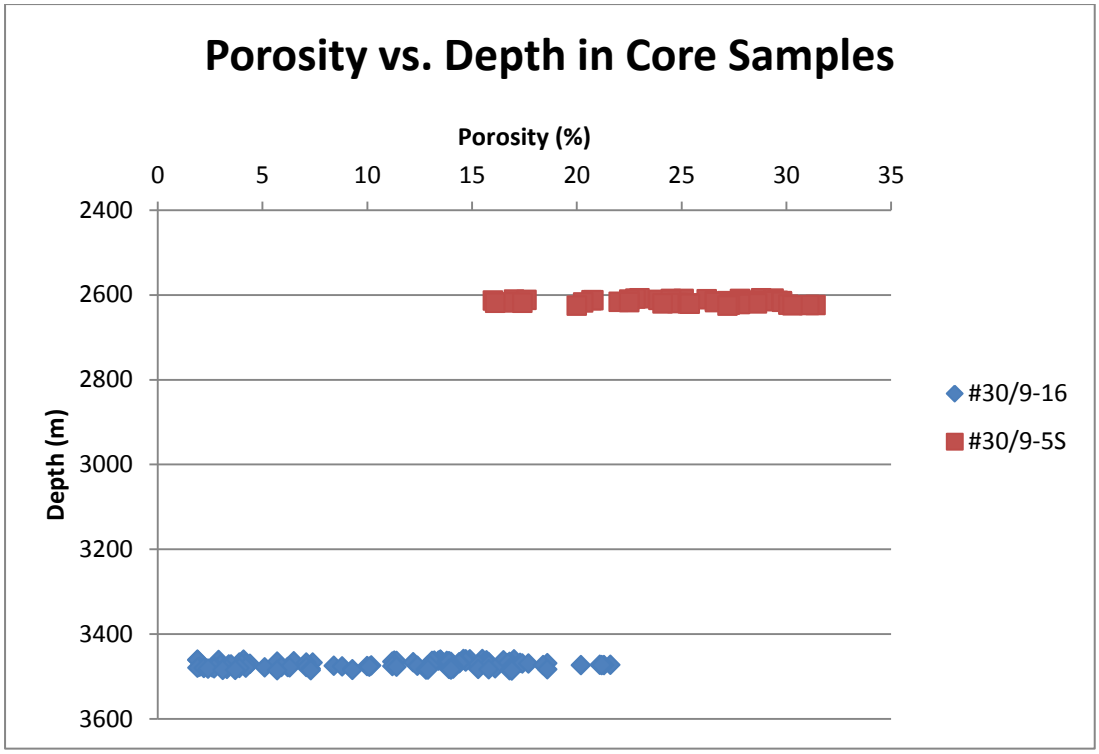

Figure 24: Graph showing the porosity differences with depth between wells 30/9-16 and 30/9-5S.

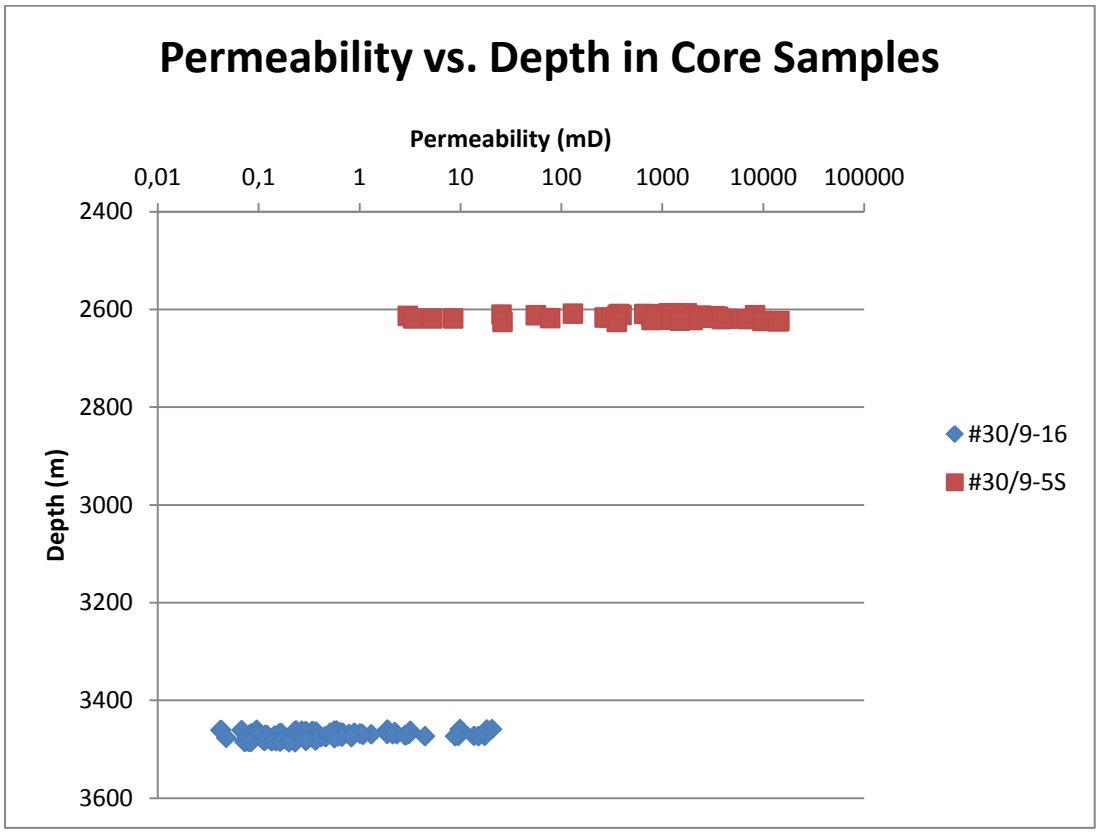

Figure 25: Graph showing the permeability differences with depth between wells 30/9-16 and 30/9-5S.

5. Seismic Input

5.1 Software

The software packages used throughout this thesis are part of the standard geological and geophysical interpretation packages that are available at Statoil. The interpretations were completed with the use of Halliburton software, namely Decision Space, SynTool, and Stratworks for seismic interpretation, synthetic creation, and geological correlations, respectively. In addition, the structural modelling was completed using IRAP RMS (ROXAR Emerson).

5.2 Seismic Data

The seismic data interpreted is a merge of three separately shot cross-line OBC surveys from 2008 and 2010. Survey ST0823 was shot over the J structure in 2008, ST10003 was shot over the C structure in 2010, and survey ST10007 was shot over the remaining portions of the field, also in 2010. The acquisition geometries of each survey are summarized in Table 5 (Dawson & Mathewson 2011). A pre-stack depth migration was performed by Western Geco on the data, with a detailed velocity model used down to the level of the Base Cretaceous Unconformity (BCU). Below this marker, the velocities are subject to more error, which needs to be kept in mind when interpreting deeper horizons that include the Statfjord Formation. The seismic is regarded as zero phase data, with an increase in acoustic impedance seen as a peak (Figure 26), and this convention applies to all seismic cross-sections throughout this thesis. All sections were interpreted in depth.

Table 5: Acquisition geometries of the three seismic surveys shot over the Oseberg South field (from Dawson & Mathewson 2011).

	J Structure	C Structure	West
Receiver Line Separation	300m	250m	350m
Receiver Station Spacing	25m	25m	25m
Source Line Spacing	300m	200m	300m
Source Point Spacing	18,75m	18,75m	18,75m

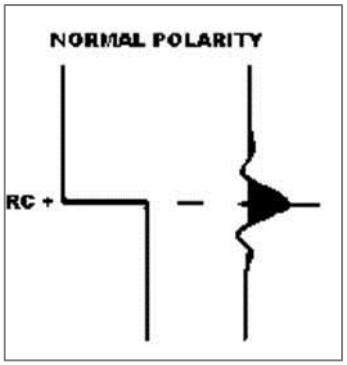

Figure 26: Polarity convention that applies to all seismic cross-sections throughout this thesis (SEG convention).

5.3 Synthetics

The creation of synthetic well traces is a critical step that ties the well log data to the seismic, and is one of the first steps when interpreting the seismic data. For this project, the Halliburton program SynTool was used to create synthetics for each of the wells that penetrated the Statfjord Formation. A consistent issue with interpreting the Statfjord Formation at Oseberg South is the lack of well penetrations.

Figure 27 shows an example of the process and output from the synthetic logs. Depths are given in TVD, and the formation markers representing the Shetland Group, Top Statfjord Formation (T Statfjord), Middle Statfjord Formation (M Statfjord), and Base Statfjord Formation (B Statfjord) are shown. The two main logs needed to create a synthetic trace are the sonic logs (µs/ft) and density logs (g/cm^3). A caliper log is used alongside the sonic and density logs to check areas where borehole issues may have affected the quality of the readings in the logs. Red arrows in Figure 27 show an example of spikes within the density log that would require manual editing to avoid erroneous creation of wavelets. In this example, spikes are also present throughout the sonic logs that require editing. At the Statfjord Formation level, it is evident that the logs are of reasonably good quality.

A downhole check shot survey is performed in each well that measures the downhole time-depth relationship (i.e., velocity). This check shot survey is used to convert all of the well data (e.g., density logs, acoustic logs) into the time domain. These converted logs are used to create the acoustic impedance log (calculated as the density multiplied by velocity), which is then used to calculate the reflection coefficient between two layers. With this data, a trapezoidal filter with frequencies of 3-6-14-50 Hz was used to create a synthetic trace that was then used to tie to the seismic. The strong trough that is typical of the Shetland Group was the most obvious reflector to aid in tying the well data to the seismic, and this is what was used to determine the time shift required to accurately tie the synthetics to the seismic

data. On all but well 30/9-5S, the time shift was roughly 30ms or less. The correct check shot survey could not be found for well 30/9-5S, and so a proper synthetic could not be created. In the absence of synthetic data, the well logs and well picks were used to best determine the Top and Base Statfjord Formation reflectors (Figure 28).

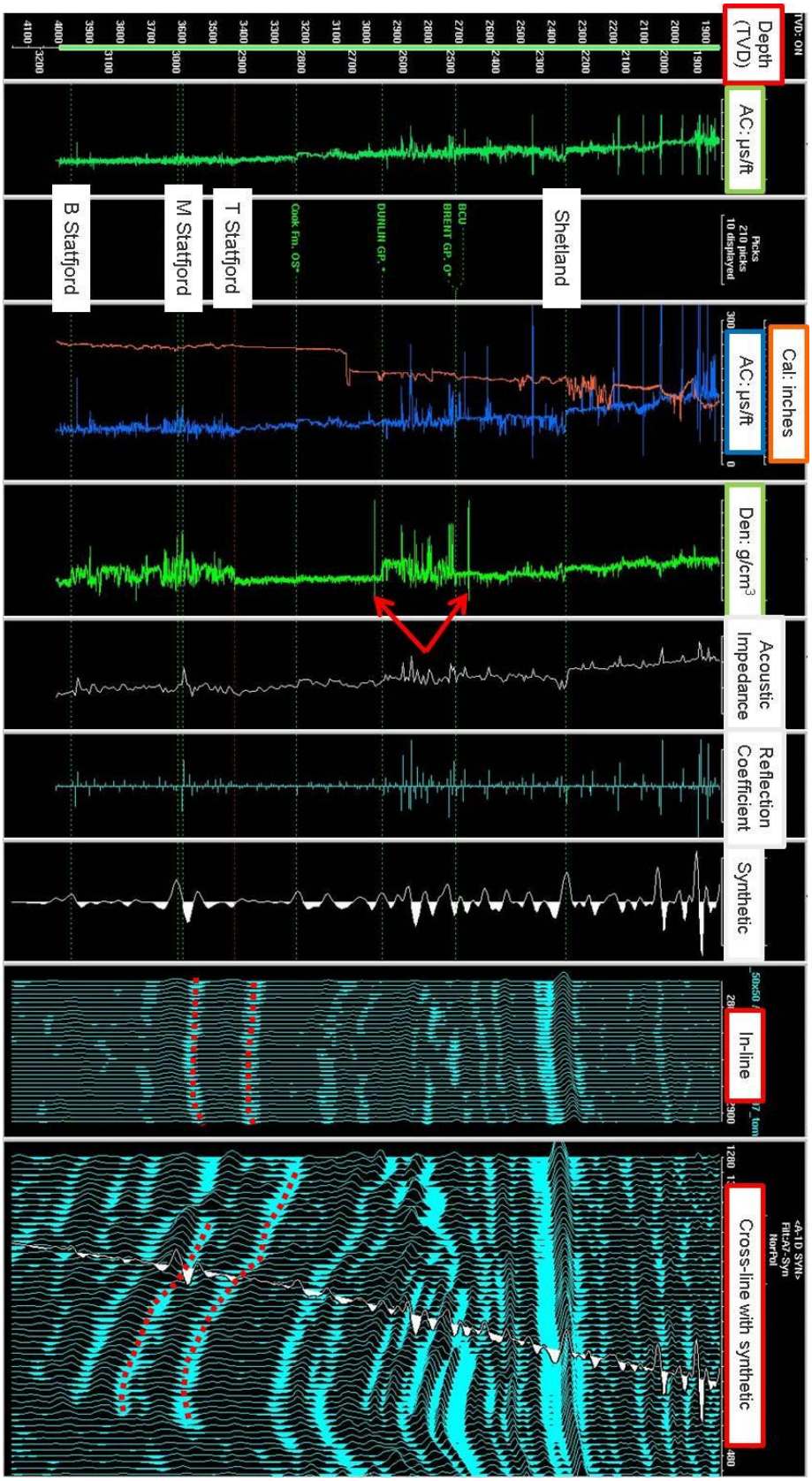

Figure 27: Example of a synthetic seismic trace for well 30/9-3A. A cross-line shows a west-east section, while in-line shows north-south. The top red dashed line on the in-line and cross-line represent the Top Statfjord Formation, while the lower dashed line represents the Middle Statfjord Formation. The strength of these reflectors is clear in the inline data.

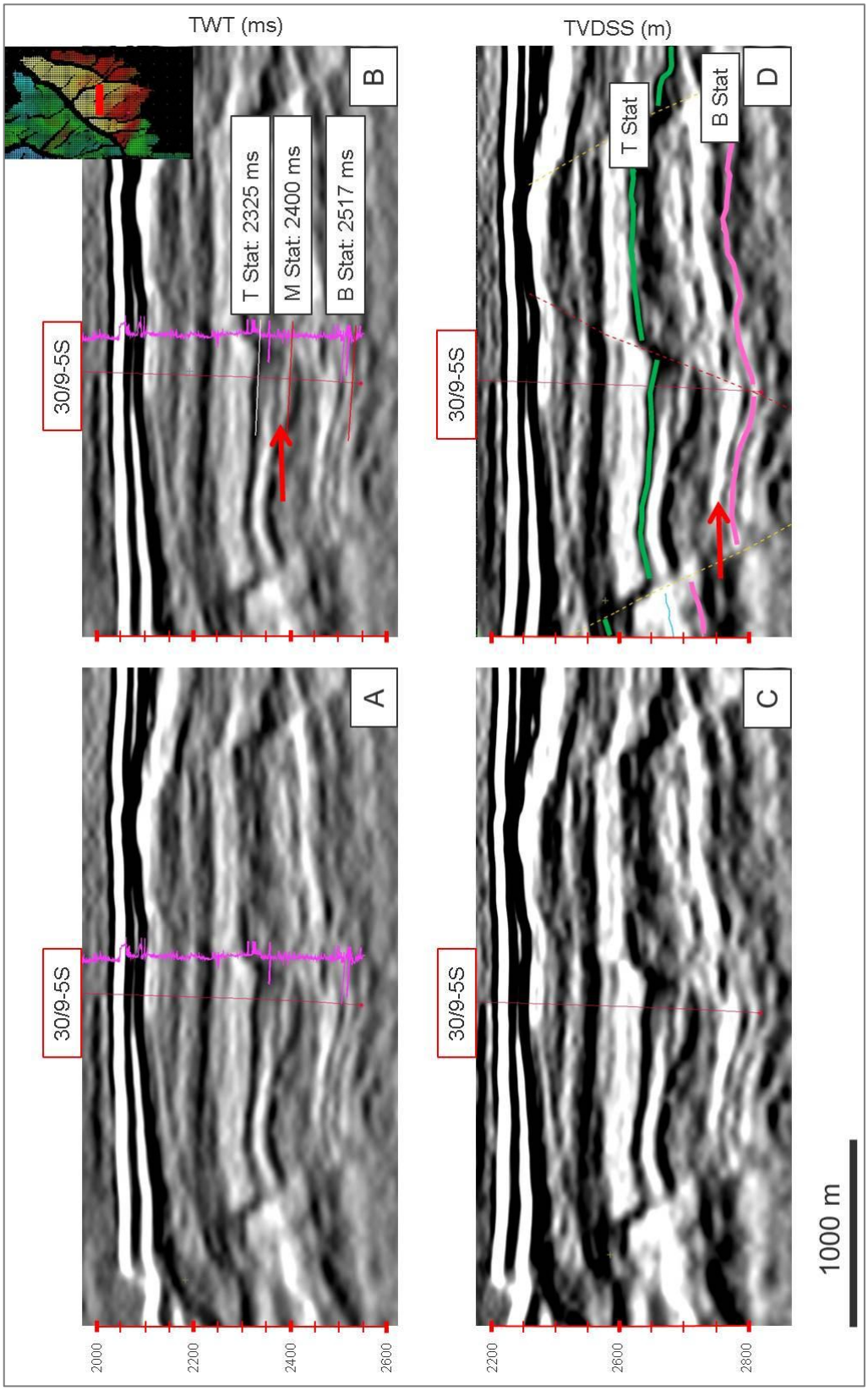

Figure 28: Example of the tie process without the use of a correct synthetic, and demonstrating uncertainties in the Middle Statfjord pick in the J structure. Panel A: Sonic log (TWT). Panel B: Sonic log with Top, Middle (red arrow), and Base Statfjord picks (TWT). Panel C: The same section shown in depth (TVDSS). Panel D: The section is shown with the Top and Base Statfjord picks (TVDSS), and a red arrow highlighting what was thought to represent the Middle Statfjord marker throughout the field, off the J structure.

5.4 Seismic Horizons

Three main horizons were interpreted, where possible, within the Statfjord Formation across much of the field. The three horizons were: Top Statfjord, Middle Statfjord, and Base Statfjord (Top Lunde Formation). The Top and Base Statfjord Formations are important horizons that help determine the thickness trends across the field, and the Middle Statfjord marker was a strong reflector in most areas that helped to constrain the interpretation where the lack of petrophysical and synthetic well data increased the uncertainty.

In most areas, the Top Statfjord marker was a strong peak, and tied well to the synthetic seismic data, as well as the well penetrations. As mentioned earlier, there are 12 exploration wells that penetrate the Statfjord Formation, in addition to another four production and injection wells located on the Gamma structure that belong to the Oseberg Main field. From these wells, it was only possible to create synthetic well data from six of them, allowing for good well-ties to the Top Statfjord Formation in the Omega structure, the J structure, and parts of the C structure.

The Middle Statfjord reflector is a strong trough that ties well to the well data in the Omega structure (Figure 31), and the nature of the reflector was generally consistent across much of the field, with the exception of the J structure. Initially, a strong trough was thought to represent this Middle Statfjord reflector in the J structure, however, neither the well data nor the synthetics supported this. Figure 28 (panel D) shows an example of the well tie to the 30/9-5S well where this strong trough has been noted with a red arrow. In actuality, the Middle Statfjord reflector is likely a much weaker trough (Figure 28, red arrow in panel B) that is located just below the Top Statfjord reflector. As a result of this uncertainty, the Middle Statfjord reflector was not picked across the J structure. The change in the reflector character from the Omega to the C and J structures can be seen in Figure 30. The dashed blue lines represent where the Middle Statfjord is thought to be, and the red arrow shows a reflector that resembles the Middle Statfjord reflector in the other parts of the field.

Unfortunately, well 30/9-6 located on the C structure does not penetrate the Middle Statfjord horizon, negating the possibility of a definite well tie. Based on the visual characteristics, however, a strong negative trough resembling the Middle Statfjord was picked. It is markedly different from the Middle Statfjord marker on the J structure, indicating that the Brage Fault separating the two structures may have played a role in the palaeogeography of the area, resulting in different geological settings and subsequent change in the nature of the reflector.

As mentioned earlier, the Base Statfjord Formation (top Lunde Formation) is generally a transitional boundary that can be difficult to pick based on lithology alone. However, at Oseberg South, the difference in acoustic impedance between the two formations is enough to create a weak, but traceable trough across much of the field. As with the Top and Middle Statfjord horizons, the Base Statfjord horizon was most consistent over the Omega structure, but became more difficult, or nearly impossible to follow in areas of the C and J structures. Only three well ties were available for the Base Statfjord Formation (wells 30/9-24T2 and 30/9-3A on the Omega structure, and 30/9-5S on the J structure).

As the field represents a large area, change in reflector characteristics is expected, and can support that changes have occurred in the depositional environments based on reflector strength and character. It is important to note that the geology is not the only influence on reflector character, and fluid changes in the formation can also significantly change the reflector, as well as other seismic artefacts such as overburden effects. Areas where there is a strong and sudden change in reflector strength should be noted for further investigation to determine the likelihood of this representing a possible hydrocarbon accumulation, or whether it is a geological artefact (e.g., pinching out, tuning, etc.). A west to east oriented cross-section in Figure 29 shows an example of reflector interpretations across the B, Omega, and Gamma structures.

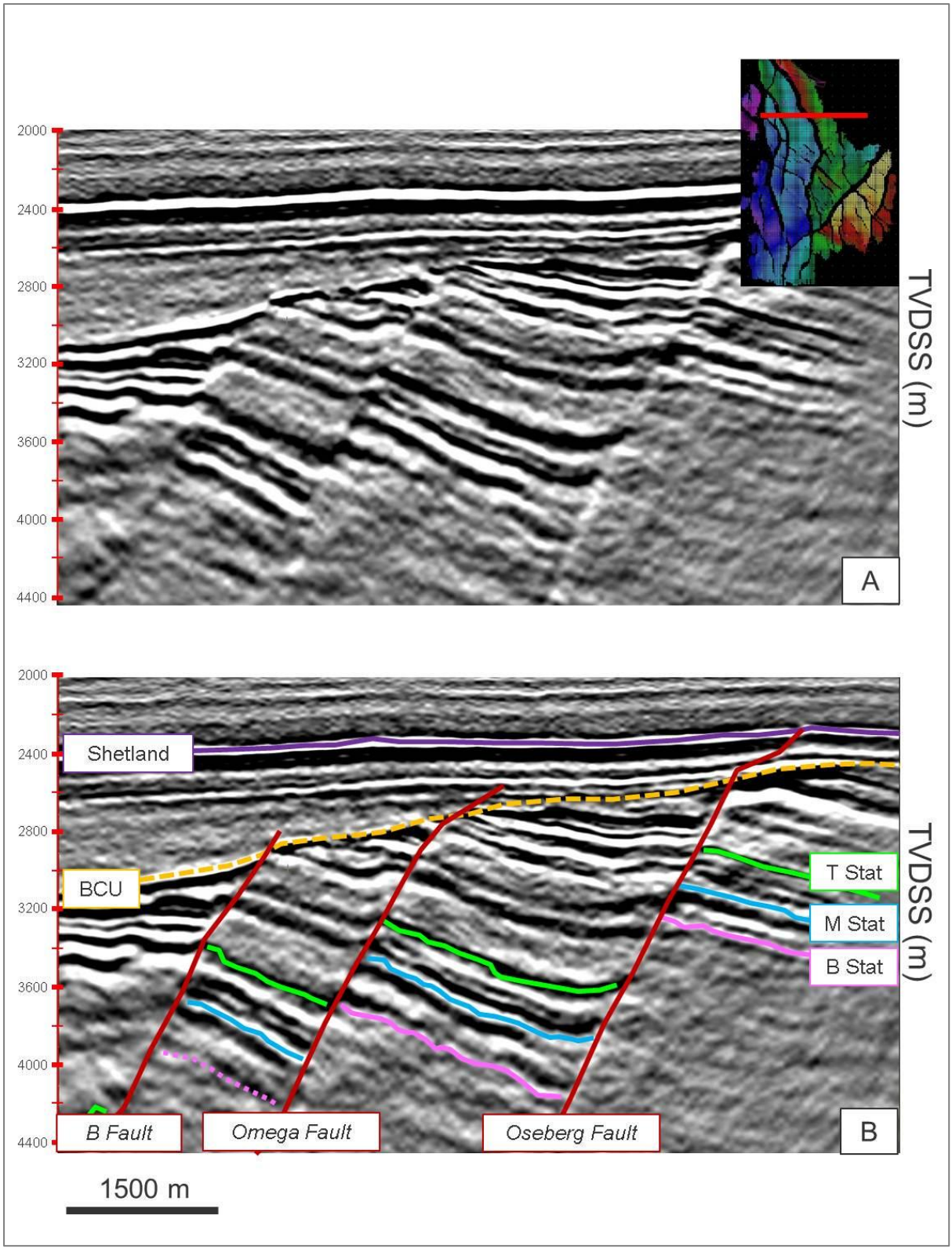

Figure 29: West to east depth section across the Omega Structure, demonstrating fault configuration and minor thickness changes across faults.

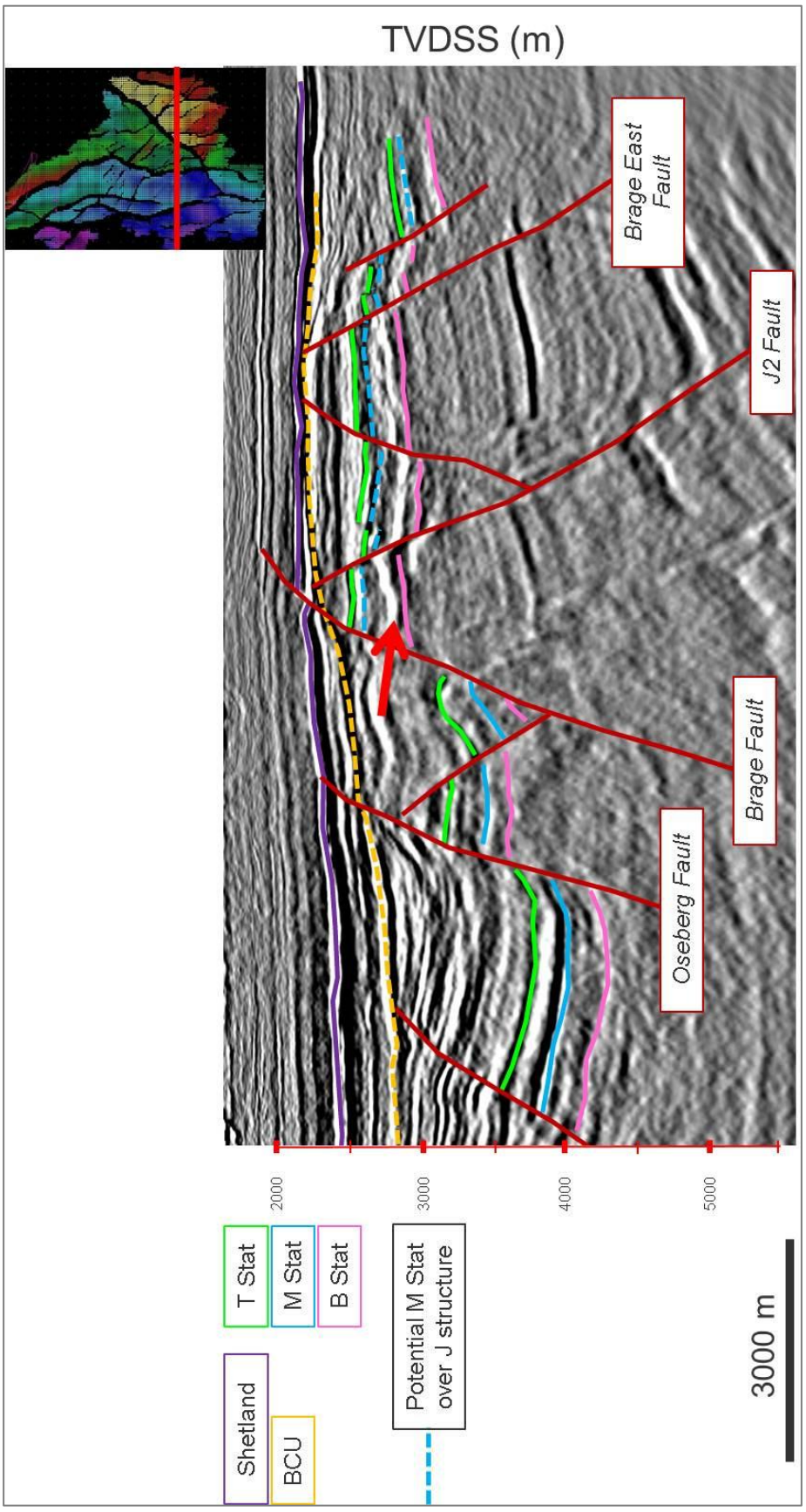

Figure 30: Seismic cross section showing the difficulties with interpreting the Middle Statfjord reflector over the J structure. The red arrow points to a reflector that resembles the Middle Statfjord in other parts of the field, while the blue dashed line represents the likely location based on well data.

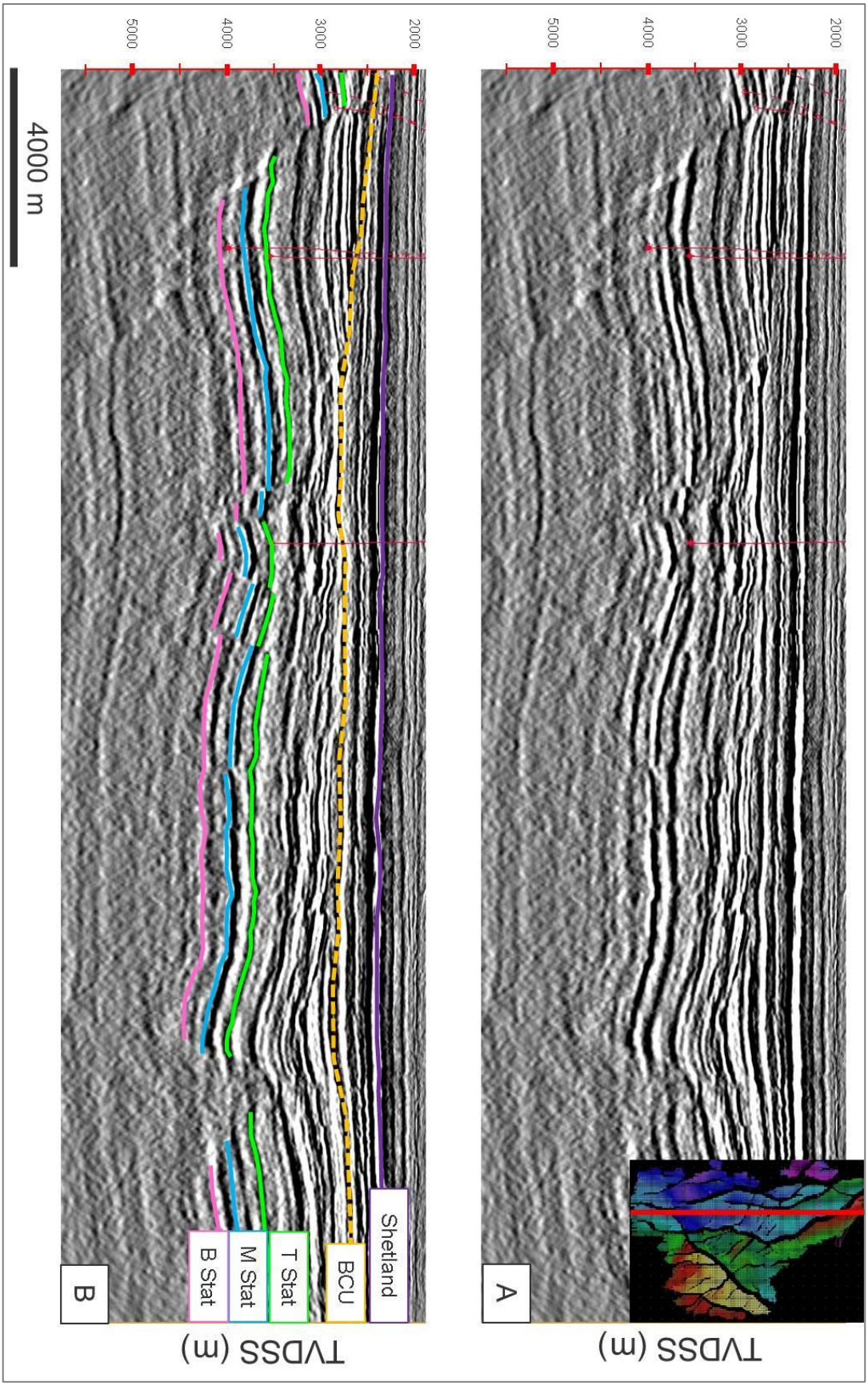

Figure 31: North to South oriented depth section across the Omega structure demonstrating the relative ease with which the reflectors are mapped in this structure.

5.5 Sources of Uncertainty

Several sources of uncertainty existed during interpretation of the data. The lack of consistent well penetration across the field means that well ties are not available for every structural block. As a result, there are several situations where the nature of the reflector appears to have changed across a fault, and the resulting interpretation may be incorrect. This was especially true in the J structure, where a strong trough looked like the Middle Statfjord reflector that was seen in other parts of the field, but upon closer investigation and examination of the well data, showed that this was not the same formation top (e.g., Figure 28). The quality of the pick in the western and deepest part of the formation was much lower than the rest of the field. There was a lack of well penetration in most of these structures, and the location near the edge of the full-fold data decreased the quality of the data, and thus the certainty in the picks. Although a best effort was made in ensuring that the correct reflector was picked, it is also possible that the incorrect one was picked in certain areas. This could be especially important to consider when interpreting thickness trends across the field.

5.6 Horizon Output

The Top and Base Statfjord reflectors were picked across nearly all structures within the field (Figures 31-33), however, near the edges of the data, and particularly in the western and deeper part of the field, the quality of the picks became highly uncertain. In these areas, the strong trough of the Middle Statfjord reflector became a good marker to determine the location within the stratigraphic section (see Figure 46), however, the quality of some of the reflectors decreased so much that making certain picks was not possible. The Top Statfjord marker was a reasonably pick in the deeper areas, but the Base Statfjord reflector was either absent, or no pick was possible. A 3D image of the top Statfjord horizon is shown in Figure 35.

5.7 Faults

A map of all faults that were picked and subsequently used in modelling in RMS is shown in the Appendix. It is evident from the map that not all of the faults in the field were interpreted

in the seismic, but the faults that were interpreted are thought to represent the most major faults that define the structural outline, and aid in understanding the evolution of the field. The remaining faults labelled in black were not part of the seismic interpretation, but were important later in the interpretations for determining the timing of the fault development. As exploration focuses in smaller and smaller areas, these smaller faults will be included in a reservoir model as they may have a significant impact on the flow properties within the formation, and thus impact the development of the field.

5.7.1 Fault Uncertainty

As seen in Figure 10 in the Introduction section, the Oseberg Fault Block sits in an area where there is a shift in polarity of the major faults, and this interaction, combined with multiple stretching phases has led to some complicated structures. The polarity switch in the faulting was seen in the J structure, with a change from westward dipping faults in the north, to eastward dipping faults in the south was encountered. Even with good quality data, the interactions between these fault phases and their cross-cutting relationships were difficult to determine. Nevertheless, an attempt was made to define the relationships between faulting phases, but this could change as understanding of the structural history in the area develops.

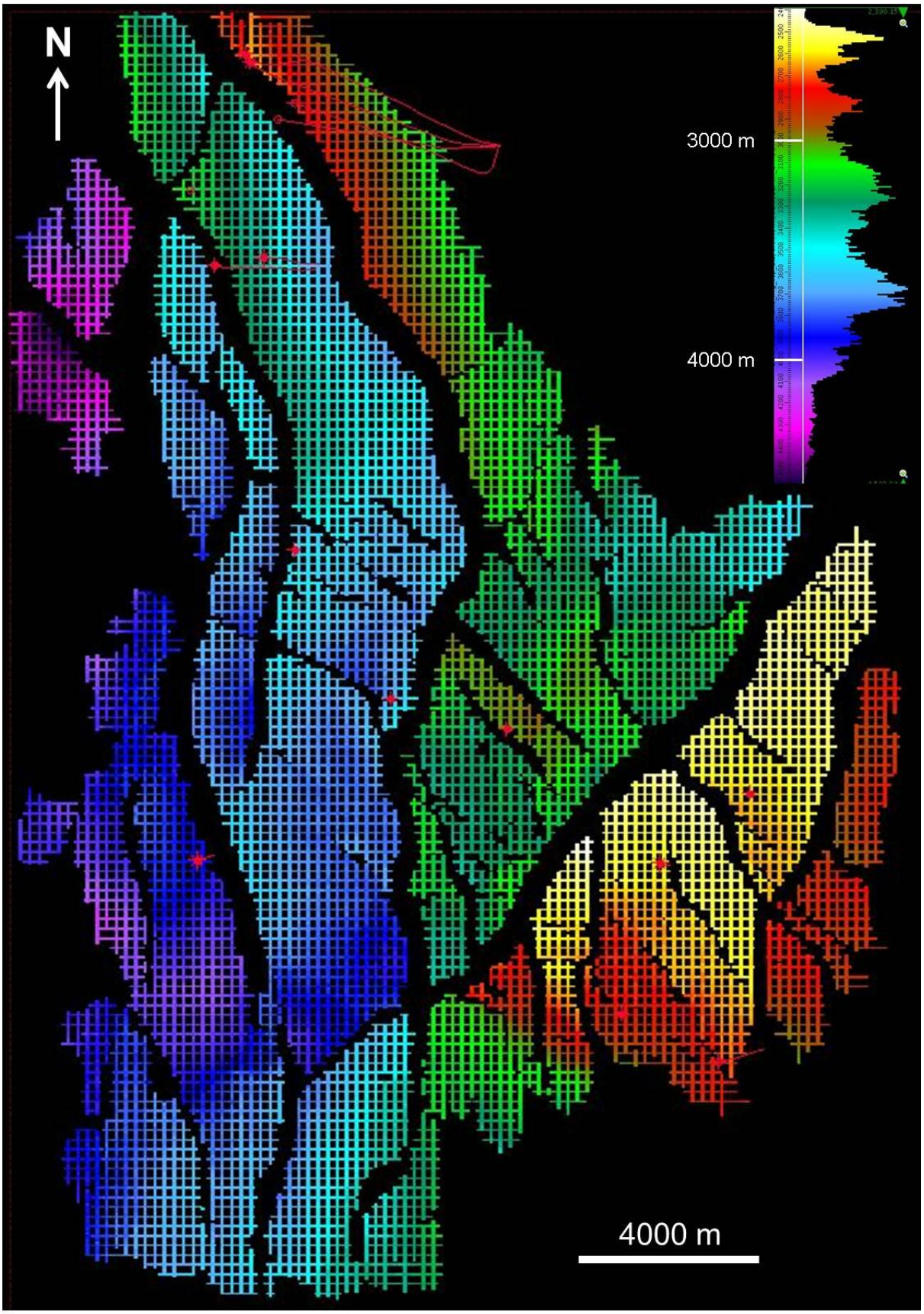

Figure 32: Top Statfjord Formation structural map. Spacing between lines is 50m.

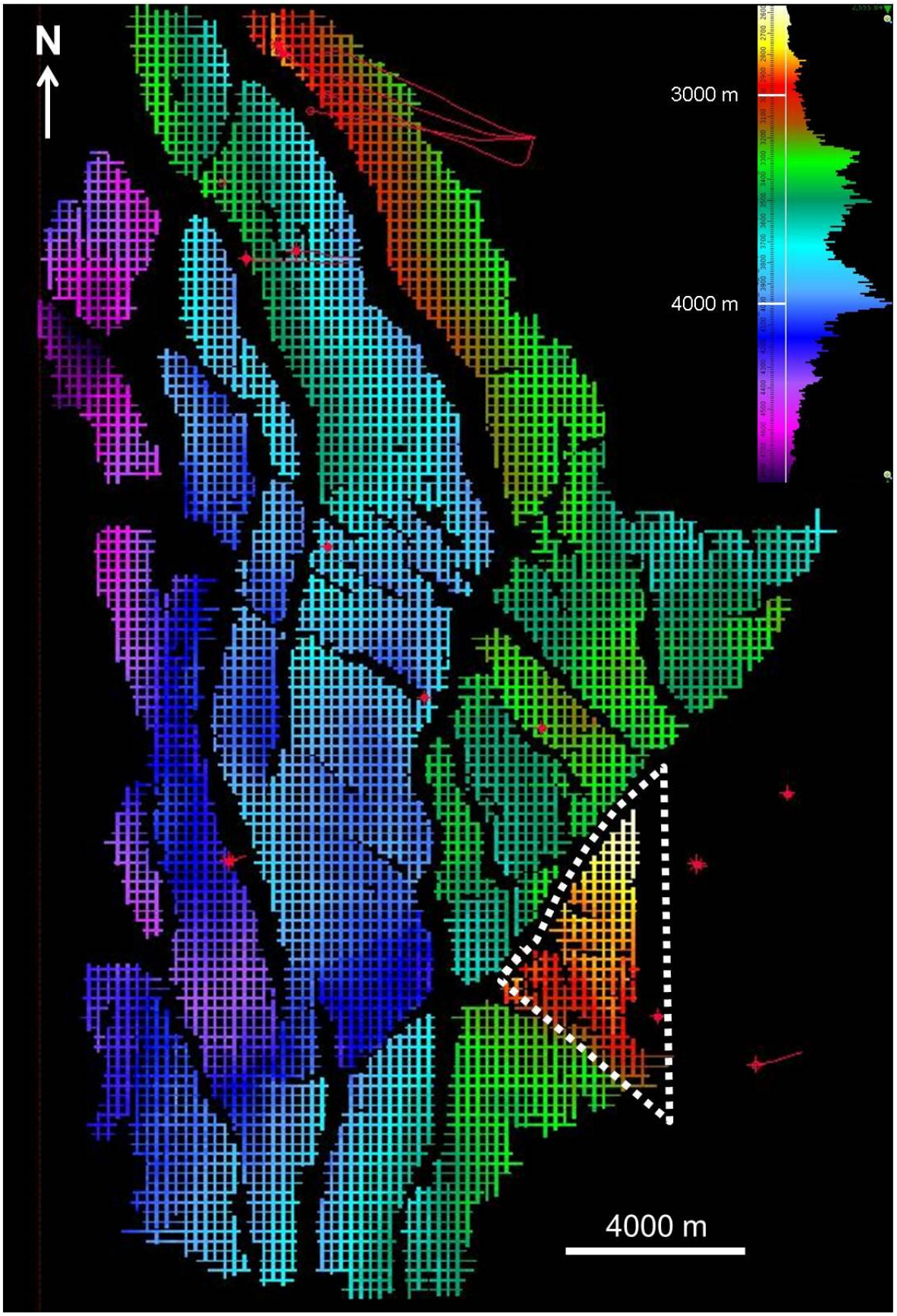

Figure 33: Middle Statfjord Formation structural map. Note the absence of interpretation over the J structure, with the interpretations in the dashed area representing uncertain picks. Spacing between lines is 50m.

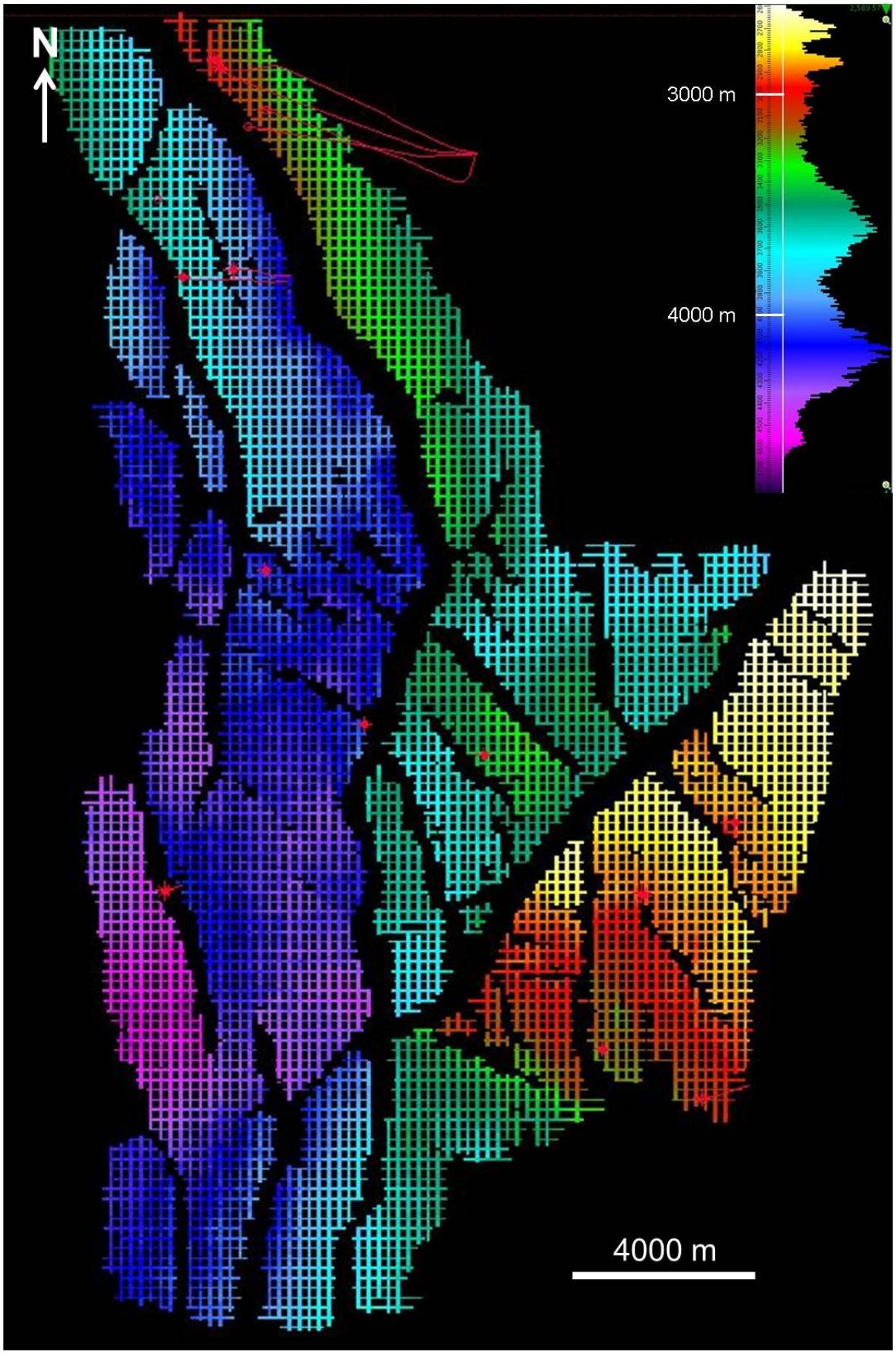

Figure 34: Base Statfjord Formation structural map. Spacing between lines is 50m.

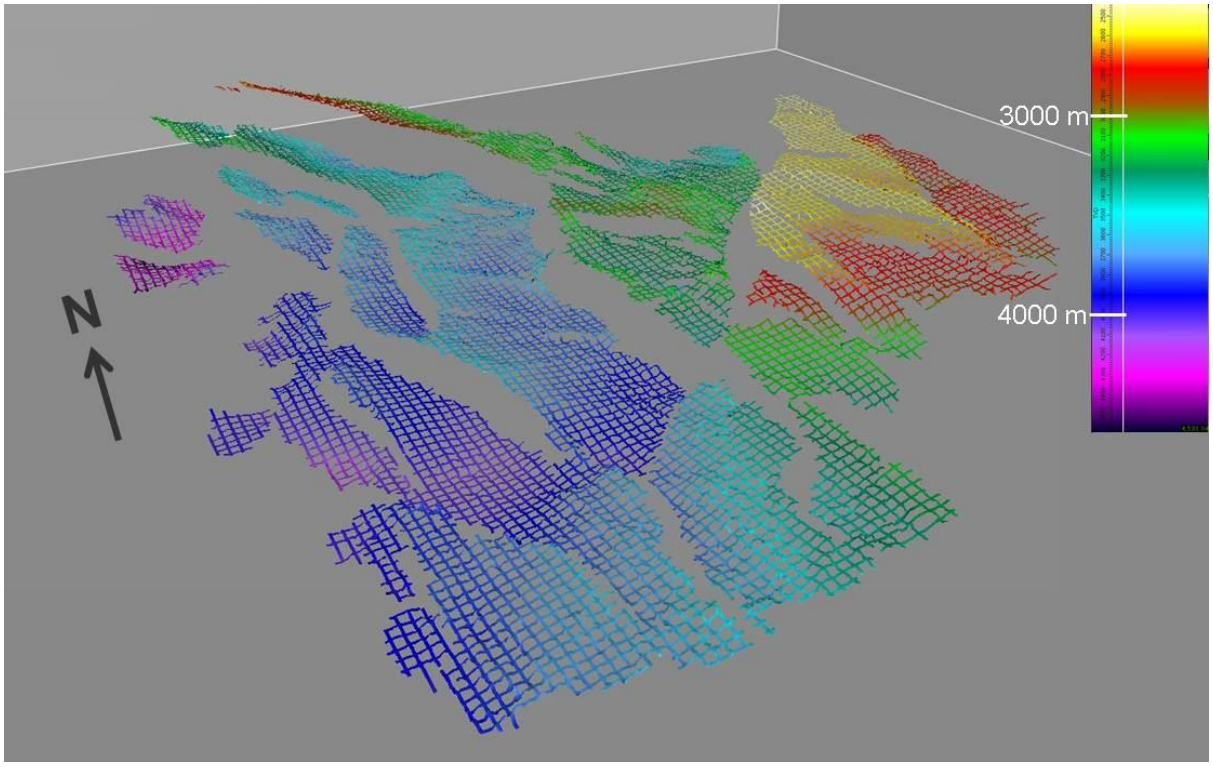

Figure 35: The Top Statfjord Formation reflector visualized in 3D.

5.8 Framework Generation

After creation of all of the horizons and faults, the data were input into a framework within the Decision Space software program. The horizon depth points were converted into a surface that extrapolated all of the points in between. The framework was best viewed in 3D, and provided a quality check for any mis-ties in the data (generally seen as large spikes), as well as an overview of each of the surfaces.

An important part of this framework was reviewing all of the faults and evaluating and defining their relationships with one another. Table 6 shows a list of the faults and associated relationships.

Table 6: Faults and their associated relationships. Bold faults indicated 'master' faults, which generally truncated the other faults.

Fault hierarchy			Status
Brage			
	J1		Truncated
	J4		Truncated
	J5		Crossing
	C1		Truncated
	C2		Truncated
	J6		Truncated
	C4		Truncated
J3			
	J2		Crossing
		J3	Truncated
Oseberg			
	Omega1		Truncated
	Omega2		Truncated
	C1		Truncated
	K		Truncated
	K1		Truncated
	C4		Truncated
Omega			
	B		Truncated
		B1	Truncated
	Omega1		Truncated
	Omega2		Truncated
K1			
	K		Truncated
J6			
	J1		Truncated

5.9 Depth Correction

The entire seismic volume has been pre-stack depth migrated. Nevertheless, the actual depths of the seismic horizons do not match the depths at which the formations are encountered within the true well data. As a last step prior to exporting the horizons to RMS for modelling, and to also quality check the interpretations, all of the grids from the interpreted horizons are imported into the depth correction program EasyDC.

Several options are available to depth shift the grid depending on the situation. Three of the possibilities (factor only, shift only, and factor & shift) were tested to determine which process best fit the data. The shift only method is used when there is a bulk shift required for all of the data (e.g., all the data is consistently off by 50 m, and thus a 50 m bulk shift could be applied), whereas the factor only method adjusts the grid to the well data when the differences in the data vary. After adjustment, a plot of the well tops versus the grid depths is plotted, giving a quality check on the adjusted data (Figure 36). In the case of the Top

Statfjord horizon, after multiplication of the horizon by the function Y = 0,9686*X + 92,02, the R^2 value of the original vs. adjusted data was 0,9993. Figure 37 shows a bar graph of the initial differences between the Top Statfjord horizon depths, compared to their actual values in the well data (blue bars). The residuals that remain after the function adjustment are seen in red in the same figure, where differences up to 40 m are still present. Within EasyDC, this is further corrected using mapping functions to further adjust the horizon to the true depth leaving only very small corrections remaining (Figure 37; green bars). However, when exporting this horizon to RMS, the grid that has only been adjusted by the function is used, meaning that it still needs to be properly depth corrected in RMS.

Both the Middle and Base Statfjord Formation surfaces fit closely with the well data, although fewer wells were available for correcting each of the surfaces. For the Middle Statfjord Formation, only four wells were used to adjust the grid, and only three were used for the Base Statfjord Formation grid. Wells within the J structure were not included with the Middle Statfjord Formation correction as the horizon was not interpreted on this structure due to its high degree of uncertainty.

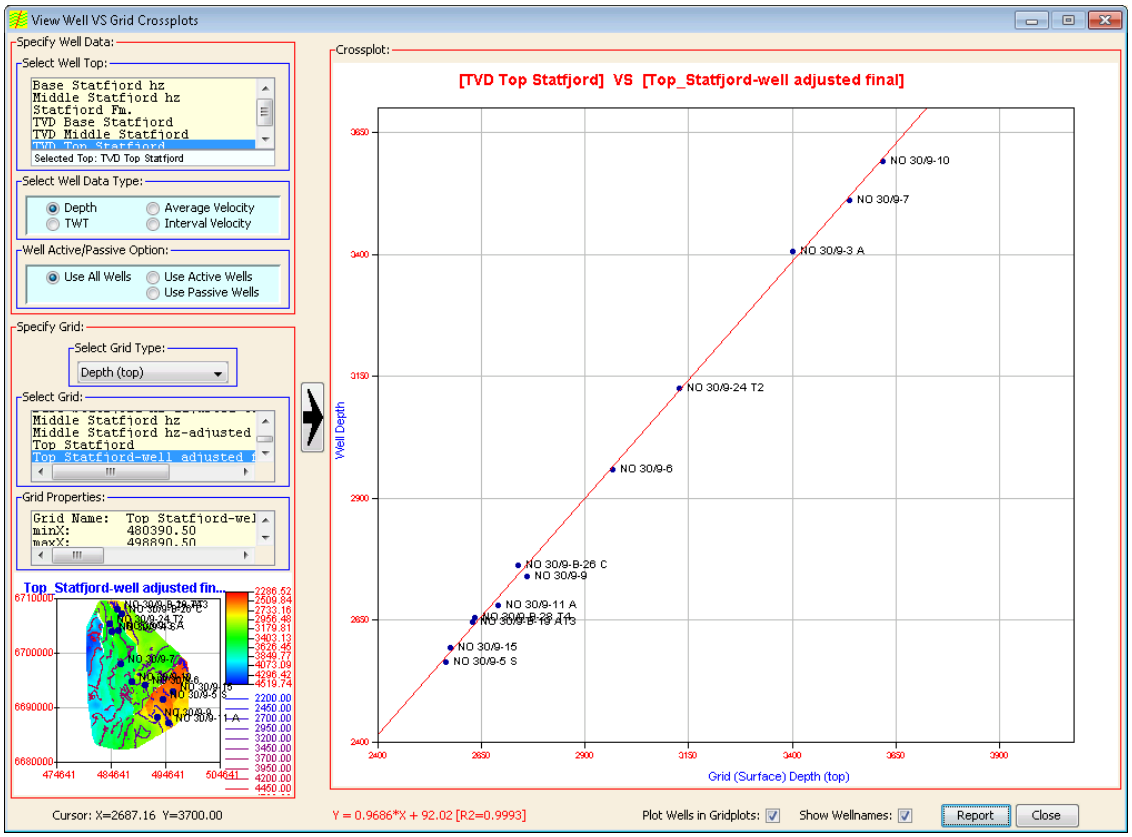

Figure 36: Cross-plot of well picks (y-axis) and grid surface (x-axis) of the Top Statfjord horizon.

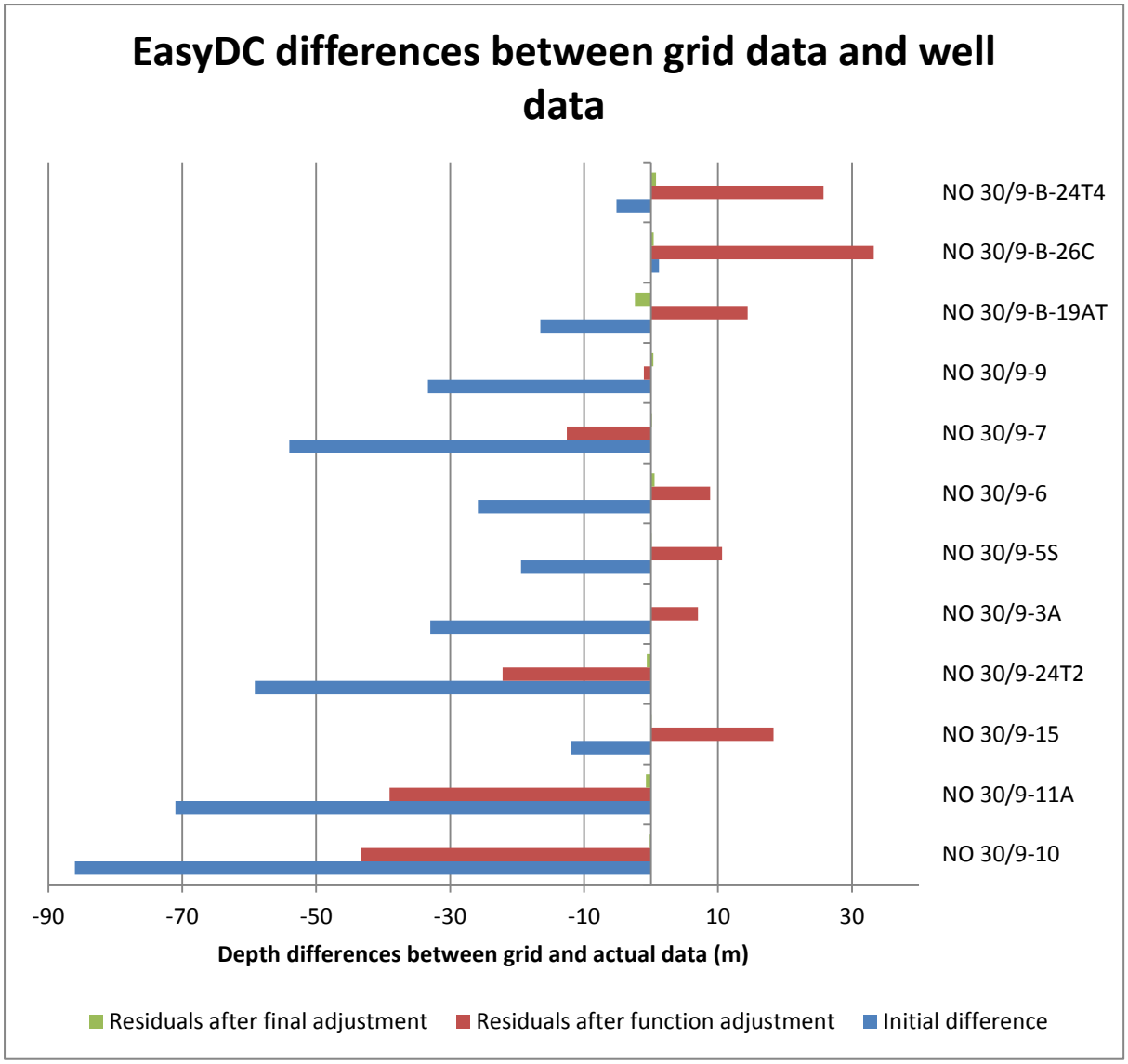

Figure 37: Graph showing the differences between the grid data and the well pick data before adjustment (blue), after the function adjustment (red), and after the final adjustment (green). Note that very little data is visible after the final adjustment as all the remaining errors were less than 2,5 m.

6. Modelling

Several data import steps are required before structural and horizon modelling can take place. The data imports include:

- Depth adjusted grid from EasyDC
- Well tops
- Petrophysical logs (Gamma Ray, Density, Neutron, Deep Resistivity, and Medium Resistivity)
- Fault framework
- Well deviation surveys

A critical step in the beginning of the project is defining the stratigraphy that will be used in the project. The naming system used for horizons in Stratworks is different from the horizon names used when interpreting seismic, and thus a common naming system needs to be created. Table 7 shows a summary of the naming system within Stratworks and Decision Space, and the resulting common scheme that was used in RMS (see also Figure 38). It is important to note the classification on each of the surfaces, where the interpreted horizons represent horizons that were interpreted from the seismic data, and the calculated horizons that will be created from well picks.

Table 7: Summary of the names of well picks, seismic horizons, and their equivalents in the RMS model. The name of the isopach layers is also included.

Stratworks	Seismic Horizons	RMS Horizons
Statfjord Fm.	Top Statfjord	Upper Statfjord
		Isopach – Upper Statfjord
Eiriksson Mbr.		Eiriksson
		Isopach – Eiriksson
Statfjord Middle Fm.	Middle Statfjord	Middle Statfjord
		Isopach – Middle Statfjord
Statfjord Lower Fm.		Lower Statfjord
		Isopach – Lower Statfjord
Lunde Fm.	Base Statfjord	Base Statfjord

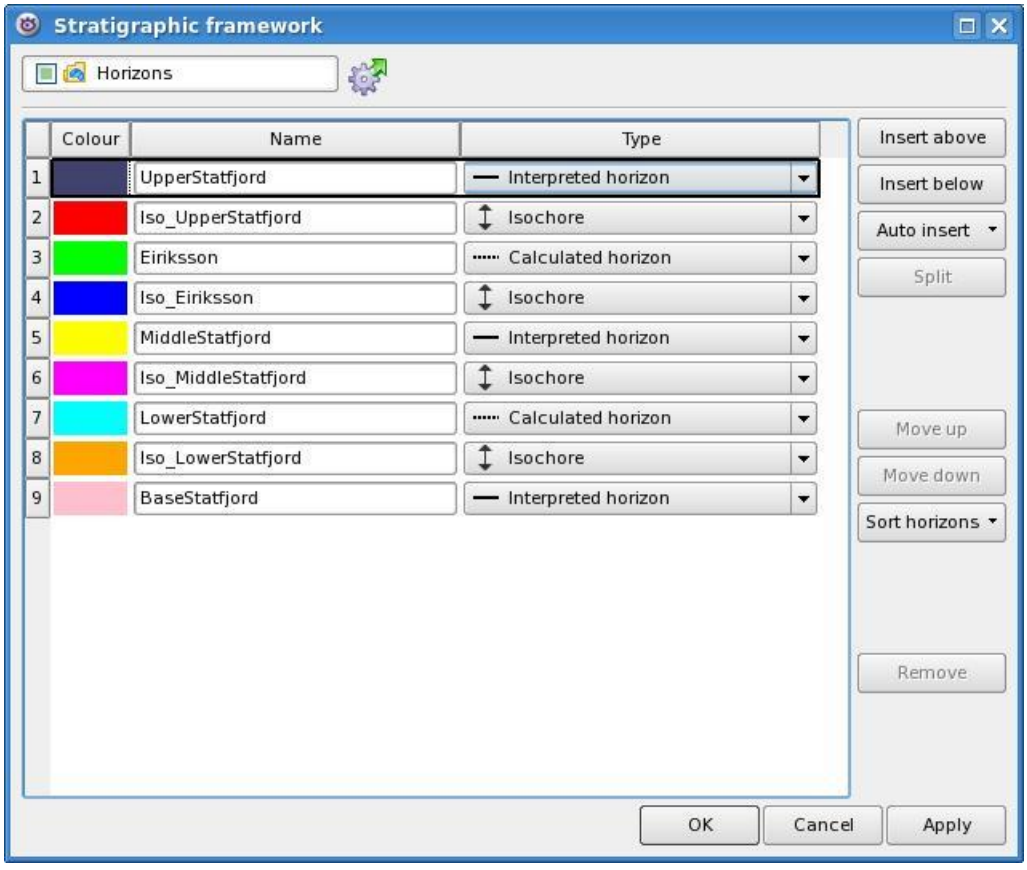

Figure 38: The stratigraphic framework within RMS.

6.1 Horizon Modelling

The first step in horizon modelling is creating surfaces for each of the depth adjusted grids that were imported from EasyDC. Recall from depth adjusting the grids in Easy DC that some depth differences remained between the well data and the grid data. In this step of horizon modelling, the created surface is forced to match perfectly to the well data, with the input and output results shown in Figure 39. Note that there is zero error remaining in the output status after this adjustment has been performed. An example of the adjusted surface is shown in Figure 40.

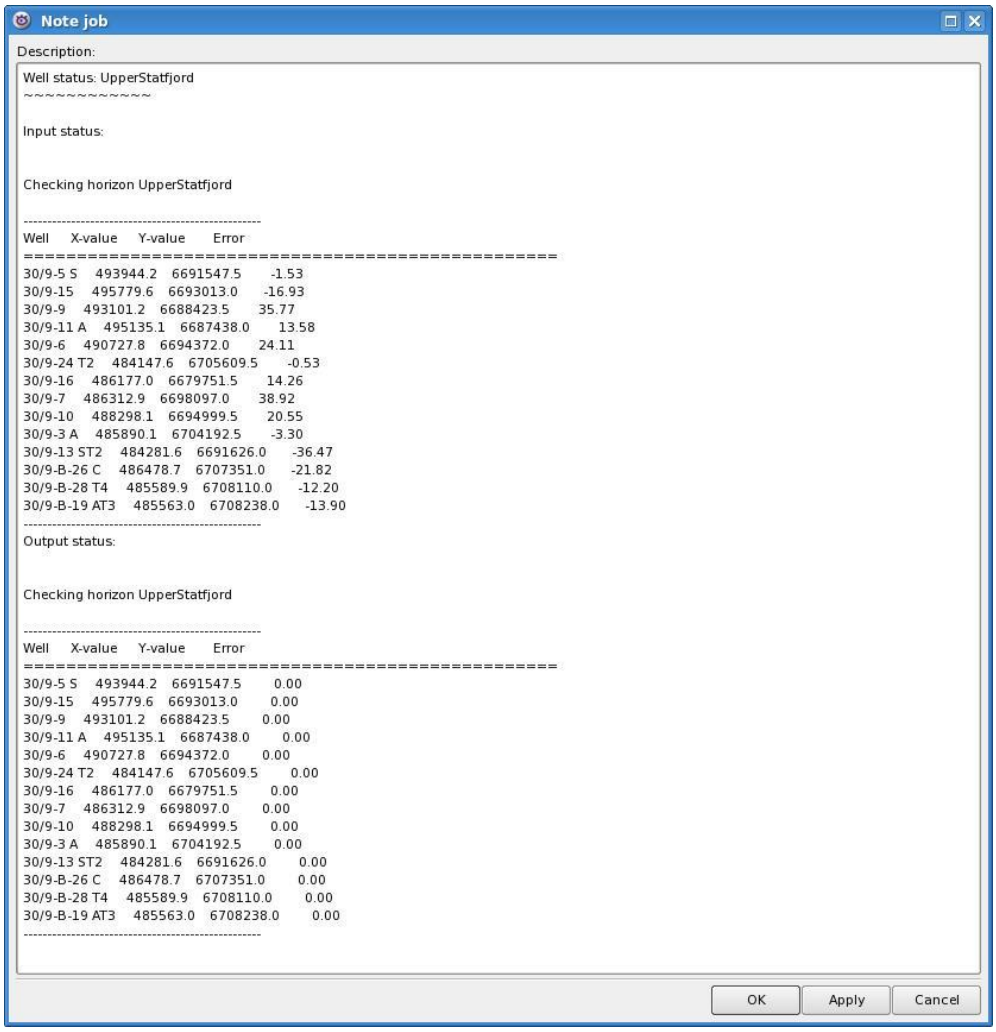

Figure 39: Grid vs. well data input errors are seen in the top table, with the lower table showing that the surface has been adjusted appropriately to the well data.

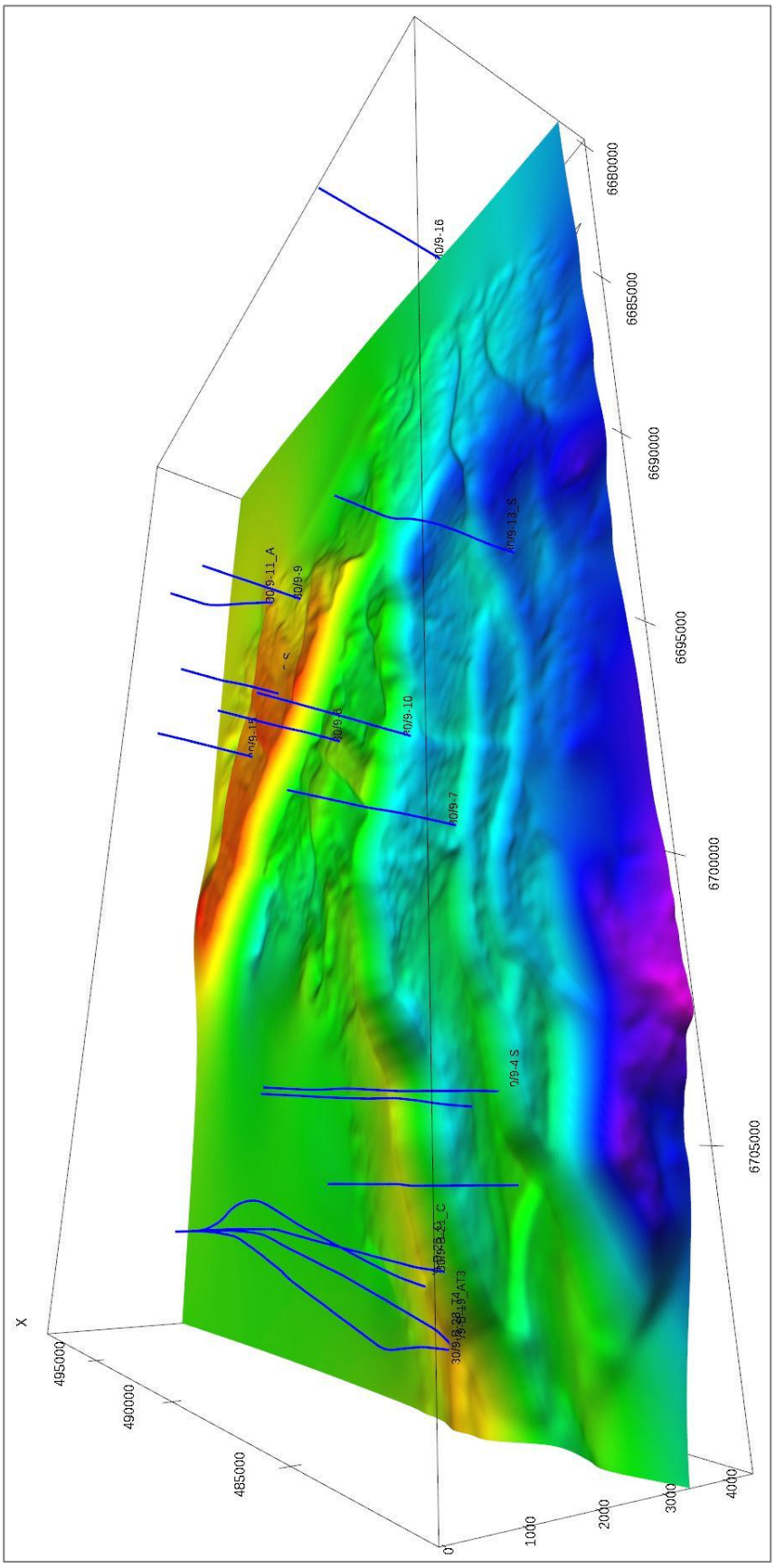

Figure 40: 3D image of the Upper Statfjord horizon after adjustment to well data. The view is towards the ESE. Hot colours represent highs, cold colours represent lows.

6.2 Structural Modelling

The quality control on the faults that was performed within the Decision Space framework helps to simplify the structural modelling process, however, there is still some quality control and editing that needs to be performed. Visualization of the faults in 3D is the simplest way to evaluate editing that needs to take place. RMS allows the user to edit the fault plane (e.g., extend horizontally, extend vertically, or smooth the surface) if necessary, and once the user is satisfied with the configuration, the fault relationships must again be defined within the program (i.e., crossing or truncated).

Once the fault relationships are defined, the next step is to edit the depth adjusted surface so that the interaction between the fault surface and the horizon is correct. As was seen earlier in Figure 40, the adjusted surface does not take into account the gap created by the fault plane, and simply treats this plane as a very steep surface. Figure 41 ('Before') demonstrates that when the fault (dashed lined) is reintroduced, the surface appears to drag up the side of the hanging wall, and down the side of the footwall.

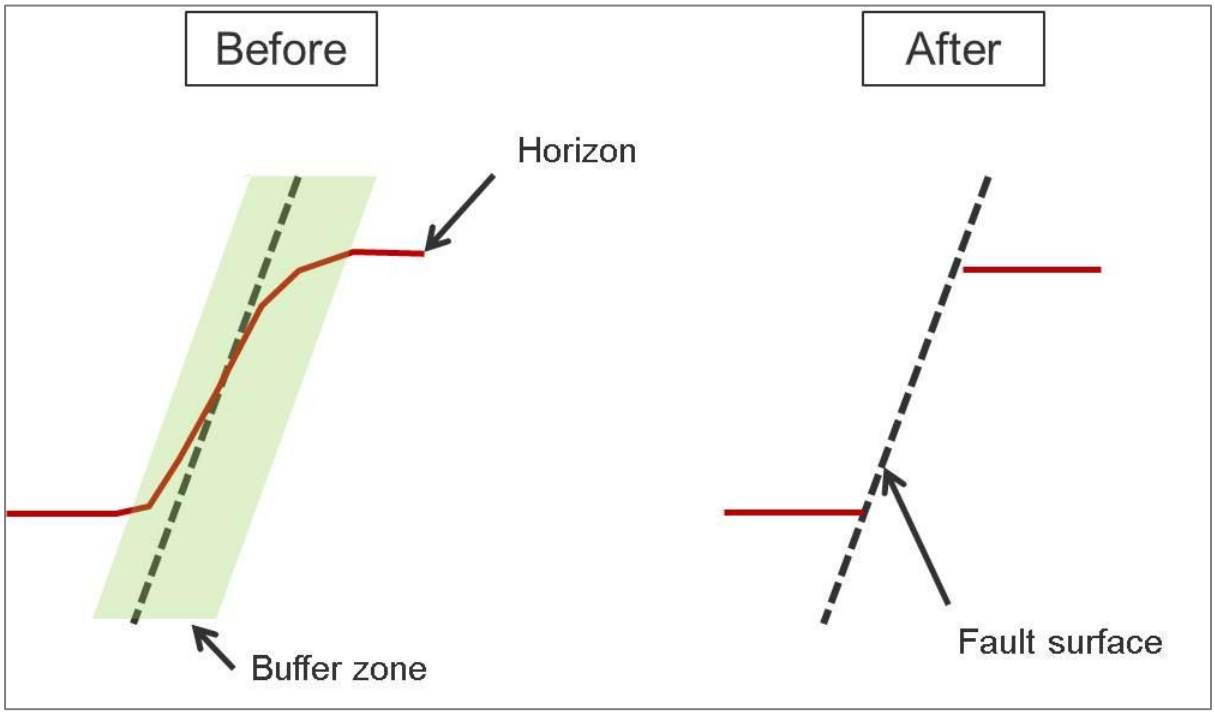

Figure 41: A schematic demonstrating why buffering and editing of the adjusted depth horizon in RMS is necessary. Note that the buffering distance can be different on the footwall and hanging wall.

The interaction between the surface and the fault is now incorrect, and shows dragging along the fault plane. In order to correct for this, a buffer zone is created on either side of the fault where a specified length of the depth adjusted horizon is deleted. The distance

required to remove this dragging effect is different from fault to fault, but is generally greater on larger faults. The ideal relationship is seen in the 'After' diagram in Figure 41. However, even after removing much of the drag on the fault surfaces, some manual editing is required. Figures 42 and 43 show before and after examples of manual editing on one of the surfaces, with the dragging effect removed. It is important to note that on some of the major fault planes, dragging of the horizon is a feature that is seen in the seismic, and it should not be removed from the model as it accurately portrays the horizon. These edited horizons are placed into a new output surface, labelled as 'filter surface data.'

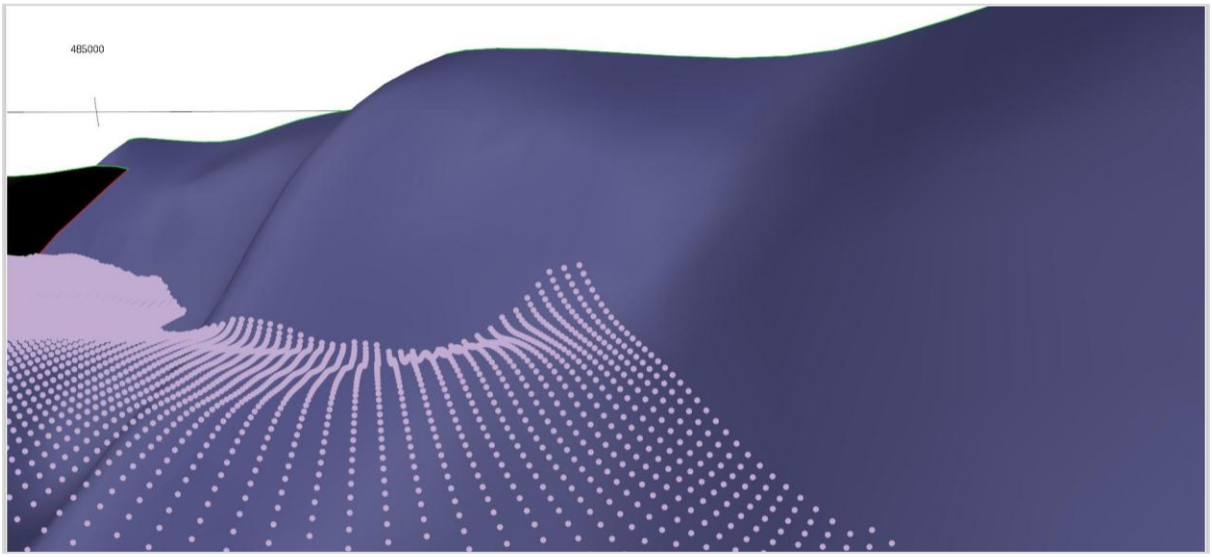

Figure 42: The dragging effect is evident on the dotted light purple points that represent the surface. The fault is dark purple.

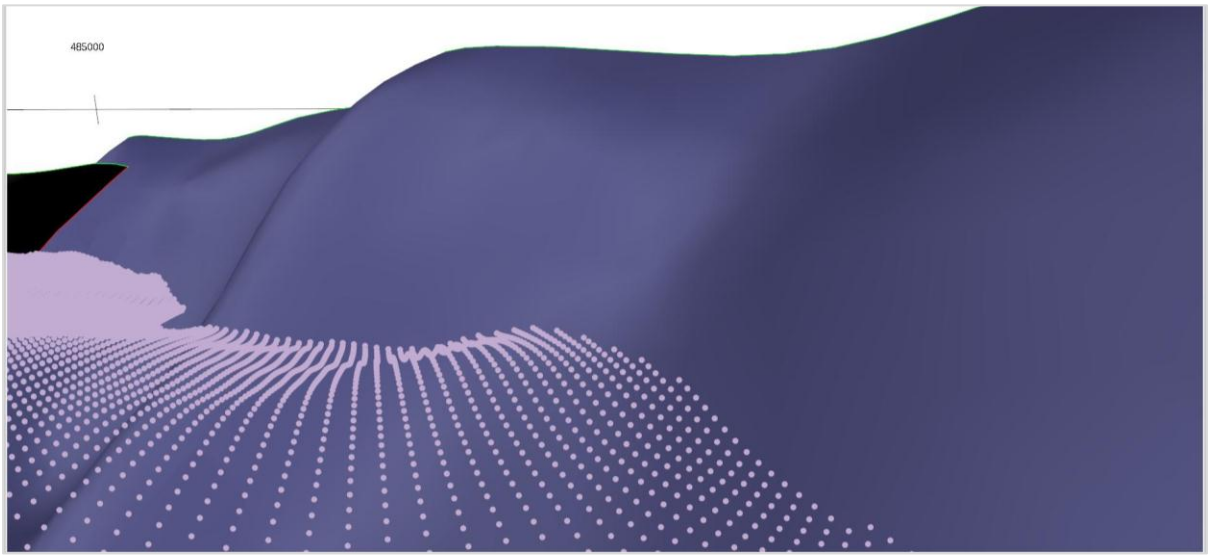

Figure 43: After manual editing, the relationship between the fault and horizon is now more appropriate.

After editing of the surfaces is complete, the full horizon model can be built, which will include creating the surfaces for the calculated horizons (i.e., the Eiriksson Member and Lower Statfjord Formation), and their associated isochores. This process is relatively simple, and first requires defining the lowermost horizon (Base Statfjord Formation), and then proceeding creating the isochores and output horizons based on the well data and the filtered surface that was just created (Figure 44). The resulting output horizons can now be viewed across the field and quality checked.

There were several problems that were noted when quality checking the resulting horizons. An expected problematic area was encountered over the J structure, where the Middle Statfjord horizon had not been interpreted on seismic. The lack of an interpreted horizon meant that both the Middle Statfjord and Lower Statfjord horizons exhibited strange and incorrect geometries. Figure 45 shows a west-east cross section of the modelled horizons through well 30/9-5S in the J structure. The modelling does a reasonable job in visualizing the expected thicknesses of the horizons throughout the same block 30/9-5S is located on, but in the right of the figure, it is evident that the lack of an interpreted Middle Statfjord horizon has created some incorrect geometries in the neighbouring fault block.

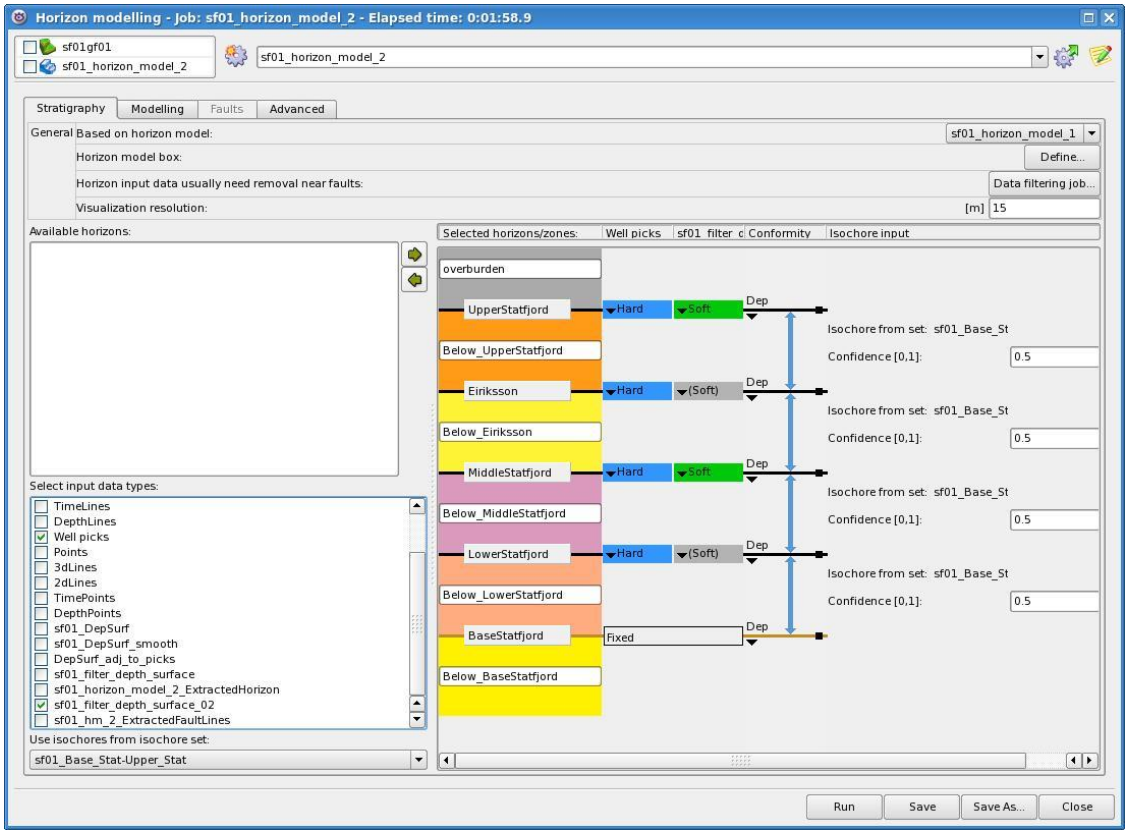

Figure 44: Creating the final surfaces and associated isochores.

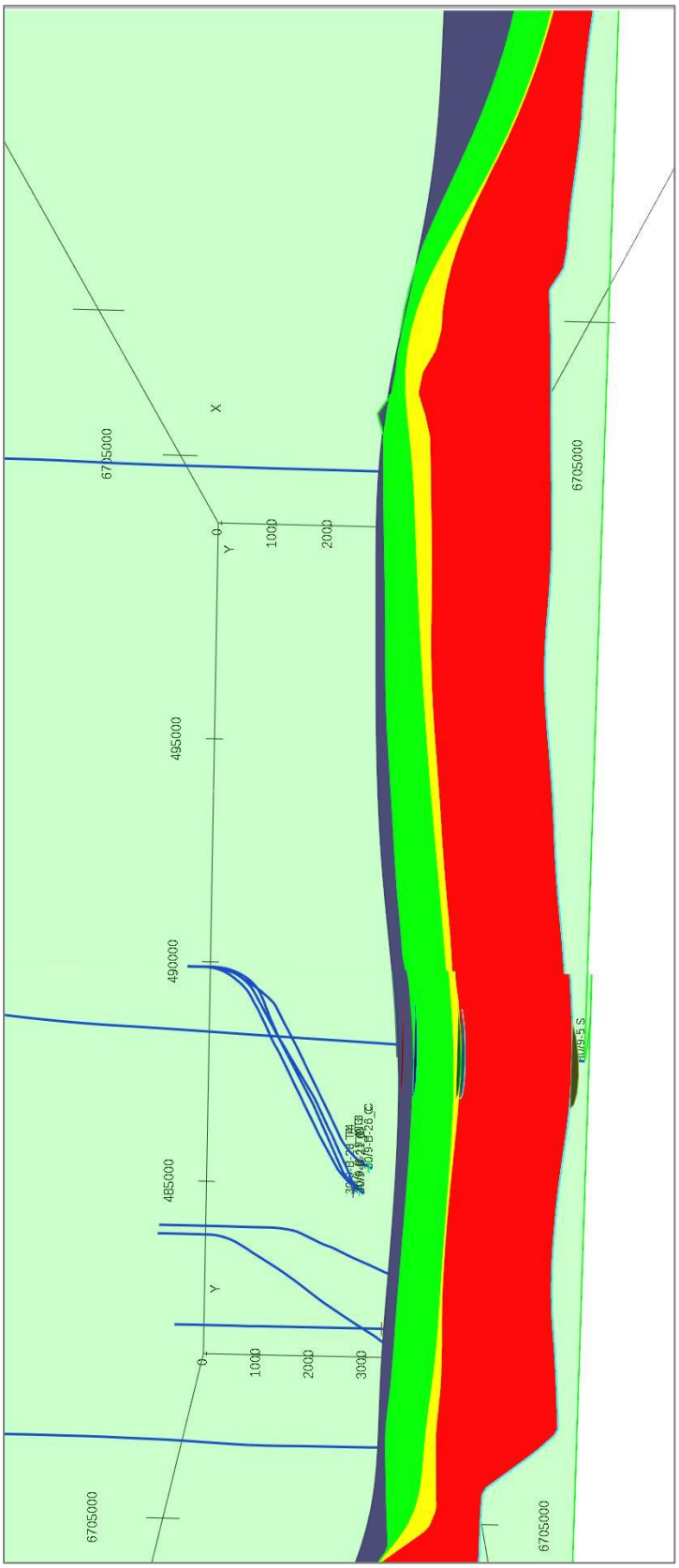

Figure 45: West to east cross section of the calculated horizons and isochores through well 30/9-5S in the J structure. Notice the unusual shapes of the isochore thicknesses in all of the horizons across the fault in the right of the figure. Red = Lower Statfjord isochore, yellow = Middle Statfjord isochore, green = Eiriksson isochore, purple = Upper Statfjord isochore.

Although the internal geometries of the isochores are incorrect over parts of the J structure, the overall isochore (from Upper Statfjord to Base Statfjord) displays expected geometries as they are constrained by the seismic interpretations. With this data, relative thicknesses of the formation can be compared across the field.

Another problem was discovered regarding well 30/9-4S, a cross-section of which can be seen in Figure 47, with problematic areas circled in Panel A (section is looking south, east is on the left, west is on the right). In the immediate vicinity of well 30/9-4S, it is evident that the Upper Statfjord Formation and Eiriksson Member well picks are not being honoured in the horizon model, and are in fact located much deeper than the horizon modelling suggests. These picks were double checked on both the well logs and in seismic, and the likely problem was revealed in the seismic data. Figure 46 shows that well 30/9-4S appears to be located off of the crest of the Omega structure, and perhaps penetrated a small downthrown block that is not visible on the seismic data. As this fault was so small, it was neither mapped nor included in the reservoir modelling, which is likely the reason for issues with modelling around this well. Due to the lack of mapping associated with the fault, and the incorrect model that was created, it was decided to rerun all of the modelling to exclude data from well 30/9-4S. Rerunning the modelling also provided the opportunity to correct for another problem that is circled in the fault in Panel A (Figure 47). Residual dragging is evident on the surfaces adjacent to the fault, which should have been better corrected during the manual editing phase of this horizon.

After rerunning the modelling and re-editing the surface, the resulting output (Figure 47, Panel B), appeared more true to what is believed to be present. The exclusion of well data from 30/9-4S, as well as manual editing on the surface has resulted in a clean looking model. However, the exclusion of data also means that the model may not be entirely representative of what is present.

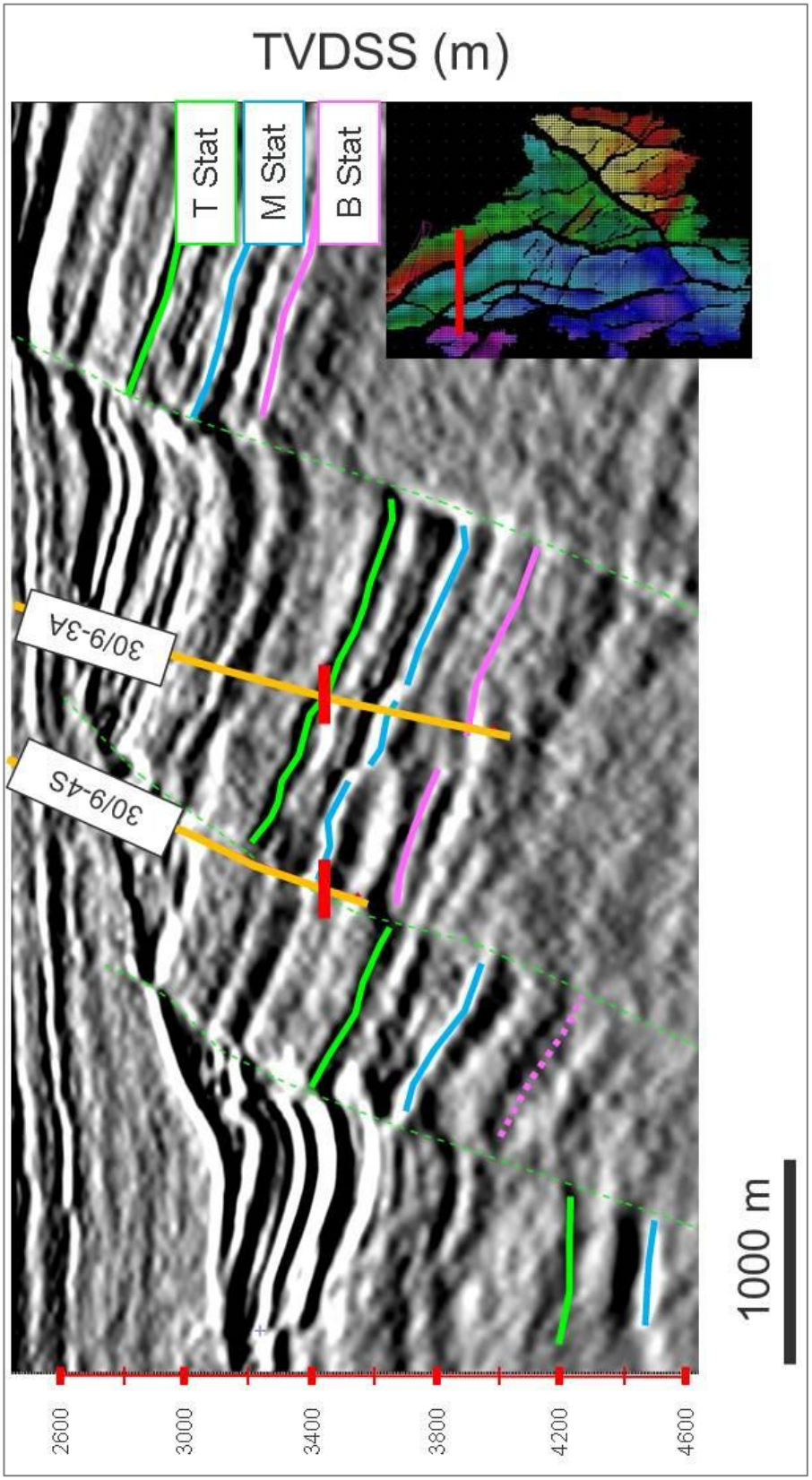

Figure 46: Seismic depth section showing the placement of well 30/9-4S with respect to the fault (section oriented west to east). The red markers indicate the well pick location for the Top Statfjord horizon. It is evident that 30/9-4S is likely located on a small, sub-seismic scale fault off of the western edge of the Omega structure. Note the strong Middle Statfjord reflector near the bottom left of the image which provides a good reference point where no tie is available for the reflectors.

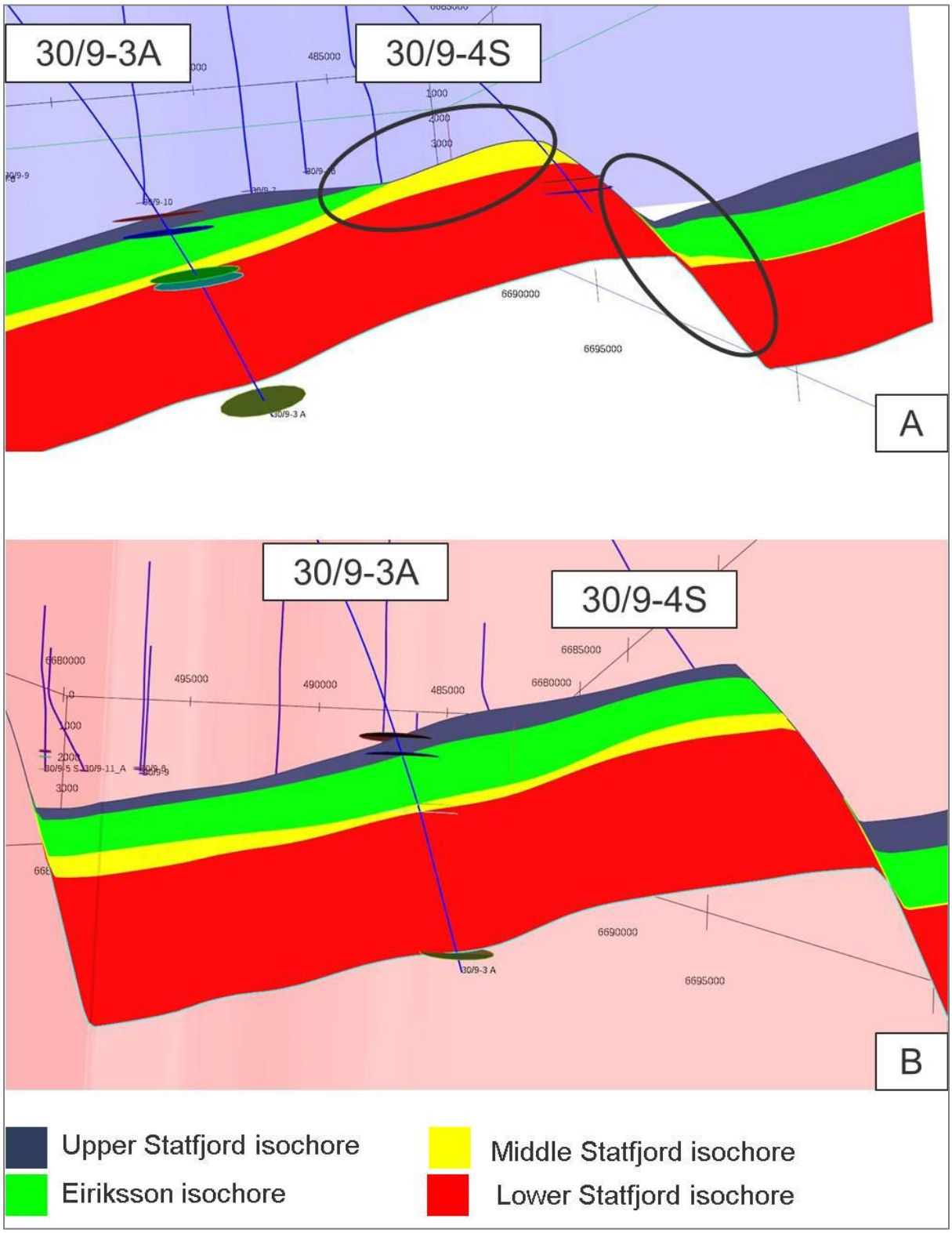

Figure 47: Panel A shows the horizon modelling prior to correction. Note that the well picks for the Upper Statfjord and Eiriksson have not been honoured in the modelling, and the remaining excessive drag located adjacent to the fault plane. Panel B shows the corrected model that has excluded well data from 30/9-4S, and where manual editing of the surface has removed the effects of the dragging against the fault. The section is looking south, with west towards the right, and east towards the left.

As a final step in the modelling process, an isopach map was created for the entire Statfjord Formation (Top Statfjord to Base Statfjord) to allow for easy visualization of the thickness changes that occur across the field, and in particular, if there are noticeable changes across the faults. Figure 48 shows the results of this mapping, with some important features noted. The cold colours (blue) represent thin areas relative to the warm colours (red). A trend of increasing thickness towards the west is visible, particularly across the Oseberg Fault that runs in a north-south orientation, which has been discussed in literature (e.g., Steel & Ryseth 1990). Thickness differences are also seen from the C structure to the J structure across the Brage Fault, however, the differences are not consistent along the length of the fault. Near the south-western portion of the fault, the thickness are similar, however, the Statfjord Formation appears to get thinner towards the northeast, with a large thickness variation across the Brage Fault at this location. This may suggest a rotational component of movement along the Brage Fault, with the northernmost portion of the J structure influenced the most by this movement. This thinning along the J structure is easily noticed in seismic (Figure 51).

6.3 Limitations and Uncertainties

There were some clear limitations with the modelling in areas where there was little data available. The modelling was best where the surfaces were based on interpretations on seismic, which was not the case for the interpolated surfaces in some areas. The most problematic area was in the J structure, where only the Top and Base Statfjord horizons were picked on the seismic data. The only information the program had available to model the internal layers was from the well picks in 30/9-5S. RMS did a good job at modelling all of the surfaces based on the well picks within the same structure, however, beyond that structure, difficulties arose in modelling these surfaces (Figure 45). Future modelling of this area will require a more detailed examination of the Middle Statfjord horizon, and how to ensure that the data is accurately represented. Despite the uncertainty with some of these horizons, the Top and Base Statfjord horizons were mapped well, and their thickness changes over faults and within fault blocks are useful in better understanding the structural evolution of the field. Both Panels of Figure 47 also show another issue that was present in some of the structures, also caused by the lack of data. Across the fault, the isochore thickness of the Middle Statfjord decreased to zero, which is not likely true considering its aerial extend across the field. In this part of the field, no wells penetrate the formation, and so these issues with internal layering are expected in the absence of data and would need to be corrected in the future.

The level of fault detail also created some issues when modelling the horizons, and resulted in the well 30/9-4S to be removed from the modelling surfaces. As mentioned earlier in this report, only the main fault surfaces were interpreted in order to keep the model as simple as possible, but also because it was thought that it could capture the bulk of the major movements within the field. This exclusion of data has demonstrated that perhaps more fault detail should be included in the model, as even the small faults have implications on the resulting structural model.

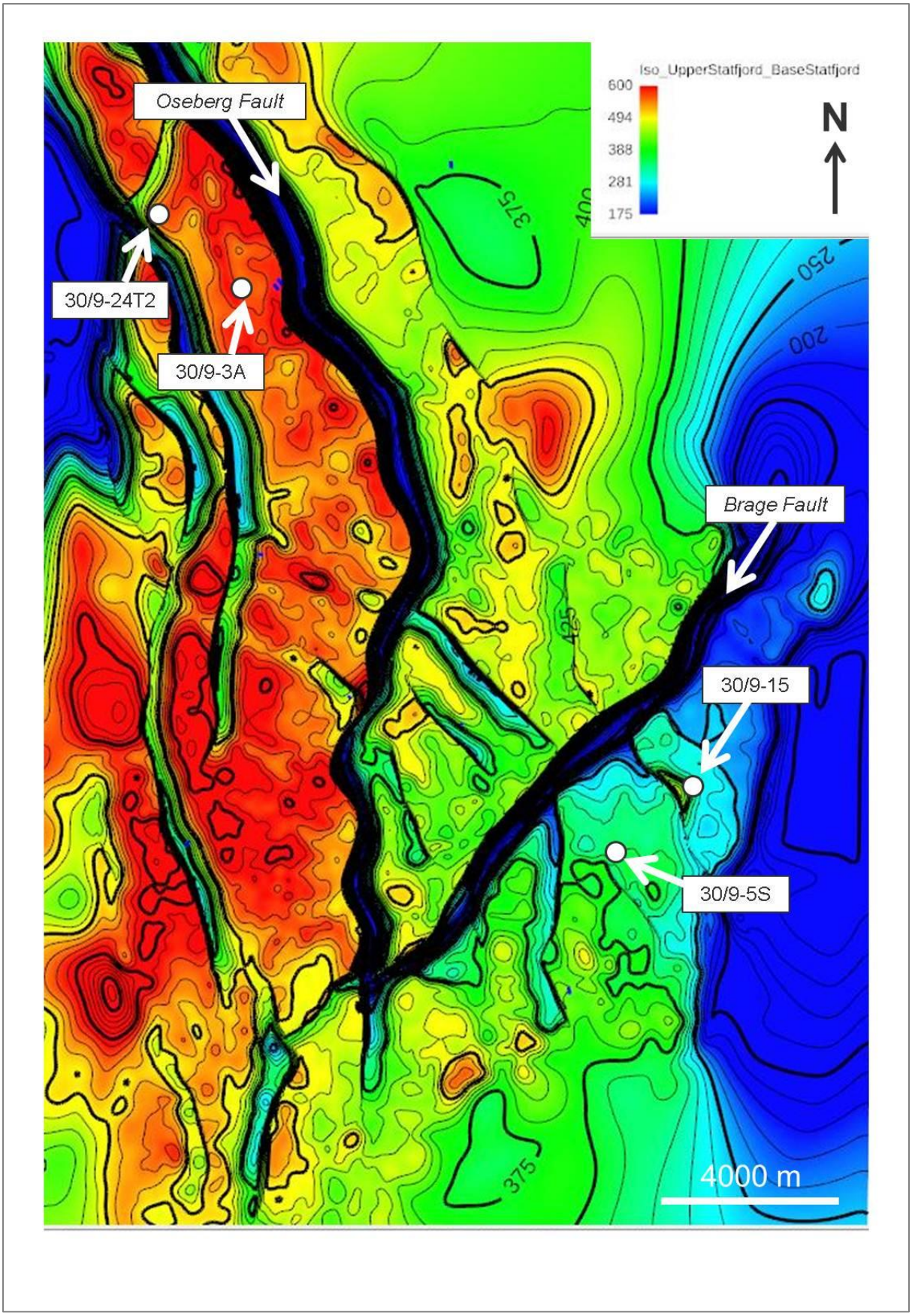

Figure 48: Isopach map of the Statfjord Formation from the RMS model, with select wells and faults highlighted.

7. Structural Interpretations

The Oseberg South field is dominated by north-south oriented faults that form the eastern edge of the Viking Graben. Although the general structural evolution of the Viking Graben is known on a regional scale, interpretations in this thesis show the variations present at a more local, field-wide scale. Several major faults cross-cut the field, with the Oseberg Fault roughly N-S oriented in the central portion, shifting towards a NNW-SSE orientation in the north, and the Brage Fault, which is roughly NE-SW oriented. Reports (e.g., Steel & Ryseth 1990, Færseth 1996, and Færseth & Ravnås 1998) have suggested that these faults were two of the more important faults during evolution of the Viking Graben, as well as during the Permo-Triassic rifting event. The Oseberg South field is located at the confluence of several structural domains, and while most of the faults are westward dipping, the polarity of the faults switches in the southern part of the field. In addition to the dominant faults, interpretations from depth seismic and from seismic tomography show that a series of northwest-southeast faults also cross-cut the field, something that has not been discussed in the literature. The high quality of the seismic data has allowed for more detailed structural interpretations to be made, and to also suggest the timing of faulting during the evolution of the field, and in particular, during deposition of the Statfjord Formation.

7.1 Fault development

Ryseth & Ramm (1996) have shown that subsidence rates within the basin played an important role in the structural architecture of the Statfjord Formation, and subsequently, its reservoir potential after burial. This suggests that understanding the structural evolution of the Statfjord Formation and how it has influenced the deposition of the formation is important for determining the location of the best quality reservoir throughout the field. These faults may also represent migration pathways or barriers during later hydrocarbon movement, but that aspect will not be discussed further in this thesis.

As mentioned earlier, evidence shows that two phases of rifting have affected this field: Permo-Triassic rifting, and mid-Jurassic rifting, which lasted until the Early Cretaceous. Both of these extension episodes were followed by post-rift thermal cooling and subsidence. Figure 2 shows a stratigraphic chart (modified from Færseth 1996) which shows the rifting events and their associated stratigraphy. In mapping the structural features of the Oseberg South field, this information was used to help guide some of the interpretations in the hopes

that it would be possible to classify faults according to their timing of initiation, and thus which phase of rifting the faults belonged to.

A map of all faults that were interpreted in the Oseberg South field is shown in Figure 55. There are some clear trends that are visible with respect to the faulting. Many of the large faults strike in a roughly north-south orientation, or a northeast-southwest orientation as seen in the faults that bound the J structure. The extension directions during both rifting events were both in a roughly east-west orientation, which is reflected in the strike of these major faults. However, a set of northwest-southeast striking faults cross-cut much of the field, but in particular the Omega, C, and J structures. The origin of these smaller faults and the reason behind their vastly different orientation from the major faults has not been discussed in the literature, but resulting interpretations suggest that they are related to the post-rift phases of both rifting events. The magnitude of the throw varies from fault to fault, and also within the fault (Figure 49, Panel B), generally decreasing in magnitude towards the south. Differential rates of subsidence and diachronism with respect to the initiation and cessation of faulting has been noted in the literature (e.g., Færseth *et al*. 1997), and is believed to have played an important part of the palaeography of the region during Statfjord deposition.

As the axes of the grabens for both rifting events were located on opposite sides of the Oseberg South field, it was expected that some of the major faults would exhibit opposite dipping orientations, namely towards the east during the Permo-Triassic rifting, and towards the west for the Jurassic rifting event. Figure 50 shows a West-East structural cross-section across the field, demonstrating the opposite dips on several of the faults.

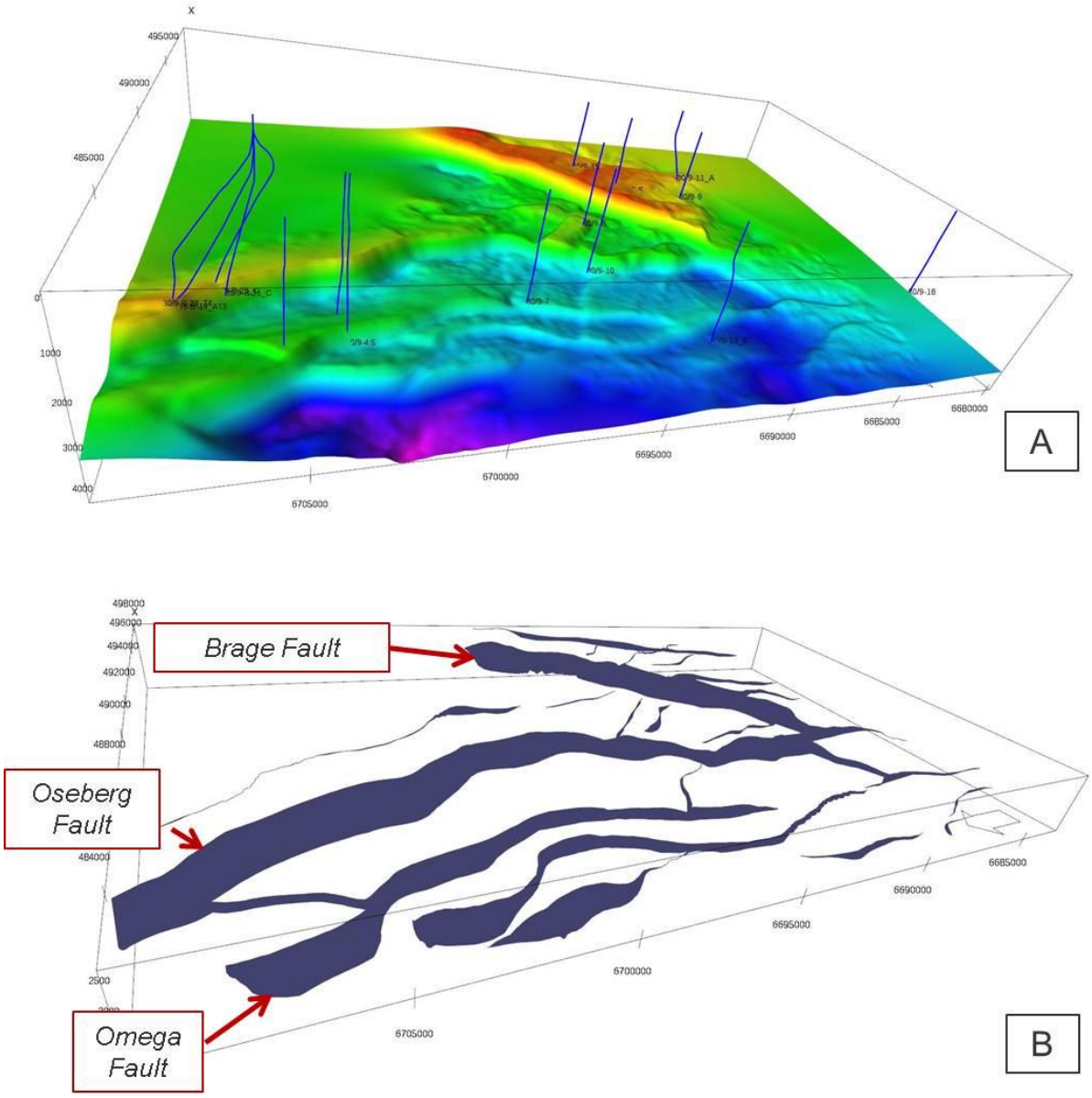

Figure 49: Panel A shows the top Statfjord structural surface from RMS, while Panel B shows the fault gaps present between the structures. Major faults are highlighted, and greater thickness in the fault gap indicates greater throw. Note the direction of the North arrow in the bottom right corner of the figure.

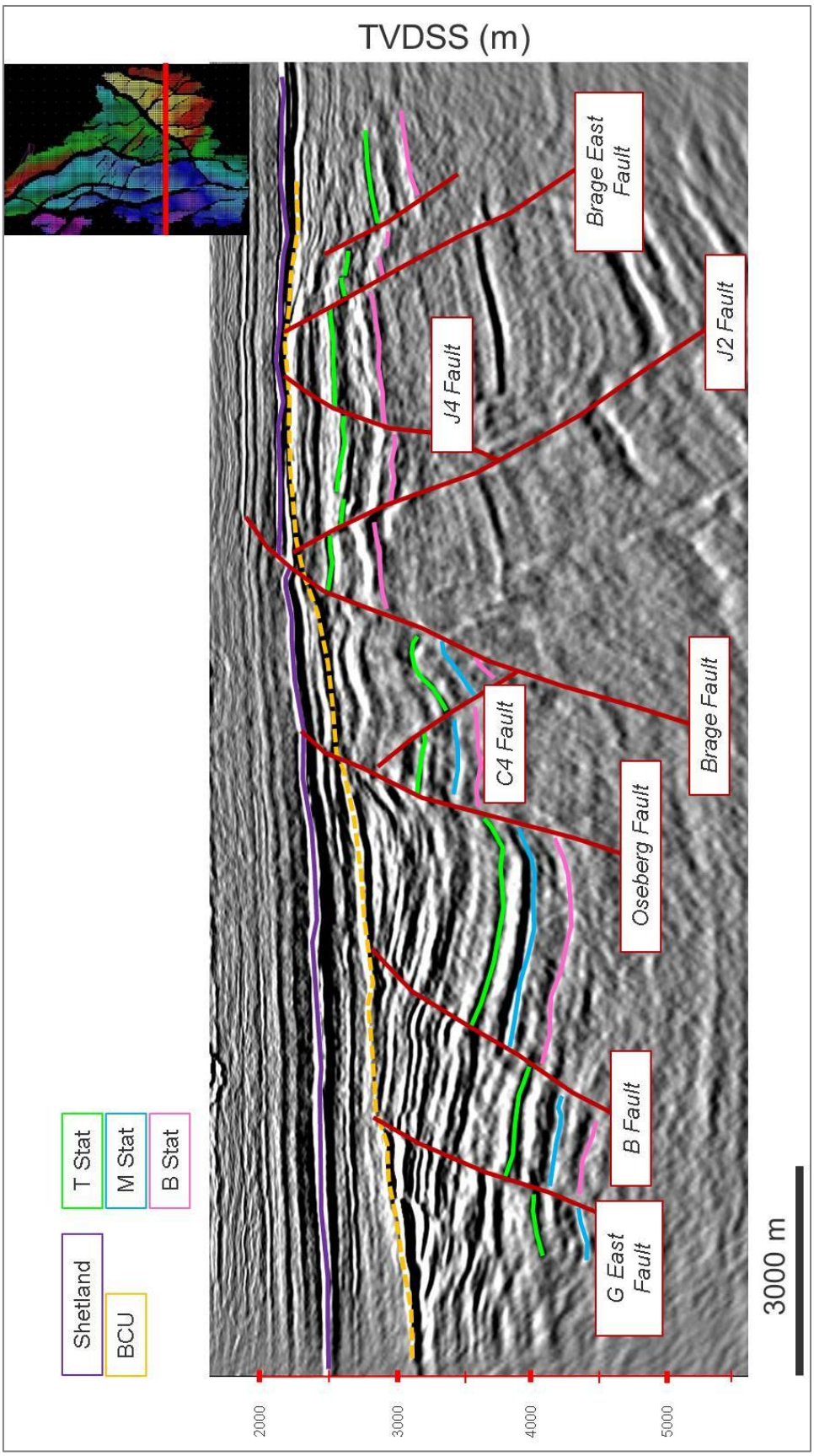

Figure 50: W-E structural cross section across the Oseberg South field. Note the deep, easterly dipping J2 and Brage East faults, and the westward dipping Brage and Oseberg Faults. Normal drag is seen on most horizons against the Oseberg Fault.

7.1.1 Permo-Triassic Faulting

Four major, east-dipping faults were interpreted in the J structure and C structure that were thought to have been initiated as a result of rifting in the Permo-Triassic. These faults include the J3 fault (likely equivalent to the Brage East Fault in the Oseberg South Field, and referred to as such in the interpretations, see Figure 9), the J2 fault, the J1 fault, and the C2 fault within the C structure (faults highlighted in Figure 56). All of the faults are deeply penetrating, as can be seen with the offset reflectors that are located well below the base of the Statfjord Formation in Figure 50. Regional literature (e.g., Færseth 1996) indicates that the axis of the Permo-Triassic graben is located to the east of the Oseberg South Field, underneath the present-day Horda Platform, with the Brage East Fault representing the westernmost boundary of the full graben. This major fault defines the eastern boundary of the J structure, and the presence of several other deep, easterly dipping faults in close vicinity of J3 fault shows that the edge of the Permo-Triassic fault blocks were heavily faulted at Oseberg South. All of the faults, with the exception of J1 show displacement in the reflectors past the Shetland Group level, indicating that not only were these faults initiated during the Permo-Triassic rifting event, but that they were also active well into the Cretaceous. Consistent with some of the other major faults in the field, two of the faults are roughly north-south oriented, however, two others are oriented in a northwest-southeast orientation.

7.1.2 Permo-Triassic post-rift thermal cooling and subsidence

This period of thermal cooling and subsidence of the crust was believed to have continued from the cessation of Permo-Triassic rifting, until at or near the onset of the mid-Jurassic rifting, 70 Ma later (Giltner 1987, Gabrielsen *et al*. 1990, Roberts *et al.* 1995, Færseth 1996). The continued subsidence after the main rifting event appears to have played an important role in the deposition of the Statfjord Formation. Steel & Ryseth (1990) demonstrated that rapid thickening of the Statfjord Formation was present across some of the major fault boundaries across the Viking Graben, including the ANH alignment, the Tampen Spur alignment as well as over a major fault that cuts in a north-south orientation across the Oseberg Fault Block. This fault is not explicitly named, but major thickening in the Statfjord Formation, as seen in the Statfjord Formation isopach in Figure 47, suggests that this fault was likely the Oseberg Fault. Other authors, e.g., Færseth 1996 and Færseth & Ravnås 1998, have also suggested that the Oseberg Fault was active during Statfjord Formation

deposition. Thickness changes were also seen across the Brage Fault from the J structure to the C structure (Figure 47). The thickness variations change along the strike of the fault, suggesting differential timing of fault movement, something that has been suggested in other major faults within the Oseberg field (e.g., Færseth *et al.* 1997). The timing of the fault suggests that its origin is related to the thermal cooling and subsidence of the crust after the cessation of Permo-Triassic rifting. The NW-SE strike of some of the faults suggests that the extension direction may have changed slightly during the post-rift subsidence, which may have just been a local phenomenon at Oseberg South.

The publications discuss the stepwise expansion of the Statfjord Formation across the major faults in the Viking Graben, but little detail has been presented with respect to thickness changes within the field itself. The OBC seismic at the Oseberg South field has revealed some thickness changes across minor faults within the J structure that suggest that minor faulting associated with post rift subsidence also played a role in the depositional architecture of the Statfjord Formation. Figure 57 shows the Oseberg and Brage Faults highlighted, as well as the numerous NW-SE oriented faults that cross-cut the J structure. These faults are also visible in a structural cross-section in Figure 51. In this figure, large, east dipping Permo-Triassic faults are visible (J1 and J2), and three graben structures are highlighted in green and are labelled A, B, and C. The J4 and J5 faults appear to be antithetic faults related to the J1 and J2 faults, respectively, with slight thickening of the sediments within graben A, and a noticeable thickening of graben sediments seen in graben B. A third graben, C, also displays thickening of graben sediments, but does not have a deep Permo-Triassic fault associated with the structure. The thickening of sediment in grabens B and C indicates that these faults existed during deposition of the Statfjord Formation, thus influencing its final thickness. Their timing with respect to influencing the Statfjord Formation deposition indicates that they were likely generated as a result of the thermal cooling and subsidence of the crust resulting from Permo-Triassic rifting. An overall thickening of the Statfjord Formation is also seen from the north-eastern part of the J structure, towards the southwest. This thickening trend was also seen in Figure 47, and may indicate differential movement of the Brage Fault throughout Statfjord Formation deposition. It may also have been a consequence of the westward paleo tilt that existed on the structures west of the Permo-Triassic graben (Færseth & Ravnås 1998). The strike of the antithetic faults within the J structure is consistently in a northwest-southeast orientation, similar to two of the major faults in the structure. The majority of these antithetic faults appear to show displacement in the reflectors up to the BCU level, indicating that they may have also played a role in the palaeogeography during the Brent Group deposition.

The interaction between the Oseberg and the Brage Faults is uncertain, but for modelling purposes, the Brage Fault has been interpreted to have been truncated by the Oseberg Fault, indicating that the Oseberg Fault was initiated first. The antithetic faults on the J structure are truncated by the Brage Fault, demonstrating the time relationships between the major faults during the thermal subsidence phase. From oldest to youngest: the Oseberg Fault, Brage Fault, antithetic faults on the J structure.

7.1.3 Mid-Jurassic rifting

The faults believed to have been initiated during the mid-Jurassic to Early Cretaceous rifting event are highlighted in red in Figure 58. The axis of the Viking Graben created during this rifting event is located to the west of the Oseberg South field, and regional data shows that the fault blocks on the east side of the graben average 15-20 km in width, separated by westward dipping faults (Færseth 1996). The westward dip of the faults and the down stepping configuration of the fault blocks towards the Viking Graben suggest that these faults resulted from mid-Jurassic rifting. Minor thickness changes have been observed across the Omega and B Faults at the Statfjord Formation level, however, it is unknown whether these thickness changes are a result of incorrect interpretation of the seismic, or whether they may indicate possible initiation of these faults during the Permo-Triassic post-rift period.

In addition to faults the faults believed to have initiated during the mid-Jurassic rifting, evidence shows that numerous older faults also showed signs of reactivation and movement (Figure 60), namely in the form of horizon drag. Horizons that sit adjacent to the Oseberg Fault show normal drag, which increases in magnitude from the Statfjord Formation to the Brent Group level within the section (Figure 50). Normal drag is believed to occur on faults with planar movement (Badley *et al.* 1984). The varying magnitude of the drag may indicate that the degree of movement along the fault has not been consistent over time. The lack of drag in layers above the BCU into the overlying Cretaceous section indicates that the bulk of the movement occurred prior to the unconformity event. Some slight reverse drag is present on reflectors against the Brage and Brage East Faults, which is believed to have been caused by rotational movement associated with listric fault movement (Badley *et al*. 1984). Detailed mapping of the Brent Group and any associated syn-rift sediments would increase the confident with respect to the timing of movement along these faults planes.

Difficulties arose when attempting to determine the origin of the Gamma Fault due to its location near the edge of the seismic data. However, its size and westward dipping

orientation suggest that it was likely initiated in either the post-rift phase of the Permo-Triassic rifting, or during the mid-Jurassic rifting. Fault drag is seen on some of the reflectors in the hanging wall of the fault up to the BCU level, indicated that although the initiation of the faulting is uncertain, it is evident that the fault experienced movement during the mid-Jurassic. Obtaining additional seismic data over this section and towards the east where no data currently exists would help to confirm thickness trends on the eastern side of the fault, and understand more about its origin.

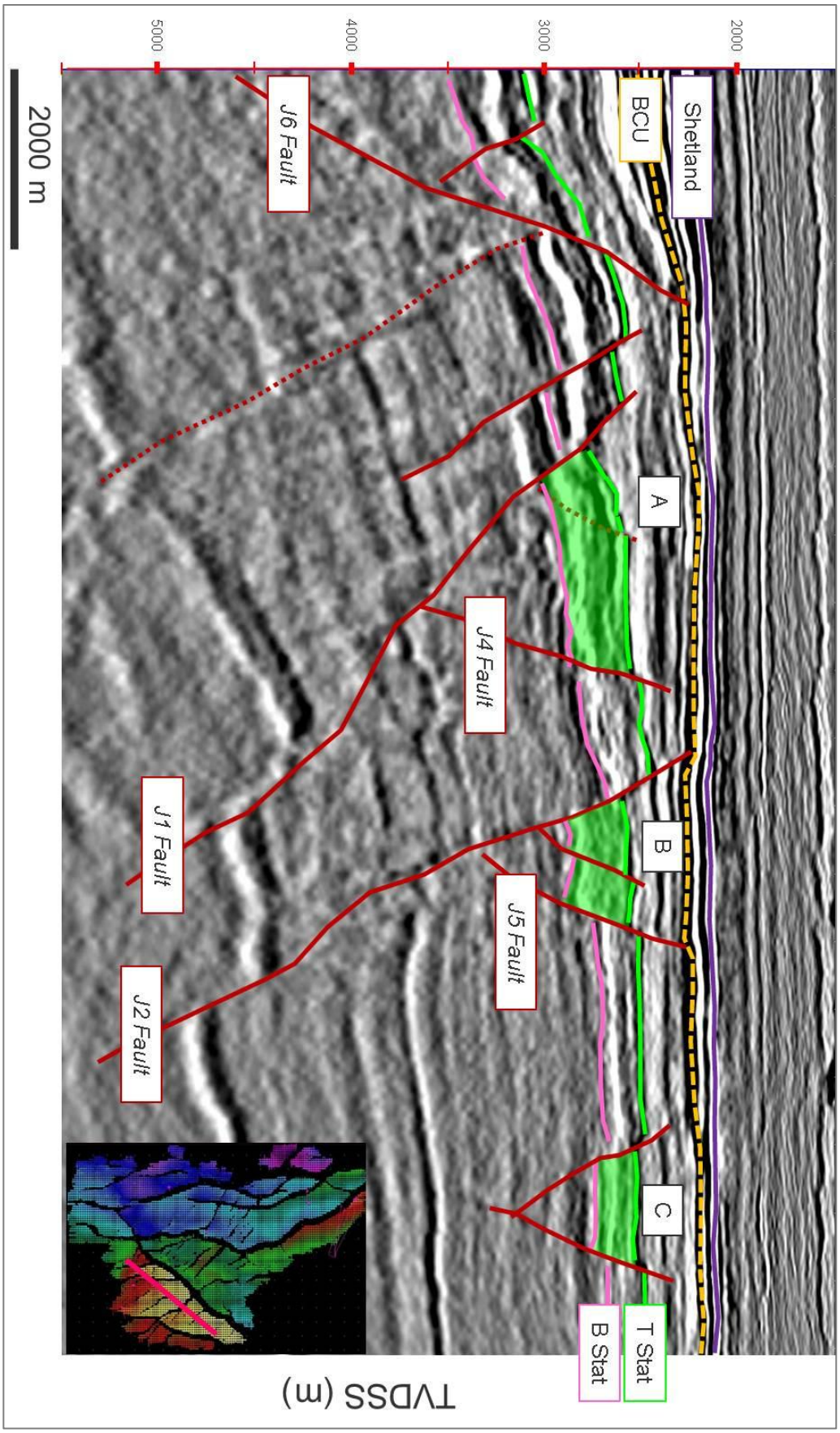

Figure 51: SW-NE oriented structural cross-section through the J structure. Labels A, B, and C refer to graben structures highlighted in green.

7.1.4 Mid-Jurassic post rift thermal cooling and subsidence

A series of NW-SE oriented faults were interpreted within the Omega and B structures of the field (Figure 58) that are believed to have been initiated during subsidence after cessation of the mid-Jurassic rifting event. Figure 52 shows a cross-section through these faults, and it is evident that no syn-depositional sedimentation appears to be present at the Statfjord Formation level, and neither do the faults extend above the BCU. The faults have a strike direction similar to those within both the J and C structures, but the lack of syn-depositional sediments suggests that this series of faults was not created until at least mid-Jurassic time. While most of the secondary faults lie within the Omega structure itself, two of the faults cross the Omega Fault and into the B structures. While timing relationships can be difficult to determine from simple crossing features, the scale of the secondary faults compared to that of the Omega Fault suggest that they formed afterwards.

The effects that primary faulting had on the formation and distribution of secondary faults with a different extension orientation were performed by Henza *et al*. (2011). Some of the resulting geometries from that study are similar to what has been interpreted in parts of the Oseberg South field, and in particular the secondary faults seen on the Omega structure. Figure 53 shows the results from the clay modelling, and shows that the some of the secondary faults were completely constrained within the first order faults, while others crossed the existing faults. It was discovered that many of the secondary faults initiated from the sides of the primary fault, in some cases continuing across the fault. Several of the secondary faults in the Omega structure terminate against either the Omega or the Oseberg Fault (green circle in Figure 59), while two others also cross the Omega Fault. The similarities of the fault expression in the Omega structure and from the modelling suggest that the NW-SE trending faults were formed after the Omega and Oseberg Faults, and also with an orthogonal extension direction.

The timing of fault development seen on the C structure remains uncertain (Figure 61), namely due to the uncertainty surrounding the interpretation of the top Statfjord Formation reflector. As seen on both the Omega and J structures, the C structure is crossed by numerous NW-SE oriented faults that create horst and graben structures, and this configuration leads to the conclusion that the faults were likely a result of one of the subsidence phases of either of the two rifting events. Should the graben display signs of syn-sedimentary deposition, the faults could be associated with subsidence after the Permo-Triassic rifting event, however, should syn-sedimentary sediments be absent, then the faulting may have been initiated during subsidence following mid-Jurassic rifting. Figure 54

shows a cross-section from the C structure displaying both of the scenarios, with the solid green line showing the interpretation that was used for modelling (and thus assigns the faults as having been initiated during post mid-Jurassic subsidence), while the dashed green line shows possible syn-sedimentary sediments. Well 30/9-6 penetrates the top of a horst within the middle of the structure, but the nature of the reflector changes within the graben, making the well tie useful only on the top of the small horst structure. As was seen with secondary faults within both the J and Omega structures, only the largest faults in the C structure extend to the BCU level, and most pinch out several reflectors below this level.

Overall, interpretations from seismic data have demonstrated that four different fault generations can be identified in the Oseberg South field, belonging to the Permo-Triassic and mid-Jurassic to Early Cretaceous rifting events, as well as their respective post rift phases. The strike of the largest faults in the field was roughly north-south oriented, and these faults belonged to the two main rifting events. Additionally, two phases of smaller NW-SE oriented faults were discovered across the Omega, C and J structures. Syn-rift sediments within the Statfjord Formation in the J structure suggests that these secondary faults were a result of post-rift subsidence following the Permo-Triassic rifting, while the absence of syn-rift sediments in the Statfjord Formation in the Omega structure suggests that these faults were generated as a result of post-rift subsidence after the cessation of mid-Jurassic rifting. The origin of the secondary faults within the C structure is uncertain, namely due to uncertainty regarding the presence of syn-rift sediments. The presence of syn-rift sediments in the grabens at the Statfjord Formation level would indicate that these faults are likely to have been generated at the same time as those in the J structure. The absence of syn-rift sediments would indicate fault generation at the same time as those in the Omega structure, indicating an origin after cessation of mid-Jurassic rifting.

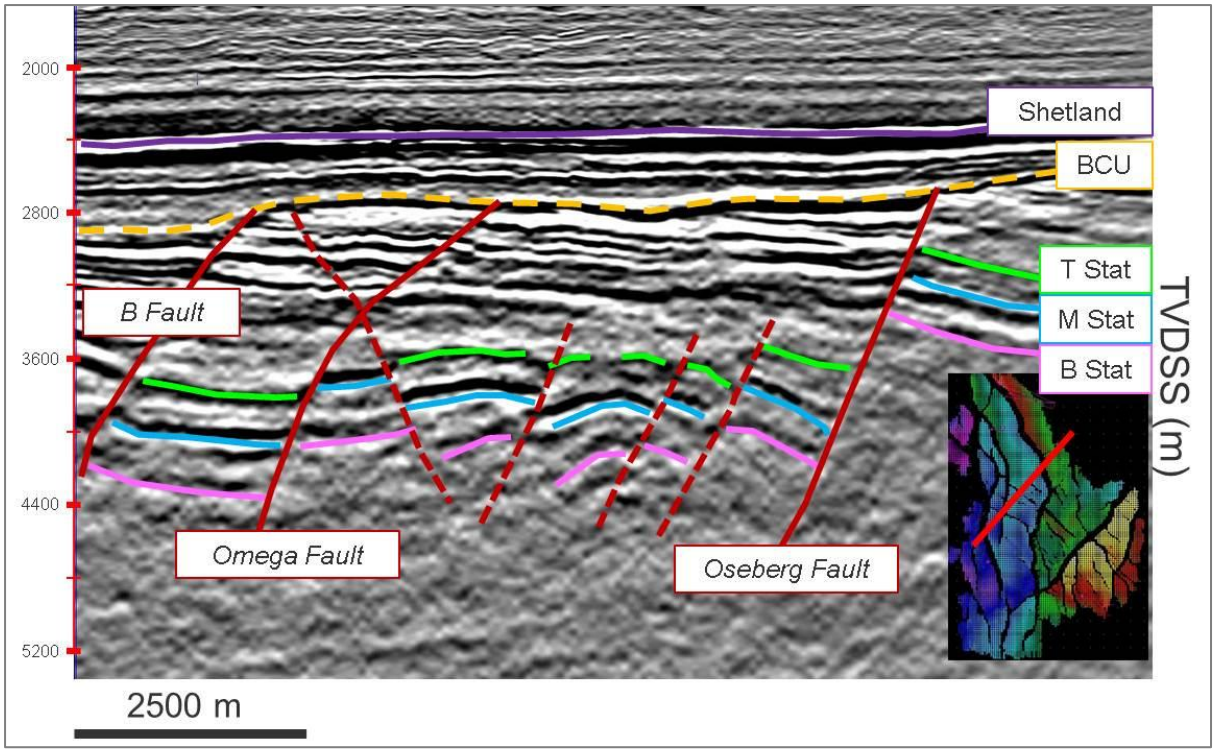

Figure 52: A SW-NE oriented structural cross-section across the Omega block. Dashed red lines indicate faults initiated post mid-Jurassic rifting. Note that one crosses the Omega fault, and does not continue past the BCU.

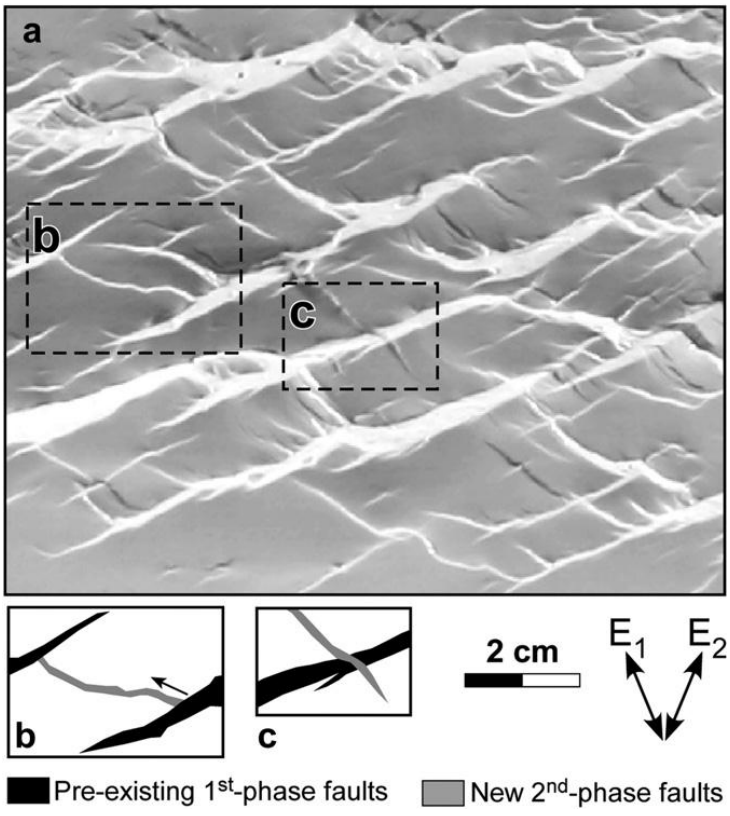

Figure 53: Results from clay modelling showing the interaction between first order extensional faults, and second order extensional faults with a different extension direction. This interacting geometry exists at the Oseberg South field (from Henza *et al*. 2011).

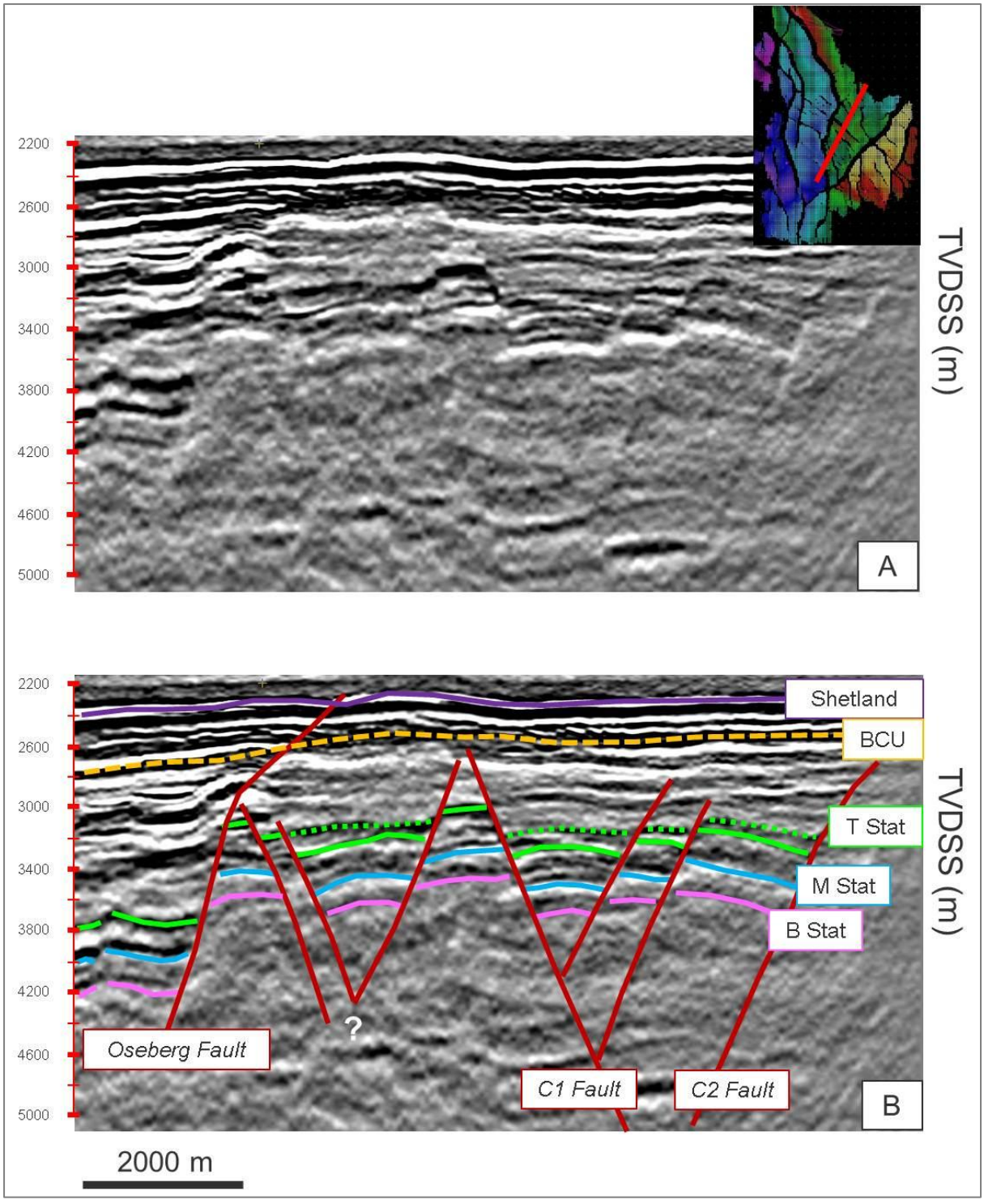

Figure 54: A SW-NE oriented structural cross-section across the C structure. Panel A shows the section without interpretations, and Panel B with interpretations. The dashed green line represents the top of possible syn-rift Statfjord sediments.

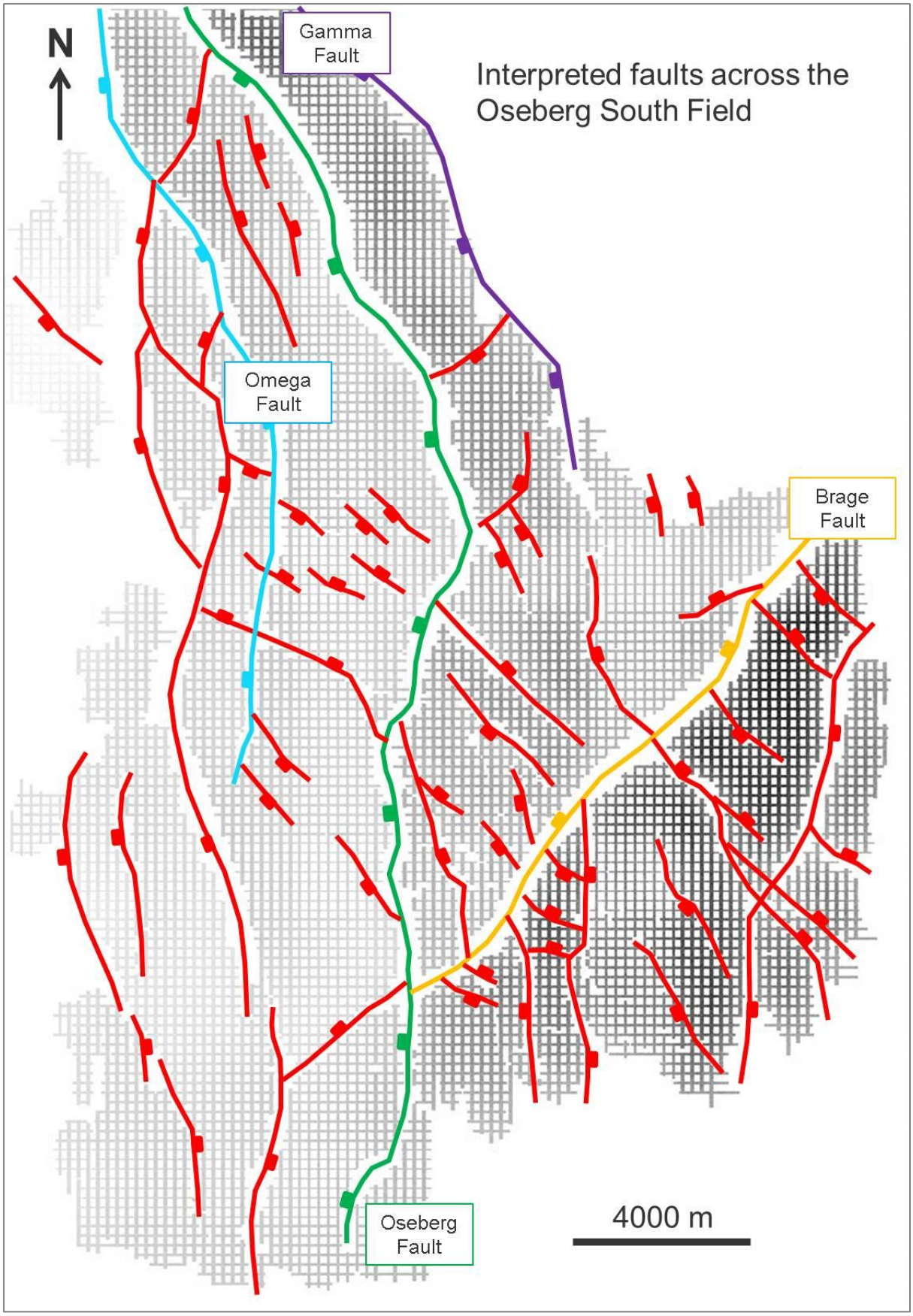

Figure 55: Plan view of interpreted faults over the Oseberg South field superimposed on the Top Statfjord structural depth map.

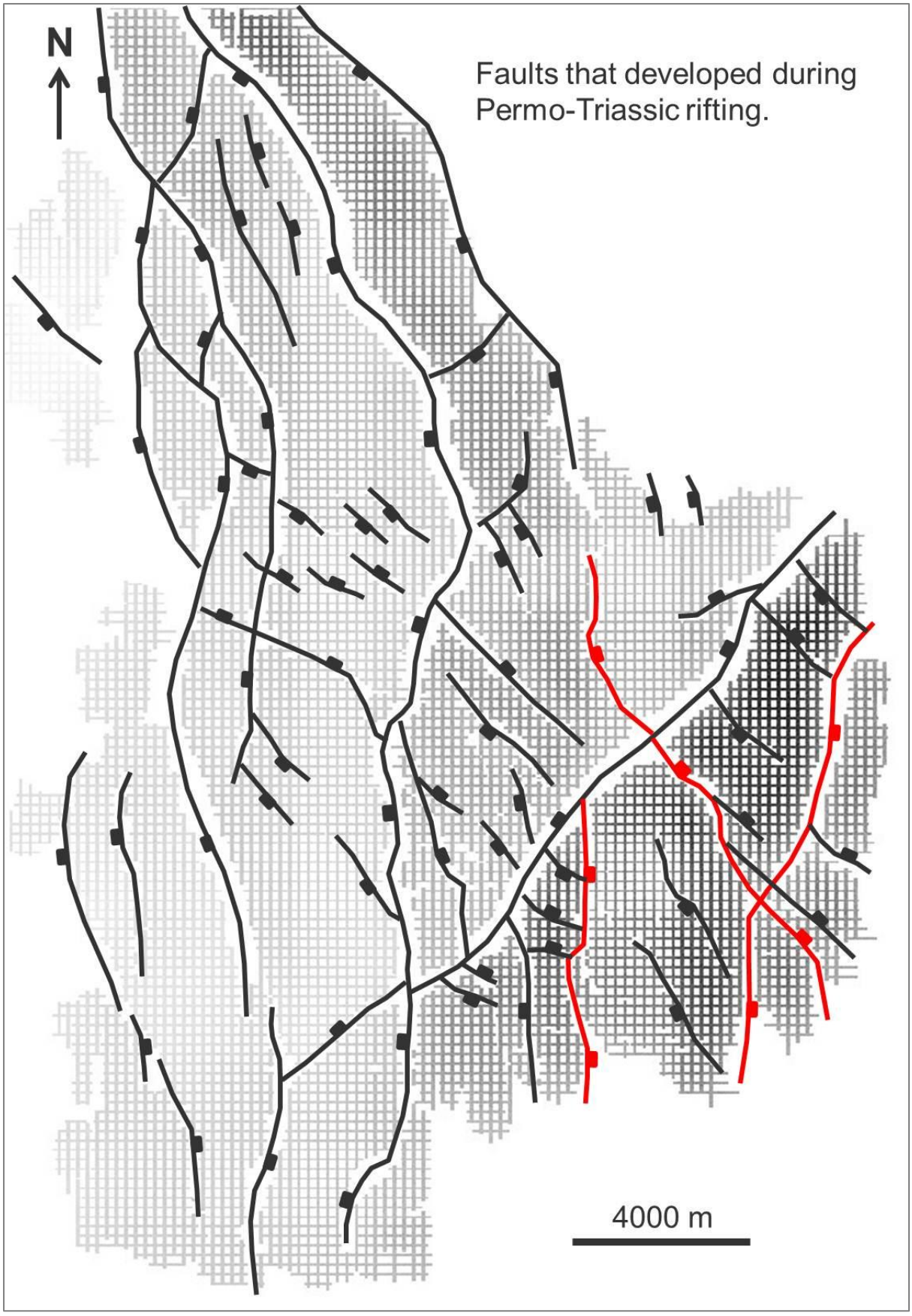

Figure 56: The red faults are believed to have been initiated during the Permo-Triassic rifting event.

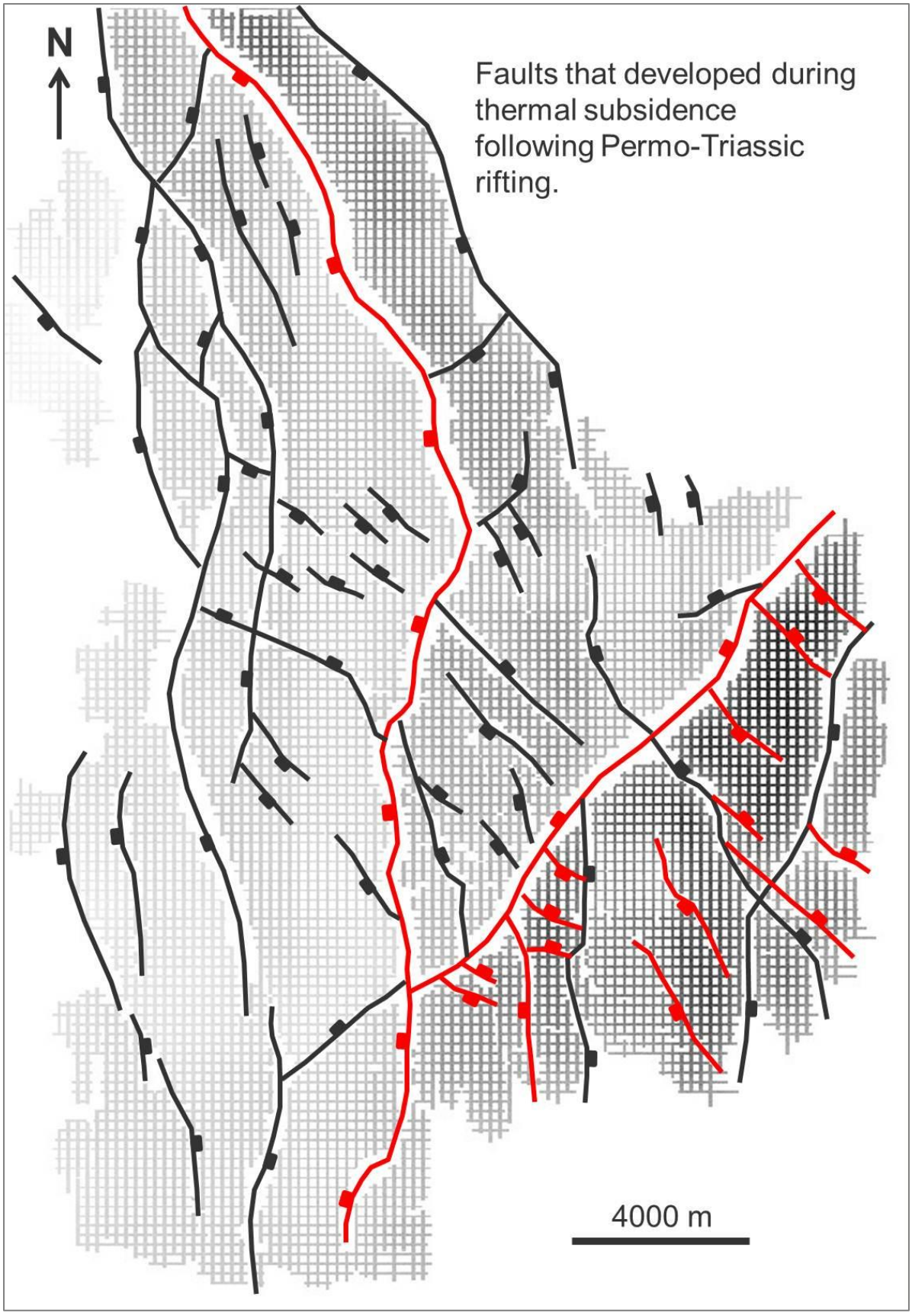

Figure 57: The red faults are believed to have been initiated during the Permo-Triassic post rift thermal cooling and subsidence phase, as exhibited by thickening of the Statfjord Formation across faults, and syn-sedimentary deposition.

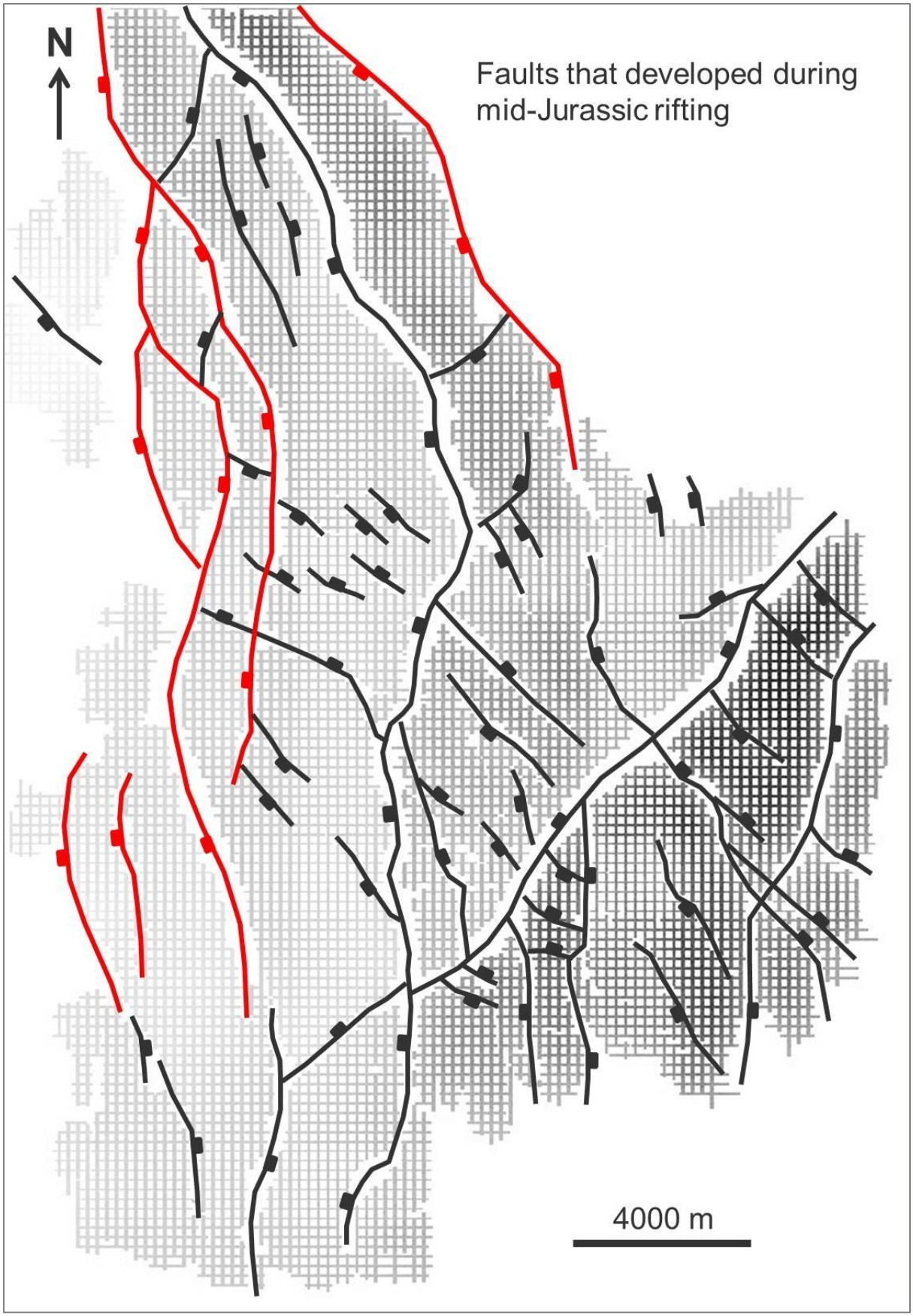

Figure 58: Red faults are believed to have been initiated during the mid-Jurassic rifting event, as exhibited by their westward dipping orientation.

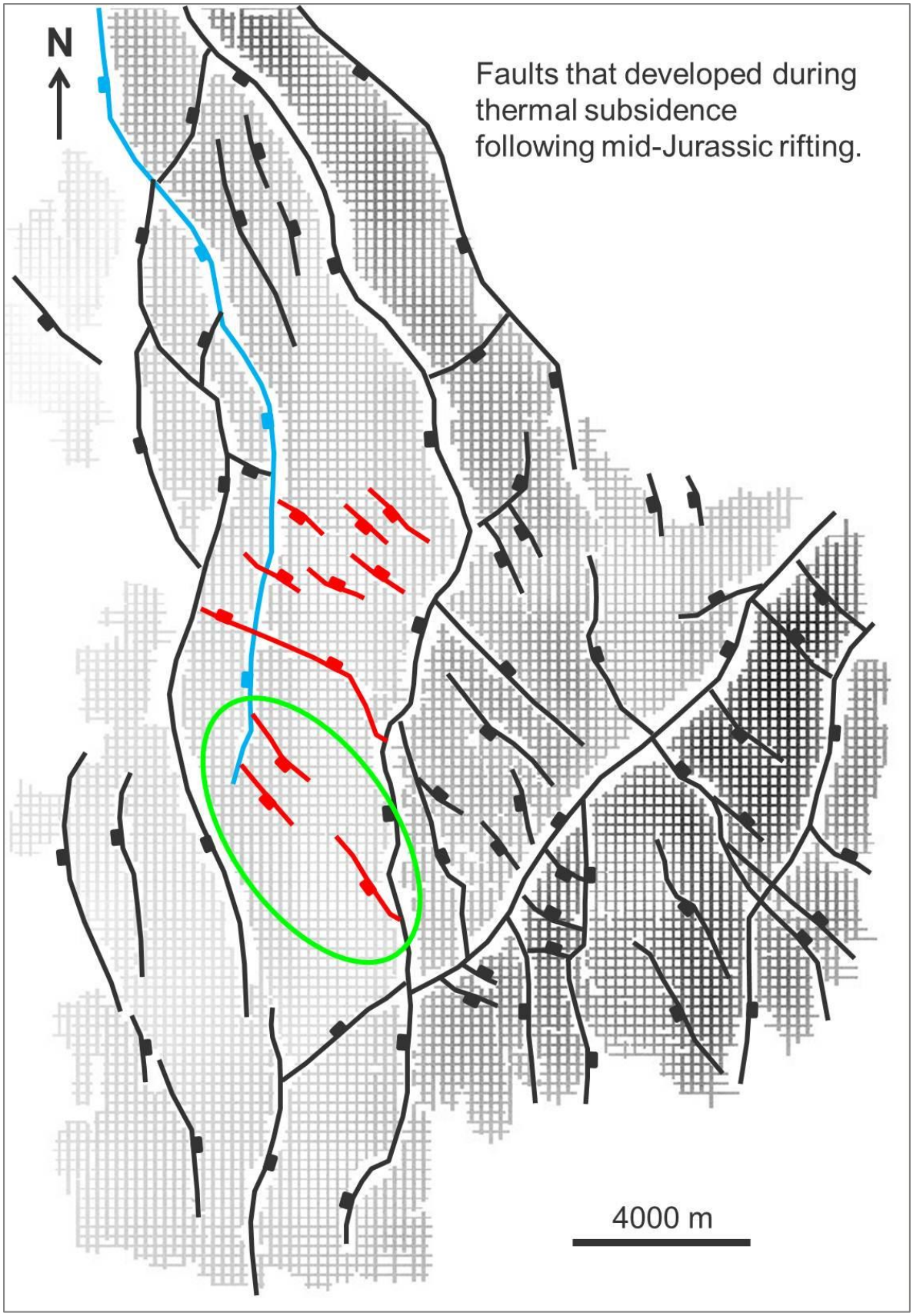

Figure 59: The red faults are believed to have been initiated during post rift thermal cooling and subsidence after cessation of mid-Jurassic rifting. The Omega Fault is highlighted in blue, while the green circle highlights faults that terminate against the Omega Fault in the west, and the Oseberg Fault in the east.

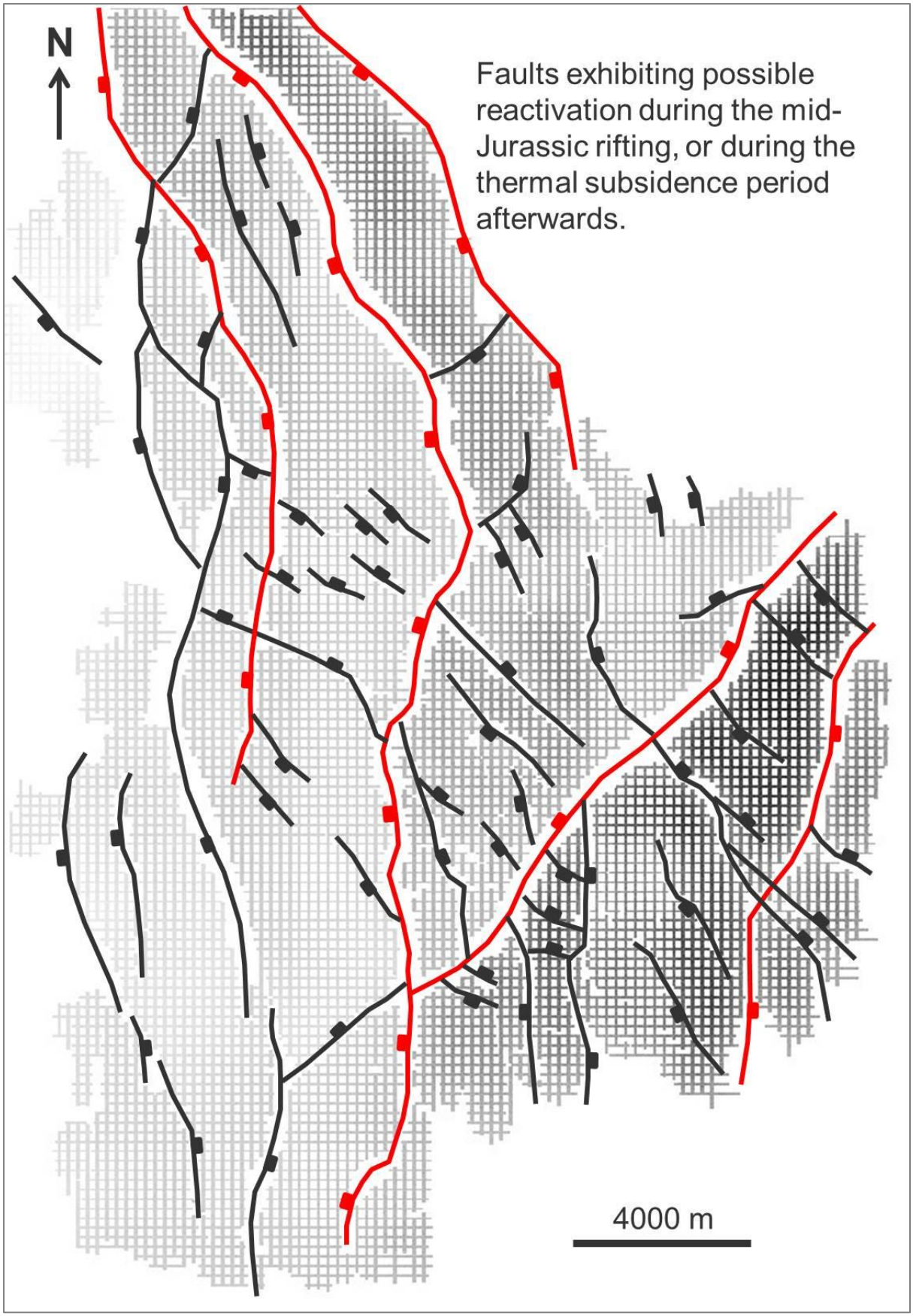

Figure 60: Red faults shown signs of reactivation during mid-Jurassic rifting, or during the thermal cooling and subsidence afterwards.

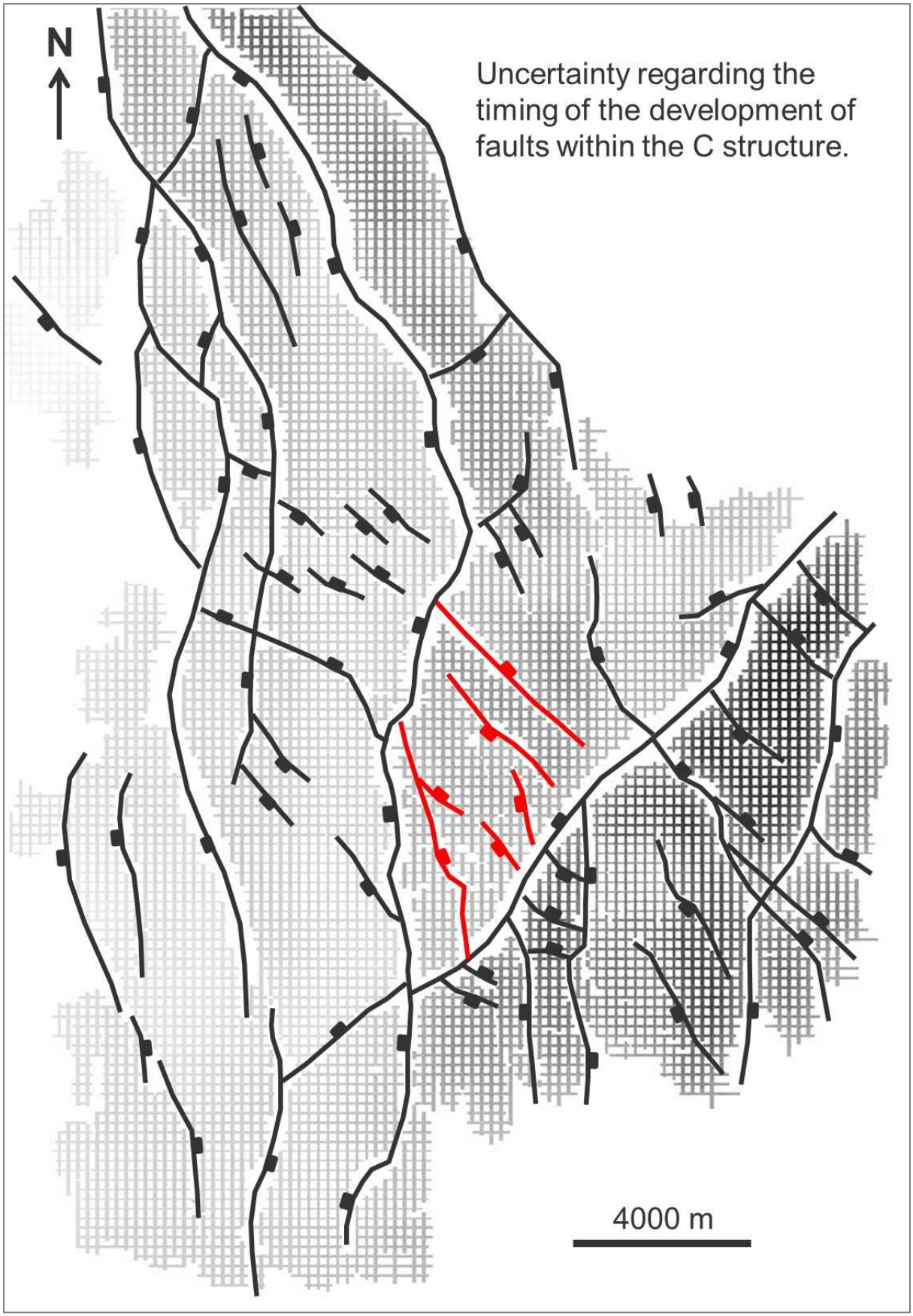

Figure 61: Uncertainty exists for the timing of the activation of the red faults highlighted in the C structure.

7.2 Faulting and Pressure Segmentation

Formation pressure data from eight exploration wells provides a glance into the effects of the faulting on the pressure distribution within the formation (Figure 62). All of the wells display typical depth/pressure trends that are characteristic of water zones, however, the pressures present in some wells do not fall in line with the expected hydrostatic pressure, indicating segmentation. The normal hydrostatic pressure is seen as pink dashes, and several of the wells (30/9-5S, 30/9-9, 30/9-15) show pressures that fall in line with what is expected at these depths. These wells are also located on the J structure, and despite the high degree of faulting on the structure, these wells appear to be in communication with one another. Wells 30/9-3A and 30/9-6 appear to follow on a higher pressure trend, while 30/9-24T2, 30/9-13S, and 30/9-10 fall on an even higher trend. Relatively few data points exist for wells 30/9-10, 30/9-13S, and 30/9-6 and so making confident interpretations regarding segmentation becomes difficult. Nevertheless, it is evident that although they are relatively close to one another, wells 30/9-24T2 and 30/9-3A are not in pressure communication with one another.

The difference in pressure between closely spaced wells 30/-924T2 and 30/9-3A highlights the importance in mapping faults throughout the formation. At first glance, the two wells appear to be both connected to each other within the Omega structure, but closer inspection reveals that a fault that separates the two wells. The differences in pressure and the presence of the fault in between the wells suggest that this fault may be sealing, with structures on either side having developed their own pressure regimes.

With regards to exploration and development of the Statfjord Formation in the Oseberg South field, understanding the influence of these supposedly small faults will play a critical role in reducing the risk during exploration, and developing an appropriate drainage strategy upon development. Previous internal Statoil projects have attempted to determine which structures have been tested by exploration wells, however, new fault maps used in conjunction with the formation pressure data may reveal that some areas previous thought to have been tested, may actually be part of a different fault segment.

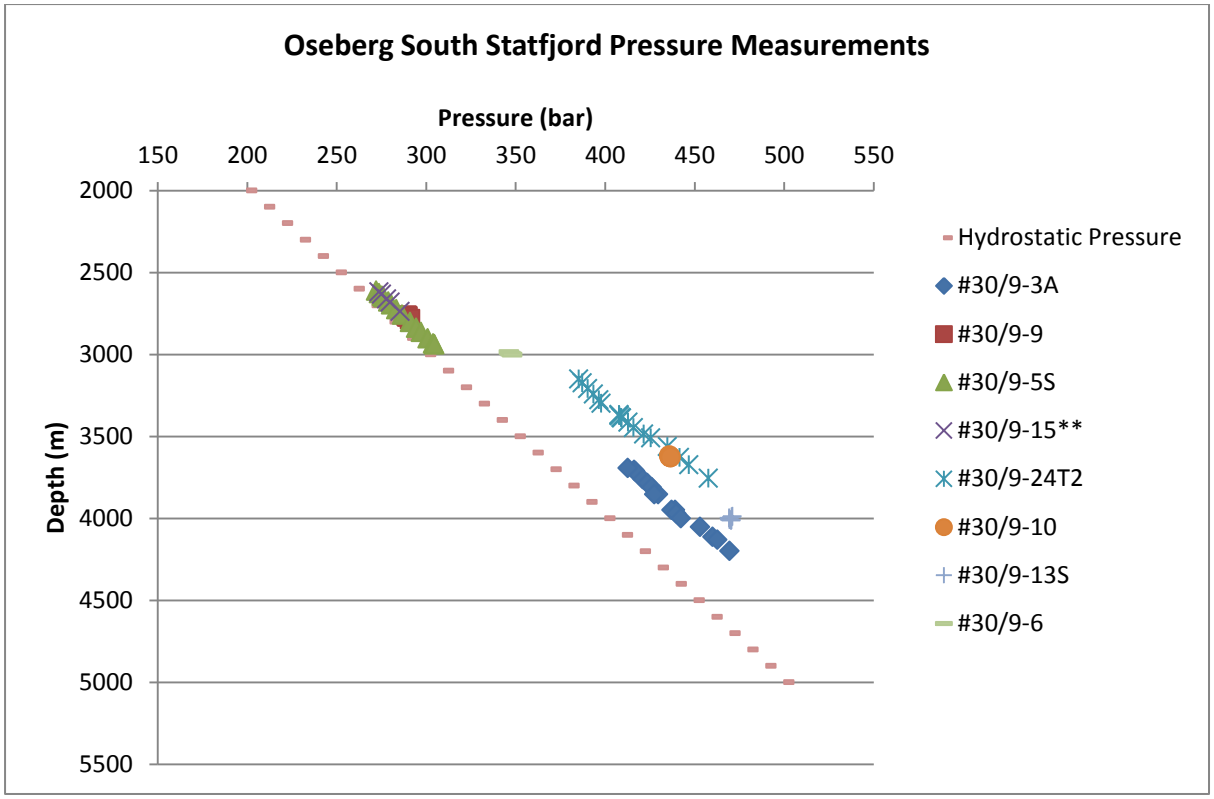

Figure 62: Formation pressure data for selected wells in the Oseberg South Field. Hydrostatic pressure is shown as pink dashes.

7.3 Implications on Palaeogeography and Reservoir Quality

The configuration of the basin, among other things, plays a large role in the distribution of sediment, and accordingly, the future potential reservoir quality. As has been demonstrated by Ryseth & Ramm (1996), the subsidence rate during the deposition of the Statfjord Formation appears to have played a large role in its reservoir quality potential. Many of the published papers have focussed on the large scale features of the sedimentary basin in the North Sea, and while this is important, this thesis has demonstrated that it is important to understand the structural geology at a reservoir level. The improvement in the seismic data quality of the OBC from the streamer data has played a tremendous role in the better understanding of the structural history in the Oseberg South field. Although the exact rates of basin subsidence are not known for each of the blocks, the information obtained from the well logs, combined with the relative rates of subsidence for the fault blocks can provide an indication of the potential reservoir quality in the blocks that have not yet been drilled, and hopefully reduce the uncertainties involved with drilling exploration wells.

Going hand-in-hand with subsidence rates, the basin configuration will also control the development and sediment transport directions of the alluvial systems within the Statfjord Formation. This also includes mapping areas which may be more prone to shale, coal, or

other type of sediment that disconnect sand bodies from one another and inhibit the flow and ultimate recovery factor of hydrocarbons from the formation.

A schematic diagram (Figure 63) shows the effects of subsidence rates on the net-to-gross ratio within the Statfjord Formation, and the vertical connectivity of the sand bodies related to the subsidence. Although higher subsidence rates lead to thicker deposits, much of the sediment is deposited as shale, and the sand bodies are not well connected to one another. Lower subsidence rates appear to reduce the amount of shale deposition and/or preservation potential, and increase the vertical connectivity between the sand bodies. Based on this theory, the active movement of the Brage and Oseberg Faults suggests that the reservoir quality of the Statfjord Formation would decrease towards the west, with large contrasts experienced across these fault boundaries. Although only three wells fully penetrated the Statfjord in the field, this reservoir quality decrease was evident. The cross section in Figure 15 shows that the Statfjord Formation in wells 30/9-24T2 and 30/9-3A, located west of the Oseberg Fault, is highly heterogeneous, with relatively thin sand bodies that are separated by abundant shale layers. The implied heterogeneities and low connectivity between the reservoir sands would provide many challenges in developing a reservoir of this nature. In comparison, the Statfjord Formation in the J structure shows very little shale deposition and/or preservation, and very high sand content. At this location, the formation is roughly 200 m thinner than in wells 30/9-24T2 and 30/9-3A, and although the data is sparse, this suggests that understanding these subsidence rates within the Statfjord Formation is especially important for finding high quality, connected reservoir sands.

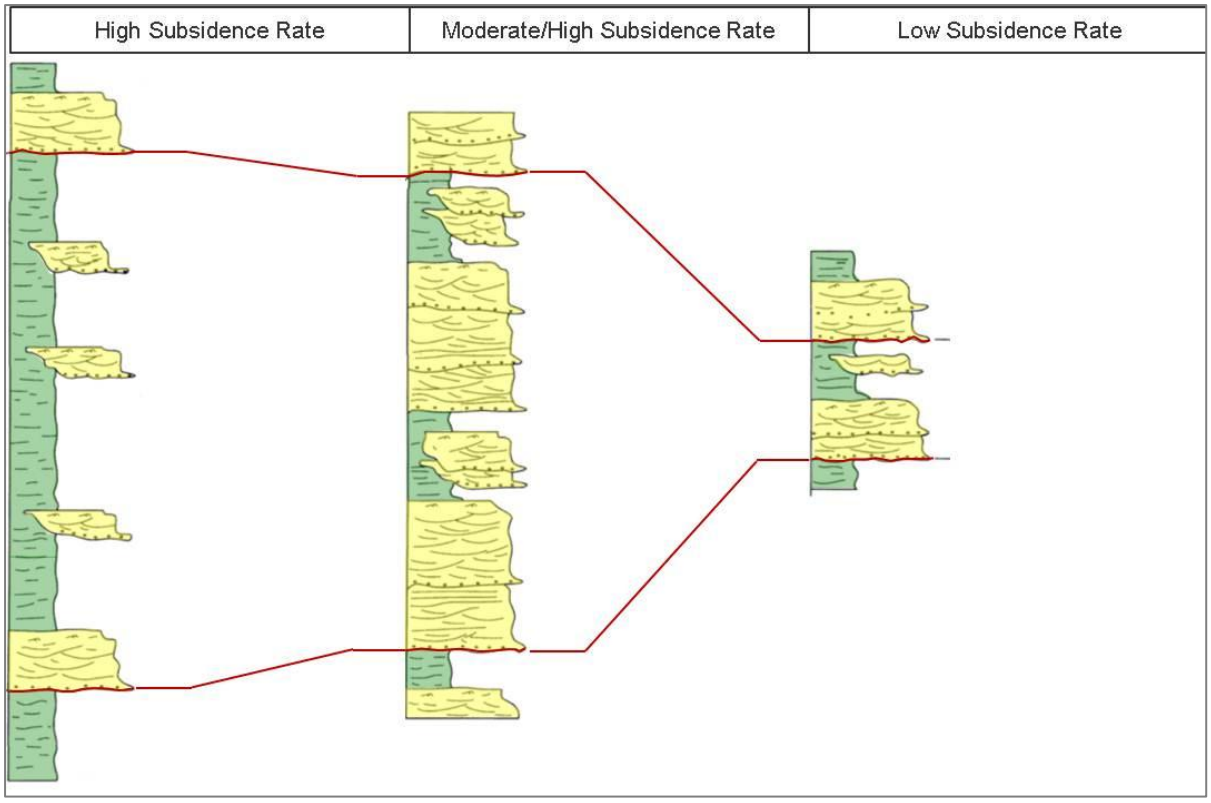

Figure 63: Schematic demonstrating the effects of subsidence rates on the volume of sand and shale within a column (modified from Ryseth & Ramm 1996)

8. Discussion

The effects and interaction of the two rifting phases in the North Sea have been long discussed, however, the effects of post-rift thermal cooling and subsidence of the crust for both events have not been well documented. Interpretations from OBC seismic data revealed that although the two rifting events played a significant role on the structural configuration of the field, smaller faults that were oriented in orthogonal directions to these main faults also played a role.

The seismic data suggest that four major faults within the J and C structures were initiated during the Permo-Triassic rifting event, with fault planes dipping towards the east in the direction of the Permo-Triassic graben located under the present-day Horda Platform. The Permo-Triassic graben was bound by four major, 35km wide westward dipping fault blocks, one of which underlies the Oseberg South field and has given a gentle paleo-dip towards the west (Færseth 1996). All but one of the Permo-Triassic faults shows evidence of movement into the Shetland Group reflector, indicating that although initiated in the Permo-Triassic, these faults have been planes of movement throughout the evolution of the basin.

Several papers (e.g., Steel & Ryseth 1990, Færseth 1996) have shown that the Statfjord Formation thickens westward from the Øygarden Fault Zone, and is thickest over the axis of the present Viking Graben. Associated with this thickening trend, large jumps in thickness are reported over some major faults that include the Oseberg and Brage Faults (Steel & Ryseth 1990). Thickness changes caused by faulting indicate that the faulting existed during the evolution of the formation, and thus, the initiation of these two major faults is interpreted to have occurred during the post-rift period of the Permo-Triassic event.

Biostratigraphic data across the field have shown good control in determining the top of the Triassic within wellbores 30/9-24T2, 30/9-3A located on the Omega structure, and 30/9-5S located on the J structure. Correlation of the relatively thin Triassic section in these wells is very good, and the thickness changes are relatively minor, suggesting that the area was not influenced by movement of the Oseberg and Brage Faults during this time. This palaeogeographic configuration was also suggested by Steel & Ryseth (1990) where a wide alluvial plain was thought to have existed during the Late Triassic. The biostratigraphic data confines the initiation of movement on the Oseberg and Brage Faults to the Hettangian stage of the Lower Jurassic.

As the post-rift subsidence continued for a 70 Ma period after the Permo-Triassic rifting (ter Voorde *et al*. 1997), the basin was continually subsiding throughout deposition of the

Statfjord Formation. The mix of biostratigraphic data and petrophysical log correlation revealed that correllable intervals between wells were of different thicknesses, increasing towards the west towards the centre of the Viking Graben (Figure 15). As mentioned, the Triassic interval Zone A appeared to have been deposited during a tectonically stable period, and little variation in thickness is seen between the wells. Zone B incorporates the time period that includes the Top Hettangian and into the early Sinemurian. The Top Hettangian was not a reliable pick using stratigraphic data, and the Middle Statfjord Formation marker, which was thought to represent a basin wide event, was used to constrain this interval. The wells within the Omega structure showed a large thickness increase from the correlated interval in the J structure. This suggests that the Oseberg and/or Brage Faults were active at this time, and that the rate of subsidence was quite high on the downthrown sides of these active faults. Zones C and D were constrained using the petrophysical data from the Top Eiriksson Member and Top Nansen Member, which defined the transition from the alluvial to the marine influenced section of the Statfjord Formation. Both of these zones exhibited thickening compared to the same zones on the J structure, with Zone D showing some rapid thickness changes close to the western edge of the Omega structure in well 30/9-24T2. The thickness changes in Zones C and D were not as large as seen in Zone B going westward over the faults, indicating that the Oseberg and/or Brage Faults experienced less movement during this time. Steel & Ryseth (1990) and Steel (1993) suggest that the degree of subsidence changed as many as seven times throughout the Permo-Triassic post rifting phase, and although the degree of detail is difficult to match at Oseberg South, the interpretations support the notion that subsidence rates were not consistent throughout this time period.

Many of the west-dipping faults that characterize the Oseberg South field are thought to have been initiated during the mid-Jurassic rifting event. There may be some slight thickness increases in the Statfjord Formation across some of these faults (e.g., Omega), however, the increase in uncertainty of horizon picks as the Statfjord Formation gets deeper makes it difficult to be certain. As a result of this uncertainty, and the west-dipping nature of the faults, they have been interpreted to have been a result of mid-Jurassic rifting. In addition to these newly initiated faults, other major faults that include the Oseberg, Brage, and J3 faults, also exhibit signs of movement during this period. Several of the horizons exhibit drag along the fault plane, which was especially evident at the Brent Group level below the BCU. Although this feature cannot constrain the timing of the movement, the extent of the rifting and initiation of nearby faults indicate that this scenario was likely. Further interpretations in the Brent Group and possible syn-rift sediments at that stratigraphic level will better constrain the timing of movement along these faults.

As was seen in the J structure, the Omega structure has a series of relatively short NW-SE striking faults, some of which cross the Omega Fault into the B structures. Unlike the J structure, however, no evidence of syn-rift sediments was seen at the Statfjord Formation level, seemingly indicating that the faults post-date Statfjord Formation deposition. Several of these smaller faults cross the Omega Fault, and others terminate against the side of the fault. Henza *et al.* (2011) discussed some of the relationships between faults resulting from two orthogonal extensional phases, with the modelling relationships showing similarities with the faults in the Omega structure. In the experiments, the primary faults appeared to control the distribution of the secondary faults, with the secondary faults beginning and/or terminating against the primary faults, or sometimes crossing it. The scale of the Omega Fault at the western edge of the Omega structure compared to the secondary faults seems to indicate that it was the primary fault, as opposed to the other way around. The orthogonal orientation of the secondary faults suggests that the secondary faults were not part of the extensional event that created the Omega Fault. The largest of the secondary faults do not extend any higher than the BCU, constraining their timing to between the end of the mid-Jurassic rifting event in the Early Cretaceous and the beginning of deposition of sediments overlying the BCU. This leads to the conclusion that the secondary faults were generated as a result of the thermal cooling and subsidence of the crust following the cessation of the mid-Jurassic rifting event.

Similar secondary faults were seen in the C structure, and contained a similar NW-SE strike that was seen in the secondary faults in both the Omega and J structures. However, uncertainty remains regarding the timing of these faults, as the presence of syn-rift sediments at the Statfjord Formation level is difficult to determine. Figure 54 shows the two possible scenarios, with the uncertainty with which reflector is the Statfjord Formation. One well (30/9-6) penetrates the structure, and has a good synthetic ties with the seismic at this location, however, the well is located on a horst, and the reflectors change from the horst into the grabens. Without a well penetrating these structures, certainty regarding the correct reflector to interpret as the Top Statfjord Formation will remain low. However, should the top reflector in dashed green (Figure 54) represent the Top Statfjord Formation, reflecting syn-rift sediments, then the origin of the secondary faults is likely to have been a result of the same event that created the secondary faults in the J structure. If the Top Statfjord Formation is located at the level of the solid green line in Figure 54, then no syn-rift sediments appear present, suggesting that they were formed as a result of the same event that created the secondary faults in the Omega structure.

All of the secondary faults within the structures strike in the same direction, regardless of the timing of the faulting. The orientation of these faults suggests that the extension direction

was in a NE-SW direction, which is orthogonal to the extensional direction in both of the main rifting events. The cause of the switch in orientation of the extension direction is unknown, but it seems possible that the configuration of the fault blocks and pre-existing faults played a role in the development of the secondary faults, created a localized extension direction that varies from the main E-W extension.

The increased understanding of the timing of the structural elements in the Statfjord Formation, and in the Oseberg South field aids in the reconstruction of the palaeogeography of the formation. The palaeogeography is important for the mapping of facies within the formation, and determining exploration locations that have the highest likely probability of encountering reservoir sands. Ryseth & Ramm 1996 have shown that the connectivity of sand bodies is dependent on the subsidence rates during deposition, and better understand of the structural geology will help to better map the location of highly connected sand bodies. Results from core interpretations have shown that at least within the Nansen Member, the facies are consistent with what has been described in the literature, however, this provides little to aid in understanding of the distribution of the facies within the Eiriksson Member, which constitutes the largest part of the Statfjord Formation. Future mapping of facies in the formation will need to rely on regional data and other data available from nearby field. In addition, the relative subsidence rates and timing of the fault movement will increase the understanding of the structural elements that influenced the deposition of the formation, leading to more confident facies interpretations, and hopefully a higher exploration success.

8.1 Future Work

Although still somewhat uncertain, the biostratigraphic data has shown some usefulness in understanding the timing of the development of the major faults in the area, and aids somewhat in the correlations across the field, which is especially important when there is such a scarcity of data. Future exploration wells drilled in the field should include full biostratigraphic analysis to help improve the understanding of the formation. The timing of movement of the faults in the field will be an important component in understanding the distribution of higher quality sands, and possibly of possible migration pathways for hydrocarbons.

Structural and horizon modelling in RMS provided a good overview of the formation, however, as only the major faults were interpreted, the model could be improved by

including the numerous smaller faults that cross the field. This will especially be helpful in understanding why different pressure regimes exist in different parts of the field.

The excellent quality data that has been obtained in the OBC survey means that it is now possible to map deeper horizons with a higher degree of confidence. Although the Top Lunde Formation was the deepest horizon mapped in this project, it would be worthwhile to map any deeper horizons, including the basement in order to better understand the development of the faulting. The current influence of the basement structure on the development of the Permo-Triassic and mid-Jurassic rifting events has been discussed in literature (e.g., Færseth 1996), but this has not been done on a local scale. Reducing the uncertainty of this relationship may help increase the understanding of the faulting, and thus the palaeogeography and subsequent reservoir quality that exists in certain areas today. Incorporating more regional facies data for both the Eiriksson and Nansen Members, in combination with the structural timing and relative subsidence throughout deposition of the formation will be required for future exploration wells.

9. Conclusion

- Structural interpretations on new OBC data revealed that four phases of faulting exist within the Oseberg South Field. Major faults resulting from the Permo-Triassic and mid-Jurassic rifting events strike in a roughly N-S orientation, and post-rift thermal cooling and subsidence of the crust in each event appear to have created a series of NW-SE trending faults. Post-rifting faulting from the Permo-Triassic event initiated some of the major faults within the field, including the Oseberg and Brage Faults, both of which appear to have predated the remaining secondary NW-SE trending faults in the J structure. Many of the west-dipping faults within the field are believed to have been initiated during the mid-Jurassic rifting event, with evidence that the Oseberg and Brage Faults were also reactivated during this time. Post-rift subsidence following mid-Jurassic rifting created a series of NW-SE trending faults within the Omega structure. The timing of secondary faults in the C structure is uncertain due to uncertainty regarding the presence or absence of syn-rift sediments.
- Biostratigraphic data has proved useful in determining the top Triassic, as well as the top Eiriksson Member/base Nansen Member. Difficulties arose in determining the top Hettangian, however, thickness changes between wells suggested that four possible relative rates of subsidence could be recorded. Alongside structural data, it appears that the rate of subsidence varied along major faults throughout deposition of the Statfjord Formation.

10. References

Aase, N.E. (2011). Petrology, reservoir quality and sedimentological study on deeply buried Statfjord Formation sandstones. Statoil Internal Report.

Badley, M.E., Egeberg, T., & Nipen, O. 1984. Development of rift basins illustrated by the structural evolution of the Oseberg feature, Block 30/6, offshore Norway, *Journal of the Geological Society*, **141**, pp. 639-649.

Badley, M.E., Price, J.D., Rambech Dahl, C., & Agdestein, T. 1988. The structural evolution of the northern Viking Graben and its bearing upon extensional modes of graben formation. *Journal of the Geological Society,* **145**, pp. 455-472.

Biostratigraphy of Exploration Well 30/9-24T2 (2010). Statoil Internal Report.

Bowen, J.M. 1975. The Brent Oil-Field. *In* Woodland, A.W. (ed), *Petroleum and the Continental Shelf of North-West Europe*, **1**, pp. 353-361.

Bysbeen, M.A., & van Veen, P. 1986. Norsk Hydro Internal report. Palynostratigraphy and palaeoenvironmental interpretation of the Statfjord Formation in 30/6-18 and 30/9-5. Norsk Hydro Research Centre, Bergen, Norway.

Collinson, J.D. 1986. *In:* Reading, H.G. (ed.) *Sedimentary Environments and Facies* (2nd edn.) Blackwell, Oxford, pp. 20-62.

Dalrymple, R.W. 1992. Tidal Depositional Systems. *In*: R.G. Walker and N.P. James (eds), *Facies Models: Response to Sea Level Change*. Geological Association of Canada, Toronto, pp. 195-218.

Dawson, A. & Mathewson, J. (2011). Oseberg Summary of PZ Fast-Track Processing. Western Geco Presentation.

Deegan, C.E. & Scull, B.J. 1977. Lithostratigraphic nomenclature for the Central and Northern North Sea. *Bull. 1*, Norwegian Petroleum Directorate, 36 p.

Eynon, G. 1981 Basin development and sedimentation in the Middle Jurassic of the northern North Sea. *In*: Illing, L.V. & Hobson, G.D. (eds) *Petroleum Geology of the continental Shelf of North West Europe*, pp. 196-204.

Færseth, R.B. 1996. Interaction of Permo-Triassic and Jurassic extensional fault-blocks during the development of the northern North Sea. *Journal of the Geological Society*, **153**, pp. 931-944.

Færseth, R.B. & Ravnås, R. 1998. Evolution of the Oseberg Fault-Block in context of the northern North Sea structural framework. *Marine and Petroleum Geology*, **15**, pp. 467-490.

Gabrielsen, R.H., Færseth, R.B., Steel, R.J., Idil, S. & Kløvjan, O.S. 1990. Architectural styles of basin fill in the northern Viking Graben. *In*: Blundell, D.J. & Gibbs, A.D. (eds) *Tectonic Evolution of the North Sea Rifts*. Clarendon Press, Oxford, pp. 158-179.

Giltner, J.P. 1987. Application of extensional models to the Northern Viking Graben. *Norsk Geologisk Tidsskrift*, **67**, pp. 339-352.

Graue, E., Helland-Hansen, W., Johnsen, J.R., Lømoe, L., Nøttvedt, A, Rønning, K, Ryseth, A. & Steel, R.J. (1997). Advance and Retreat of Brent Delta System, Norwegian North Sea. In *Petroleum Geology of Northwest Europe*, eds J. Brooks and K.W. Glennie, pp. 915-937.

Helland-Hansen, W., Ashton, M., Lømoe, L., & Steel, R.J. (1992). Advance and retreat of the Brent delta; recent contributions to the depositional model. In *Geology of the Brent Group*, eds A.C. Morton, R.S. Haszeldine, M.R. Giles and S. Brown, pp. 107-127. *Geological Society of London* Special Publication **1**.

Holden, A. 1992. Norsk Hydro 30/9-13S and 30/9-13X Norwegian North Sea wells: biostratigraphy of the interval 1040-4027mTD. Simon-Robertson. Norsk Hydro Internal Document.

Henza, A.A., Withjack, M.O. & Schlische, R.W. 2011. How do the properties of a pre-existing normal-fault population influence fault development during a subsequent phase of extension? *Journal of Structural Geology*, **33**, pp. 1312-1324.

Johannesen, E.P., Mjøs, R., Renshaw, D., Dalland, A. & Jacobsen, T. (1995). Northern limit of the 'Brent delta' on the Tampen Spur – A sequence stratigraphic approach for sandstone prediction. In *Sequence Stratigraphy on the Northwest European Margin*, eds R.J. Steel, V. Felt, E. Johannessen and C. Mathieu, pp. 213-256. Norwegian Petroleum Society Special Publication **5**.

Miall, A.D. 1992. Alluvial Deposits. *In*: R.G. Walker and N.P. James (eds), *Facies Models: Response to Sea Level Change*. Geological Association of Canada, Toronto, pp. 119-142.

Miles, N.H., Minnis, J., Regnault, E.A., & Titterton, R. 1984. Norsk Hydro Internal Report. Norsk Hydro 30/9-3A Norwegian North Sea well: Biostratigraphy of the interval 2800-4300mTD.

Millennium Atlas. Petroleum Geology of the Central and Northern North Sea. Evans, D., Graham, C., Armour and Bathurst, P. (editors and coordinators). The Geological Society of London 2003.

Norwegian Petroleum Directorate (www.npd.no). Accessed 30 January 2012.

Pemberton, S.G., MacEachern, J.A. & Frey, R.W. 1992. Trace Fossil Facies Models: Environmental and Allostratigraphic Significance. *In:* R.G. Walker and N.P. Janes (eds), *Facies Models: Response to Sea Level Change*. Geological Association of Canada, Toronto, pp. 47-72.

Ramm, M. & Ryseth, A.E. 1996. Reservoir quality and burial diagenesis in the Statfjord Formation, North Sea. *Petroleum Geoscience*, **2**, pp. 313-324.

Ravnås, R., Bondevik, K., Helland-Hansen, W., Lømoe, L., Ryseth, A. & Steel, R.J. (1997). Retreat and drowning of the Brent delta as a response to initial middle Jurassic rifting: the uppermost Ness, Tarbert and lower Heather formations, Oseberg-Brage area, northern North Sea. *Norsk Geologisk Tidsskrift*, 77.

Ravnås, R., Nøttvedt, A., Steel, R.J., & Windelstad, J. 2000. Syn-rift sedimentary architectures in the Northern North Sea. *From*. Nøttvedt, A. *et al.* (eds) *Dynamics of the Norwegian Margin*. Geological Society, London, Special Publications, **167**, pp. 133-177.

Roberts, A.M., Yielding, G. & Kusznir, N.J., Walker, I.M., & Dorn-Lopez, D. 1995. Quantitative analysis of Triassic extension in the northern Viking Graben. *Journal of the Geological Society,* **152**, pp. 15-26.

Ryseth, A.E. & Ramm, M. 1996. Alluvial architecture and differential subsidence in the Statfjord Formation, North Sea: prediction of reservoir potential. *Petroleum Geoscience*, **2**, pp. 271-287.

Ryseth, A.E. 2001. Sedimentology and palaeogeography of the Statfjord Formation (Rhaetian – Sinemurian), North Sea. *Sedimentary Environments Offshore Norway – Palaeozoic to Recent* edited by O.J. Martinsen and T. Dreyer. NPF Special Publication 10, pp. 67-85. Published by Elsevier Science B.V., Amsterdam. Norwegian Petroleum Society (NPF).

Røe, S.L. & Steel, R. 1985. Sedimentation, sea-level rise and tectonics at the Triassic-Jurassic boundary (Statfjord Formation), Tampen Spur, Northern North Sea. *Journal of Petroleum Geology*, **8**-2, pp. 163-186.

Seilacher, A. 2007. Trace Fossil Analysis. Springer-Verlag Berlin Heidelberg.

Statoil Internal Data (2012). Early-Jurassic-Latest Jurassic Chronostratigraphy, Biostratigraphy, Lithostratigraphy.

Steel, R.J. (1993). Triassic-Jurassic megasequence stratigraphy in the Northern North Sea: rift to post-rift evolution. In *Petroleum Geology of Northwest Europe*, ed. J.R. Parker. *Proceedings of the 4th Conference, Geological Society of London*, pp. 299-315.

Steel, R. & Ryseth, A. 1990. The Triassic – early Jurassic succession in the northern North Sea: megasequence stratigraphy and intra-Triassic tectonics. *In*: Hardman, R.F.P., Brooks, J. (eds), *Tectonics Events Responsible for Britain's Oil and Gas Reserves*, Geological Society Special Publication No. 55, pp. 139-168.

ter Voorde, M., Færseth, R.B., Gabrielsen, R.H. & Cloetingh, S.A.P.L. 1997a. Repeated lithosphere extension in the northern Viking Graben: a coupled or decoupled rheology? *In:* Nøttvedt *et al.* (eds), *Integrated Basin Studies: Dynamics of the Norwegian Margin*, Geological Society of London, Special Publication 167, pp.59-81.

ter Voorde, M., Ravnås, R., Færseth, R. & Cloetingh, S. 1997b. Tectonic modelling of the Middle Jurassic synrift stratigraphy in the Oseberg-Brage area, northern Viking Graben. *Basin Research*, **9**, pp. 133-150.

Vollset, J. & Doré, A.G. 1984. A revised Triassic and Jurassic lithostratigraphic nomenclature for the Norwegian North Sea. *Norwegian Petroleum Directorate Bulletin*, No. 3.

Wood, R. & Barton P. 1983 Crustal thinning and subsidence in the North Sea, *Nature*, **304**, p. 561.

Yonge, B., Myrland, R., Taylor, H. & Ruble, C.L. 1975. A preliminary report from the Jurassic stratigraphic nomenclature sub-committee in Norway. NPF – Jurassic Northern North Sea Symposium, Stavanger, **29**, pp. 1-14.

Ziegler, P.A. 1982. *Geological Atlas of Western and Central Europe*, Shell Internationale Petroleum Maatschappij BV., the Hague.

Appendix

Main structures within the field

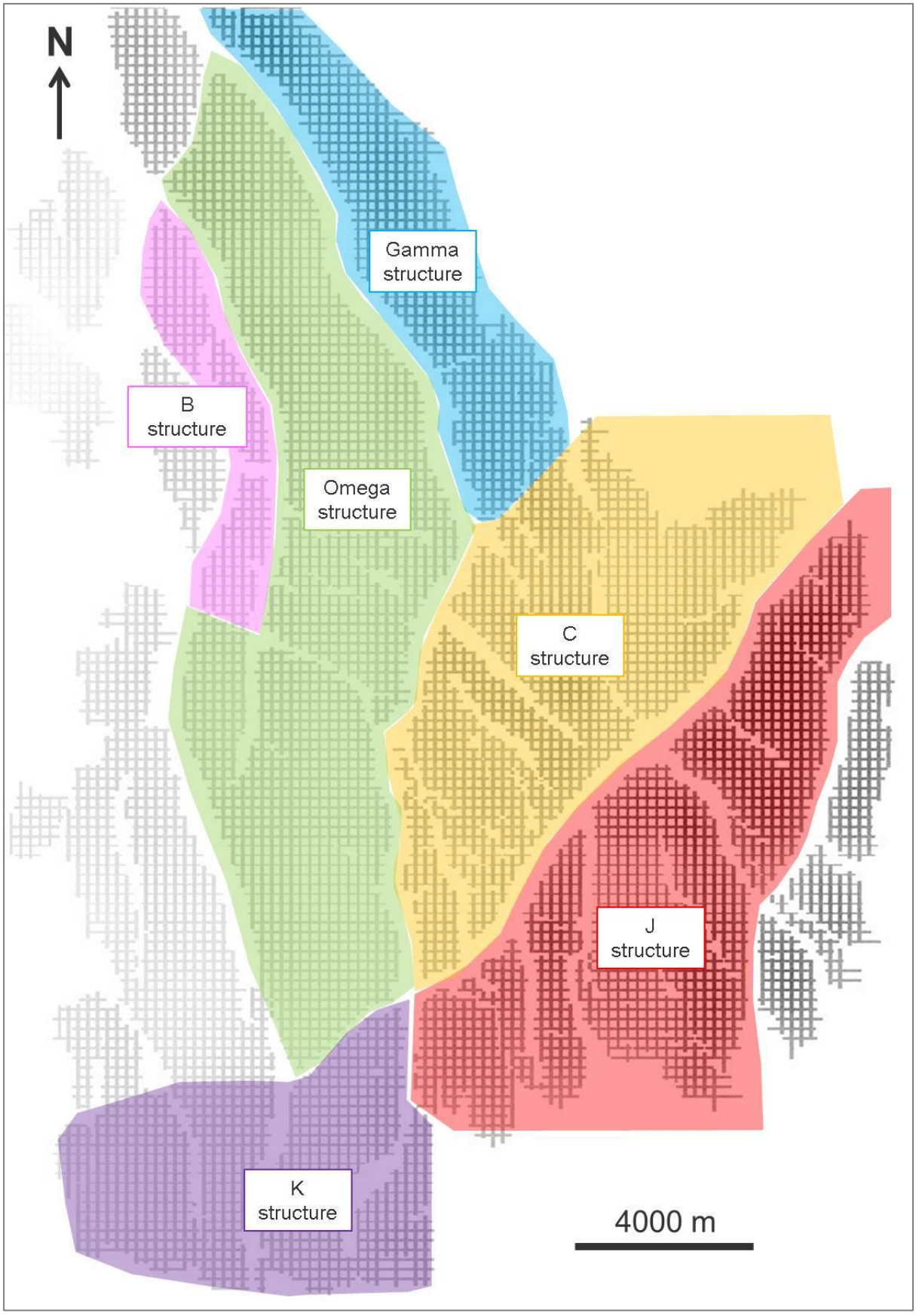

Facies codes for well 30/9-16

Depth (mMD)	Facies	Depth (mMD)	Facies	Depth (mMD)	Facies	Depth (mMD)	Facies
3459	Sm	3463,8	Swa	3468,7	Sm	3473,7	Sm
3459,1		3463,9	Fl	3468,8		3473,8	
3459,2		3464		3468,9		3473,9	
3459,3		3464,1		3469		3474	
3459,4		3464,2		3469,1		3474,1	Hl
3459,5		3464,3		3469,2		3474,2	
3459,6		3464,4		3469,3		3474,3	
3459,7		3464,5	Sm	3469,4		3474,4	
3459,8		3464,6	Fl	3469,5		3474,5	
3459,9		3464,7		3469,6		3474,6	
3460		3464,8		3469,7		3474,7	
3460,1		3464,9	Sm	3469,8		3474,8	
3460,2		3465		3469,9		3474,9	
3460,3		3465,1		3470		3475	
3460,4		3465,2	Fl	3470,1		3475,1	
3460,5		3465,3		3470,2		3475,2	
3460,6		3465,4		3470,3		3475,3	
3460,7		3465,5		3470,4		3475,4	
3460,8		3465,6	Sx	3470,5		3475,5	
3460,9		3465,7		3470,6		3475,6	
3461		3465,8		3470,7		3475,7	
3461,1		3465,9		3470,8		3475,8	
3461,2		3466		3470,9		3475,9	
3461,3		3466,1		3471		3476	
3461,4		3466,2		3471,1		3476,1	
3461,5		3466,3	Sm	3471,2		3476,2	
3461,6	Sb	3466,4		3471,3	Sx	3476,3	
3461,7		3466,5		3471,4		3476,4	
3461,8		3466,6		3471,5	Sr	3476,5	
3461,9		3466,7	Sx	3471,6		3476,6	
3462		3466,8		3471,7		3476,7	
3462,1		3466,9	Sm	3471,8		3476,8	
3462,2		3467		3471,9		3476,9	
3462,3		3467,1		3472		3477	
3462,4		3467,2		3472,1		3477,1	
3462,5	Swa	3467,3		3472,2		3477,2	
3462,6		3467,4		3472,3	Sm	3477,3	Fl?
3462,7		3467,5		3472,4		3477,4	St
3462,8		3467,6		3472,5		3477,5	
3462,9		3467,7		3472,6		3477,6	
3463		3467,8		3472,7		3477,7	
3463,1		3467,9		3472,8		3477,8	
3463,2		3468		3472,9		3477,9	
3463,3		3468,1		3473		3478	
3463,4		3468,2		3473,1		3478,1	
3463,5		3468,3		3473,2		3478,2	
3463,6		3468,4		3473,3		3478,3	
3463,7		3468,5		3473,4		3478,4	Fl
		3468,6	Sm	3473,5		3478,5	
				3473,6		3478,6	

Depth (mMD)	Facies	Depth (mMD)	Facies
3478,7	Fl	3483,5	Sb
3478,8	St	3483,6	
3478,9	Fl	3483,7	
3479		3483,8	
3479,1		3483,9	
3479,2		3484	
3479,3		3484,1	
3479,4		3484,2	
3479,5		3484,3	Sl
3479,6		3484,4	Sx
3479,7		3484,5	Sb
3479,8		3484,6	
3479,9		3484,7	
3480		3484,8	
3480,1		3484,9	
3480,2		3485	
3480,3		3485,1	
3480,4		3485,2	
3480,5		3485,3	
3480,6	Fb	3485,4	
3480,7		3485,5	
3480,8		3485,6	
3480,9		3485,7	
3481		3485,8	
3481,1	Sl	3485,9	
3481,2		3486	
3481,3		3486,1	
3481,4		3486,2	
3481,5			
3481,6			
3481,7			
3481,8	Fl		
3481,9			
3482			
3482,1			
3482,2			
3482,3			
3482,4			
3482,5	Sm		
3482,6			
3482,7	Fb		
3482,8	Sm		
3482,9			
3483	Sb		
3483,1			
3483,2			
3483,3			
3483,4			

Facies codes for well 30/9-5S

Depth (mMD)	Facies	Depth (mMD)	Facies	Depth (mMD)	Facies
2608	Sm	2614,1	N/A	2620,4	
2608,1		2614,2		2620,5	
2608,2		2614,3		2620,6	
2608,3		2614,4		2620,7	
2608,4		2614,5	Sx	2620,8	Sw
2608,5		2614,6		2620,9	
2608,6		2614,7		2621	Rubble
2608,7		2614,8		2621,1	
2608,8		2614,9		2621,2	
2608,9		2615		2621,3	Sl
2609		2615,1		2621,4	
2609,1		2615,2		2621,5	
2609,2	Sx	2615,3		2621,6	
2609,3		2615,4		2621,7	
2609,4		2615,5		2621,8	
2609,5		2615,6		2621,9	
2609,6		2615,7		2622	
2609,7		2615,8		2622,1	
2609,8		2615,9		2622,2	N/A
2609,9		2616		2622,3	
2610	Sm	2616,1	Sr/Sx?	2622,4	Rubble
2610,1		2616,2		2622,5	
2610,2	Sp	2616,3		2622,6	
2610,3		2616,4	Sx	2622,7	
2610,4		2616,5		2622,8	
2610,5		2616,6		2622,9	
2610,6	N/A	2616,7	Hl?	2623	
2610,7		2616,8		2623,1	
2610,8		2616,9		2623,2	
2610,9	Sp	2617		2623,3	
2611		2617,1		2623,4	
2611,1		2617,2		2623,5	Sx
2611,2	Sx	2617,3		2623,6	
2611,3		2617,4		2623,7	
2611,4	Sp	2617,5	Sm	2623,8	
2611,5		2617,6		2623,9	
2611,6		2617,7	N/A	2624	Rubble
2611,7		2617,8		2624,1	Sm
2611,8		2617,9		2624,2	
2611,9		2618	Swa	2624,3	
2612		2618,1		2624,4	
2612,1	Sx	2618,2		2624,5	
2612,2		2618,3		2624,6	
2612,3		2618,4		2624,7	Sh?
2612,4		2618,5		2624,8	Sm
2612,5		2618,6		2624,9	
2612,6		2618,7		2625	Rubble
2612,7		2618,8		2625,1	
2612,8		2618,9		2625,2	
2612,9		2619		2625,3	
2613		2619,1		2625,4	N/A
2613,1		2619,2		2625,5	
2613,2	Fl	2619,3		2625,6	Sr
2613,3		2619,4		2625,7	
2613,4		2619,5		2625,8	
2613,5		2619,6		2625,9	
2613,6	Sr	2619,7		2626	
2613,7		2619,8		2626,1	
2613,8	Fl	2619,9		2626,2	
2613,9		2620			
2614		2620,1			
		2620,2			
		2620,3			

Biostratigraphy for well 30/9-24T2

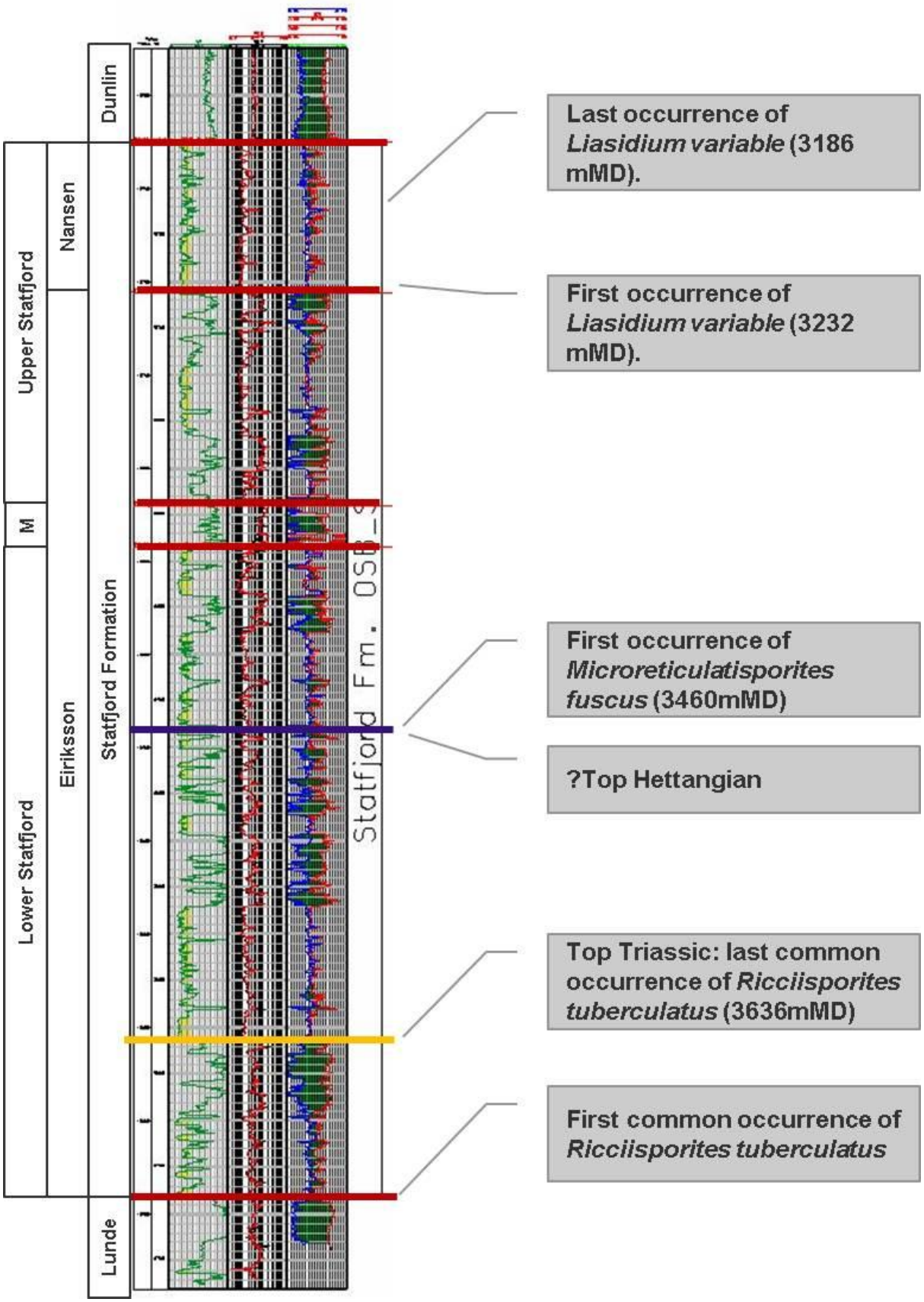

Biostratigraphy for well 30/9-3A

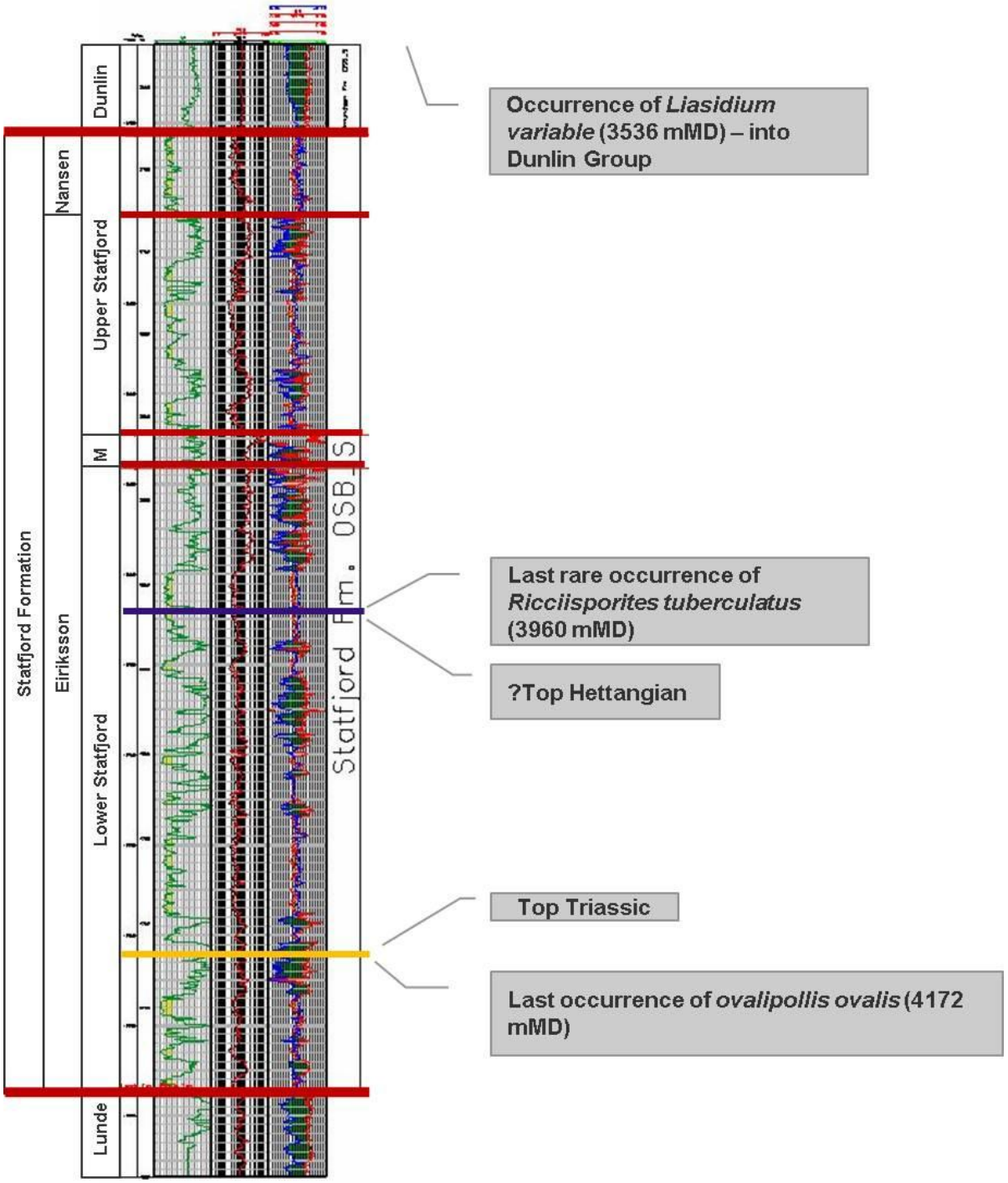

Biostratigraphy for well 30/9-5S

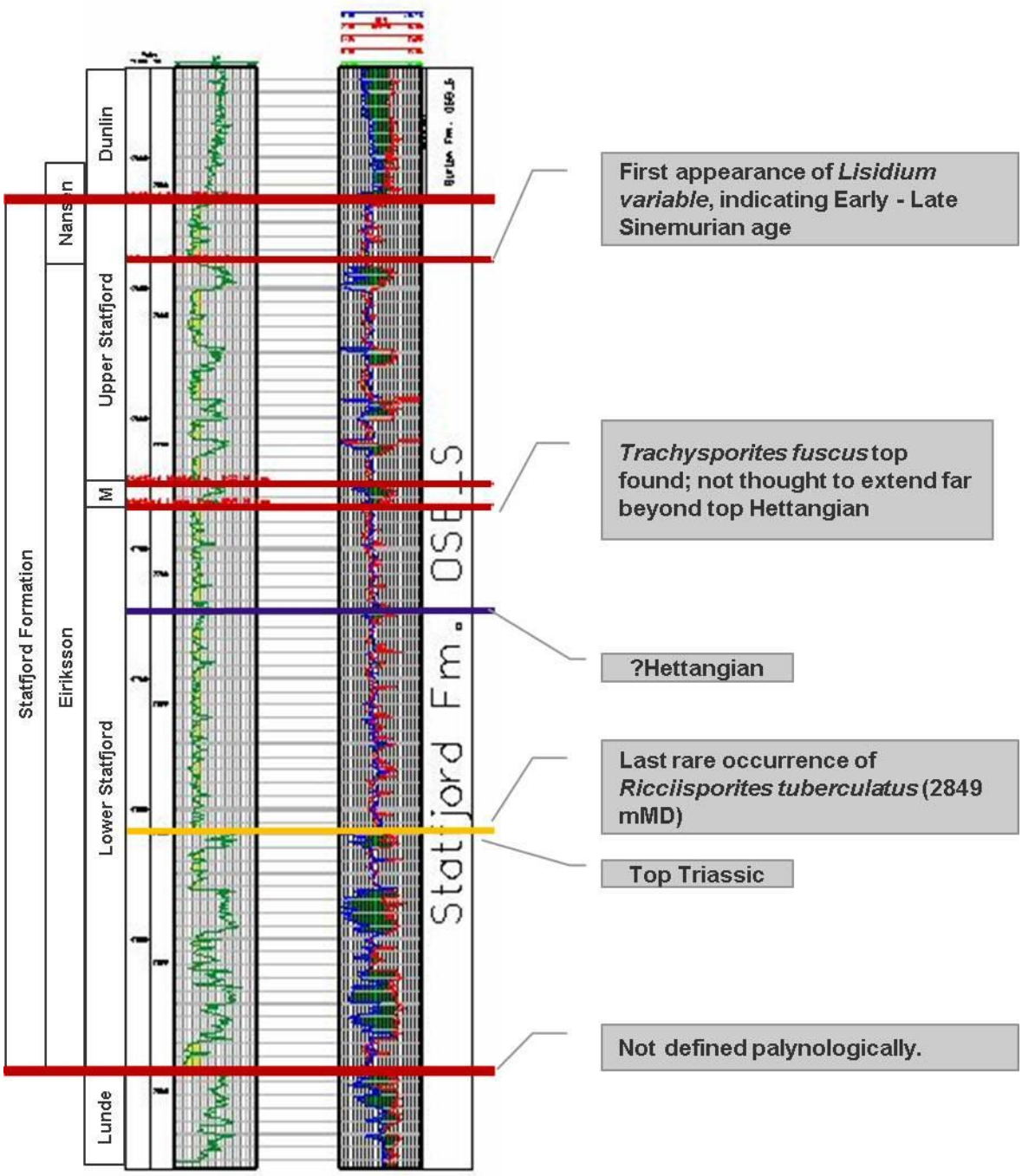

Faults used in modelling